5-3-2016

Identification and Quantification of Heterogeneity in Freezing and Primary Drying Steps of Lyophilization

Pooja Sane
University of Connecticut, pooja.sane@gmail.com

Identification and Quantification of Heterogeneity in Freezing and Primary Drying Steps of Lyophilization

Pooja P. Sane, Ph.D.

University of Connecticut, 2016

Abstract

The ultimate goal of the freeze-drying process is to deliver a consistently stable, efficacious, easily reconstitutable, and non-immunogenic final product to the patient at an affordable cost. However, heterogeneity in the heat transfer to vials across the batch and in mass transfer resistance to sublimation were found to lead to variation in the factors affecting product quality both intra- and inter-batch. The overall objective of this research was to identify and quantify the sources of variation in the freeze-drying process, which alter the thermal history of the product and investigate their effects on the product quality attributes.

Effects of processing parameters on the measurement of vial heat transfer coefficient (K_v), one of the major factors affecting the product temperature and drying time, were studied. This study found several nuances and pitfalls of K_v measurement. Calculation of K_v for developing a cycle for a new product should be based on measurements made at target shelf temperatures and chamber pressures, using the vial and fill volume of the new product. Experimentally obtained distribution in K_v across a batch of vials was combined with variations in three other input parameters – dry product layer resistance, fill volume and shelf temperature –

in a first principles based, steady-state heat and mass transfer model to quantitatively predict the distribution in primary drying times in vials in the batch.

A method was developed to experimentally measure the spatial variation in pressure in the drying chamber using a differential capacitance manometer and custom-made rig installed in a laboratory freeze-dryer. These measured pressure gradients were found to have an insignificant effect on drying time in comparison to the variations in the position-based K_v or ice nucleation temperature-dependent dry product layer resistance.

Lastly, the effect of heterogeneity in the freezing and the primary drying steps of lyophilization on the reconstitution time for a lyophilized high concentration monoclonal antibody was investigated. Differences in product temperature and drying times affected the cake properties such as wetting, disintegration and hydration, altering reconstitution times.

Identification and Quantification of Heterogeneity in Freezing and Primary Drying Steps of Lyophilization

Pooja P. Sane

B.Pharm., Mumbai University, [2007]

M.S., Northeastern University, [2009]

A Dissertation

Submitted in Partial Fulfillment of the

Requirements for the Degree of

Doctor of Philosophy

at the

University of Connecticut

[2016]

Approval Page

Doctor of Philosophy Dissertation

Identification and Quantification of Heterogeneity in Freezing and Primary Drying Steps of Lyophilization

Presented by

Pooja P. Sane, M.S.

Major Advisor _____

Robin H. Bogner

Associate Advisor _____

Michael J. Pikal

Associate Advisor _____

Devendra Kalonia

Associate Advisor _____

Serguei Tchessalov

Associate Advisor _____

Joseph Rinella

University of Connecticut

[2016]

Dedication

To my mom, dad and sister for all the love, care and patience throughout these years,

&

My best friend, Nilesh for letting me be myself

Acknowledgements

The day I decided to make the list of people I wanted to thank, I realized I have tons of people to acknowledge for their support either in my thesis or in my life, directly or indirectly.

I consider myself to be very privileged to have worked in the Bogner-Pikal group. I would first like to express my heartfelt gratitude to my major advisor, Dr. Robin Bogner for her enthusiastic support and guidance through every step of my thesis work, and for everything she has taught me both at a professional as well as at a personal level. She's one of the most approachable people I have ever met who would make me understand difficult concepts with a very simple approach. I am very much thankful to Dr. Pikal as well for his contagious passion for freeze-drying, continuous guidance and inspiration throughout these five and half years. Regarded as the "King of Lyophilization", I consider myself very fortunate to have worked under his excellent mentorship. Now as I stand on the cusp of my professional career, I would like to thank both Dr. Bogner and Dr. Pikal for giving me a platform to evolve as a better scientist as well as an individual. I will really miss them both!

I would also like to thank my associate advisors:

- Dr. Kalonia for his thought provoking questions during seminars and committee meeting and especially the "always keep smiling" comment he made in my first year which I took rather seriously throughout my stance at UCONN.
- Dr. Serguei Tchessalov for giving me an opportunity to work at Pfizer for two consecutive summers, for his incessant contribution with regards to my thesis and for teaching me that it is ok to get crazy when it comes to research!
- Dr. Joe Rinella for his interest and involvement in my work and very helpful suggestions during committee meeting.

My work at UCONN has comprised of several collaborative projects, which would not have been possible without the help of several people.

- First and foremost, I am very grateful to Dr. Bakul Bhatnagar for helping me understand a lot about reconstitution of proteins when working at Pfizer as a summer intern. He has been an excellent mentor, a very patient listener and my go-to person whenever I needed help in writing, understanding concepts, job search and the list goes on.
- I would like to thank Dr. Steve Nail for the elaborate and helpful discussions on the vial heat transfer coefficient measurement project.
- I also thank Dr. Alina Alexeenko, Dr. Arnab Ganguly and Nikhil Varma for educating me about computational fluid dynamics when collaborating on the project to investigate the presence of spatial pressure variation.
- I thank Cyrus Agarabi for the insightful discussions on the lyo model project.
- And Jim Jenks who was always just a call away if I had any problems with the freeze-dryers!

I am grateful to the entire Pharmaceutics faculty for the rigorous and comprehensive coursework, which has laid a strong scientific background, and for arranging seminars and external talks that enabled me to understand the different facets of pharmaceutical research along with giving me the opportunity to interact with the subject experts.

I would also like to thank:

- Mark Armati for being extremely kind and helpful whenever I needed to place an order for lab supplies. I literally feel he has 10 hands and probably an XL sized brain!

- Administrative staff at the School of Pharmacy: Leslie Lebel, Kathy Koji, Laura Burnett, Jackie Petri, Sharon Giovenale, Mina Boone, Skip Copeland, Debbie Milvae, Liz Anderson for their support.
- Past and present lab-mates: Puneet (who gave me a Freeze-Drying in the Lab 101 and made sure I could plot the data for my first lyo-cycle using Excel by standing behind me all the while I did it!), Kelly and Ken (for their guidance), Mary (for her energy), Arushi (for being Arushi!), Lauren (for a constant source of information), Loren, Hiro, Kaz, Norman, Meena, Kim, Ilaria.
- Ekneet, Rajani, Ashlesha, Megha, Vibha, Upasana, Mamta, and Viru for the fun times at UCONN.
- Other friends at UCONN: Shreya (for her contagious laughter), Japneet (for her inputs), Chitra, Avnish, Saurabh, Bing, Jie, Rajan, Janki, Sahil, Joseline, Priya, Johana, Gayathri.
- Friends outside UCONN: Utkarsh and Aparna (who had awarded me my PhD degree right in my first year!), Aditi, Shweta, Tony, Rujuta, Babu, Amit and Kamiya, Suvarna and Abhishek, Robin, Keyur, Rahul, Sheetal
- Friends from Undergrad: Sean, Juee, Anuja, Yash and Anup for giving me some laughs.

I am really grateful to Neera Jain and Suresh Babu, my mentors at Synta Pharmaceuticals for helping me through a rough time in life and then directing me towards the right path. Further, I would also like to thank Nimita Dave who went out of her way to help me choose the right school for my graduate studies.

My life at UCONN has been a very memorable experience and that would not have been possible without the presence of a few special people. I would like to extend a very special thank you to Masha (for being an awesome friend and companion all these years and for always remembering the exact gift I wanted at all the special occasions), Vamsi (for being my 24/7 helpline to answer my silly questions on literally any topic), Rui (for always making me feel good about myself), Pawel (whose early morning greeting "Hello, how are ya?" would make my day), Namita (for being the awesomest roommate and a lovely friend I have ever had!!), Rishabh (for looking out for me), Liz (for the crazy times and yes of course for the last minute eggplant parmigiana!).

I would like to express my heartfelt gratitude to my parents, Nanda Sane and Prasad Sane for being a constant support throughout my life. I am what I am today only because of the lessons of life that I have learnt from them and the umpteen number of sacrifices they have made throughout these years. I don't express this quite often but I really love you guys a lot! I would also like to thank my younger sister, Sayali Sane for being there for me, for making me smile all these years and for acting like an elder sister when required ☺. I want to thank my parents-in-law for their constant encouragement throughout this long journey

The last but the most important person in my life who I want to thank today is my best buddy, my husband Nilesh Kuchekar. He has been my constant source of inspiration since the past 11 years. His unconditional love and support throughout my graduate school made this time fly by very quickly. Thank you for being my rock, my anchor; for keeping me grounded when I felt like I might otherwise blow away. Thank you for making fun of me when I deserved it, and for loving me when I didn't. Thank you for being you and letting me be me! I will always love you (more than you do)!

Table of Contents

Chapter 5:

Chapter 6:

Chapter 1

Introduction, Aims and Organization of the Thesis

INTRODUCTION

Freeze-drying or lyophilization is a process commonly used to improve the stability of labile injectable drugs such as therapeutic proteins. In the freeze-dried solid state, chemical and physical degradation reactions are inhibited or sufficiently decelerated, resulting in improved long-term stability (Carpenter et al. 1997). The process of freeze-drying consists of three main steps: (a) freezing, (b) primary drying and (c) secondary drying. Variation in the parameters of any of these stages will influence the performance of the later stages with an ultimate effect on the product quality. There is a considerable amount of heterogeneity involved in the freezing and primary drying steps of lyophilization, which will be discussed below. A thorough quantification of this heterogeneity will enable a better process control of the individual steps of freeze-drying leading to a successful process development to produce a quality product. Moreover, the extended freeze-drying cycles and the costs associated with them can be reduced by optimization of the freeze-drying process.

Heterogeneity in Freezing:

The freezing step is critical in lyophilization since the overall performance of the drying process depends on this stage. Freezing cycle parameters especially the degree of supercooling and the rate of ice crystallization are used to define the freezing process (Pikal, Rambhatla, Ramot 2002).

The degree of supercooling which is the difference between the equilibrium freezing point and the actual ice nucleation temperature determines the number of ice nuclei formed. Given that the total amount of water that freezes remains constant, the size of the ice crystals formed will be determined by the degree of supercooling. A high degree of supercooling produces large number of small ice crystals leading to the formation of small pore sizes in the

dried layer of the product during primary drying. During primary drying, the sublimation front moves from the top to the bottom of a vial with the dry layer forming on the top. This layer poses a resistance to the movement of water vapor from the frozen plug to the empty space in the vial. Thus, a higher degree of supercooling reduces the sublimation rate during primary drying (Pikal et al. 1983). The small pore size essentially creates a higher specific surface area in the dried product, which increases the sublimation rate during secondary drying and decreases the time (Pikal et al. 1990). Due to the inherent stochastic nature of ice nucleation achieving homogenous nucleation and growth in all the vials in a batch is a challenge leading to a further variation in primary and secondary drying behavior.

Further, the rate of ice crystal growth affects the residence time of the solutes in the freeze concentrated state, which can affect the stability of certain labile drugs such as biotherapeutics. Faster the growth of ice crystals lesser is the exposure of the solutes in the formulation to the freeze concentrated phase thereby reducing the degradation (Carpenter et al. 1997; Pikal 2002).

Synchronizing the ice nucleation and introducing an annealing step prior to primary drying are some of the options available to control the size and distribution of the ice crystals (Kasper and Friess 2011). There are several methods available for controlling the ice nucleation namely ice fog technique (Ling 2015; Rowe 1990) and the depressurization method (Konstantinidis et al. 2011). Annealing the sample by holding the product temperature above the glass transition temperature (T_g') of the freeze-concentrate for a predetermined time is another way to overcome the heterogeneous ice crystal size and obtain larger crystals (Searles, Carpenter, Randolph 2001b).

Heterogeneity in Primary Drying:

Primary drying is the removal of ice from the frozen product by sublimation at a reduced pressure. The higher amount of water present during primary drying poses a constraint of maintaining the product below a *maximum allowable product temperature* that is defined by the collapse temperature (T_c) for the amorphous solutes and the eutectic melting temperature (T_{eu}) for the crystalline solutes. During primary drying, the target product temperature is maintained 2-3 °C below the T_c or T_{eu} as a safe margin. If the product temperature exceeds the critical temperatures (T_c, T_{eu}) viscous flow is initiated and the cake structure collapses, often adversely affecting the stability, reconstitution time and/or appearance of the end product (Schersch et al. 2010). The product temperature cannot be controlled directly, but is manipulated by balancing the heat removed from the product by sublimation with the heat input to the product. The heat input to the product is controlled by adjusting the chamber pressure and shelf temperature during primary drying to obtain a certain vial heat transfer coefficient. The resistance to the vapor flow due to the dry layer formed during primary drying and the driving force for sublimation given by the difference between the pressure at the sublimation interface and the chamber pressure govern the heat removed from the product by sublimation. Even with the advanced process understanding of heat and mass transfer during primary drying found in the literature (Pikal, Roy, Shah 1984; Rambhatla and Pikal 2004), often the shelf temperature and chamber pressure for a new product are determined by empirical "trial and error" experimental approaches, which can be time and material consuming.

In pharmaceutical freeze-drying applications, heat transfer to the vial is the sum of three contributions, namely contact conduction arising from the direct heat transfer between the vials and the shelf, radiation from the warmer non-temperature-controlled surfaces in the chamber and

gas conduction between the shelf and the bottom of the vial (Pikal 1985). The contribution from radiative heat transfer varies depending on the location of the vial on the shelf (Rambhatla and Pikal 2003). At the low temperatures employed in freeze-drying thermal radiation is not a dominant mechanism of heat transfer for vials in the center (Nail 1980) but it becomes significant for edge vials from relatively warm surfaces such as the door and chamber walls. The edge vials, which are close to the walls and the door, receive more heat and dry faster than an average center vial; this is referred to as "the edge vial effect" (Rambhatla and Pikal 2003). Additionally, vials closer to the duct, which connects the chamber to the low temperature condenser, lose energy by radiation thus experiencing colder temperatures leading to decreased sublimation rates.

The heat transfer due to gas conduction between the vial bottom and the shelf beneath is a very strong function of the chamber pressure (Nail 1980). Usually the chamber pressure in a typical laboratory freeze-dryer is controlled at a fixed location. The pressure at this port can vary by 1 - 2 mTorr during the entire process. However, recent theoretical calculations using Computational Fluid Dynamics (CFD) simulations show the presence of significant pressure gradients along the shelves, especially in the large-scale units with decreased clearance between the shelves (Rasetto et al. 2008; Rasetto et al. 2010). No experimental verification for the same exists. Increase in the local pressure near a vial increases the collisions of gas molecules between the bottom of the vial and the shelf leading to an increase in the vial heat transfer coefficient, sublimation rate and product temperature. Thus, pressure variation can be a significant source of inter-vial variation in product temperature affecting the product quality especially if one is operating at the edge of failure.

Further, differences in the ice nucleation temperatures, dryer configurations, position of the condenser with respect to the chamber and the position of the vials on the shelf between a laboratory-scale and a manufacturing-scale freeze-dryer further complicate the scale-up of an existing cycle from a laboratory-scale (Rambhatla and Pikal 2004).

Effect of Heterogeneity in Freeze-Drying on the Reconstitution Time of Protein Formulations at High Concentrations:

A lyophilized product is reconstituted using an appropriate diluent prior to administration. Reconstitution time is one of the important quality attributes especially if the times are long such as in the case of protein formulations at high concentrations (Shire, Shahrokh, Liu 2004). Several studies have been published in the literature focusing on the alteration of the freezing step to explore its effect on the reconstitution time for high protein concentration systems. Effect of controlled ice nucleation at higher temperatures (Geidobler, Konrad, Winter 2013) and use of different cooling rates (Beech et al. 2015) during freezing on the reconstitution times of amorphous systems containing proteins at high concentrations has been explored. As discussed earlier, the ice nucleation temperature during freezing and freezing rate affect the pore structure in the final freeze-dried product, which can alter the reconstitution times.

When a bulking agent such as mannitol was present in the crystalline phase in a high concentration lyophilized protein product the reconstitution time was shortened (Cao et al. 2013). Cooling rate influences the extent of crystallization of excipients like mannitol and glycine (Hsu et al. 1996) (another bulking agent) that can in turn affect the reconstitution times especially in the absence of an annealing step. Crystallization of excipients can also be promoted by annealing (Searles, Carpenter, Randolph 2001b) which can improve the reconstitution times for lyophilized

high concentration protein formulations. Even varying the annealing temperatures can cause a change in the reconstitution time (Krishnan et al. 2007).

STATEMENT OF THE PROBLEM

A variation in the different stages of freeze-drying could lead to a variation in the thermal history of the product both intra- and inter-batch. The thermal history of a lyophilized product determines its appearance, stability during and post freeze-drying, reconstitution times and efficacy. Controlling the product temperature judiciously will consistently result in a product of the same quality. Any improvement in the process by achieving more homogenous drying conditions and shortening the primary drying time will improve the cost efficiency of the process leading to a decrease in the overall cost of the product to the end user.

OBJECTIVES AND AIMS

The overall objective of the dissertation research was to identify and quantify the sources of heterogeneity in the freeze-drying process followed by exploring their effects on the processing time and product characteristics such as the reconstitution time.

Specific Aims:

a. To explore factors such as chamber pressure, shelf temperature, vial fill height and vial position on the vial heat transfer coefficient and develop well-defined protocols for its measurement.
b. To model vial-to-vial variation in the maximum product temperature and drying time during the primary drying step of lyophilization based on the natural variation in several input parameters, such as vial heat transfer coefficient and the resistance of the product to sublimation of ice.

c. To measure any spatial variation in the chamber pressure during the primary drying step of a freeze-drying cycle in a laboratory freeze-dryer and calculate its effects on scale-up and batch uniformity.

d. To determine the effect of protein concentration, ice nucleation temperature and drying conditions on the reconstitution times of an amorphous lyophilized formulation containing high concentration monoclonal antibody.

CHAPTER ORGANIZATION AND OUTLINE

Chapter 2 probes the heterogeneity in heat transfer rates to the product based on the position of the vial on the shelf for a range of processing conditions. The chapter outlines the different types of vial heat transfer coefficients that can be calculated for either an individual, group or a batch of vials based on the method used to measure sublimation rate and product temperature during a freeze-drying cycle. The conventional gravimetric method is compared and contrasted with the Process Analytical Technology (PAT) tool, Tunable Diode Laser Absorption Spectroscopy (TDLAS) for determination of sublimation rate with a special emphasis on the calculations involved in determining the vial-to-vial variation in the heat transfer coefficient across a batch of vials. Effects of several processing variables such as chamber pressure, shelf temperature, fill volume, nature of the pre-lyophilized solution and other additional factors are discussed in detail.

Chapter 3 presents the application of a first principles model based on quasi steady-state heat and mass transfer theory for the primary drying step of lyophilization to quantify the distribution of maximum product temperature and primary drying time, within a batch of vials. To obtain a distribution in these key output parameters, distributions in fill volume, shelf temperature, vial heat transfer coefficient and product resistance are provided as input

parameters. The agreement of the calculated distribution in drying times with experimental results was used to assess the model.

Chapter 4 discusses the experimental verification of the local chamber pressure gradients in a lab-scale freeze-dryer at a target chamber pressure. Pressure differences between the center and the edges of a lab-scale freeze-dryer shelf were measured using a differential capacitance manometer as a function of sublimation flux and clearance between the sublimation front and the shelf above. The data were extrapolated to manufacturing-scale to better understand the consequences of the pressure gradients at that scale.

Moving to a more recent challenge in freeze-drying, the reconstitution behavior of lyophilized formulations containing high concentration monoclonal antibody (mAb) is the subject of **Chapter 5**. It specifically describes experimental approaches to investigate the underlying mechanisms, namely wetting, disintegration and hydration in order to better understand the reconstitution of the lyophilized high concentration proteins. The effect of heterogeneity in the freezing and primary drying steps of lyophilization on the reconstitution behavior was investigated by altering the ice nucleation temperature and drying conditions at a low and high protein concentration.

Chapter 6 summarizes the key findings of the thesis work, discusses their implications and suggests additional areas of inquiry.

REFERENCES

Awotwe-Otoo D, Agarabi C, Read EK, Lute S, Brorson KA, Khan MA, Shah RB. 2013. Impact of controlled ice nucleation on process performance and quality attributes of a lyophilized monoclonal antibody. Int J Pharm 450(1):70-8.

Beech KE, Biddlecombe JG, van der Walle, Christopher F, Stevens LA, Rigby SP, Burley JC, Allen S. 2015. Insights into the influence of the cooling profile on the reconstitution times of amorphous lyophilized protein formulations. European Journal of Pharmaceutics and Biopharmaceutics 96:247-54.

Bhambhani A, Meyer BK, Blue JT. 2010. Methods for producing high concentration lyophilized pharmaceutical formulations.

Bhatnagar BS, Bogner RH, Pikal MJ. 2007. Protein stability during freezing: Separation of stresses and mechanisms of protein stabilization. Pharm Dev Technol 12(5):505-23.

Bhatnagar BS, Tchessalov S, Lewis LM, Johnson R. Encyclopedia of pharmaceutical science and technology. .

Brülls M and Rasmuson A. 2002. Heat transfer in vial lyophilization. Int J Pharm 246(1):1-16.

Cao W, Krishnan S, Ricci MS, Shih L, Liu D, Gu JH, Jameel F. 2013. Rational design of lyophilized high concentration protein formulations-mitigating the challenge of slow reconstitution with multidisciplinary strategies. Eur J Pharm Biopharm 85(2):287-93.

Carpenter JF, Pikal MJ, Chang BS, Randolph TW. 1997. Rational design of stable lyophilized protein formulations: Some practical advice. Pharm Res 14(8):969-75.

Chang BS, Kendrick BS, Carpenter JF. 1996. Surface-induced denaturation of proteins during freezing and its inhibition by surfactants. J Pharm Sci 85(12):1325-30.

Colandene JD, Maldonado LM, Creagh AT, Vrettos JS, Goad KG, Spitznagel TM. 2007. Lyophilization cycle development for a high-concentration monoclonal antibody formulation lacking a crystalline bulking agent. J Pharm Sci 96(6):1598-608.

Costantino HR and Pikal MJ. 2004. Lyophilization of biopharmaceuticals. Springer Science & Business Media.

Dix D, Bowers K, Chimanlall G. 2006. IL-1 antagonist formulations.

Fissore D, Pisano R, Barresi AA. 2011. Advanced approach to build the design space for the primary drying of a pharmaceutical freeze-drying process. J Pharm Sci 100(11):4922-33.

Flink J. 1977. Energy analysis in [food] dehydration processes. Food Technol 31.

Forny L, Marabi A, Palzer S. 2011. Wetting, disintegration and dissolution of agglomerated water soluble powders. Powder Technol 206(1):72-8.

Gan KH, Bruttini R, Crosser OK, Liapis AI. 2005. Freeze-drying of pharmaceuticals in vials on trays: Effects of drying chamber wall temperature and tray side on lyophilization performance. Int J Heat Mass Transfer 48(9):1675-87.

Geidobler R, Konrad I, Winter G. 2013. Can controlled ice nucleation improve Freeze-Drying of Highly-Concentrated protein formulations? J Pharm Sci 102(11):3915-9.

Gieseler H, Kramer T, Schneid S. 2008. Quality by design in freezedrying: Cycle design and robustness testing in the laboratory using advanced process analytical technology. Pharm Technol 10:88-95.

Gieseler H, Kessler WJ, Finson M, Davis SJ, Mulhall PA, Bons V, Debo DJ, Pikal MJ. 2007. Evaluation of tunable diode laser absorption spectroscopy for in-process water vapor mass flux measurements during freeze drying. J Pharm Sci 96(7):1776-93.

Giordano A, Barresi AA, Fissore D. 2011. On the use of mathematical models to build the design space for the primary drying phase of a pharmaceutical lyophilization process. J Pharm Sci 100(1):311-24.

Greco K, Bergman TL, Bogner R. 2011. Design and characterization of a laminar flow-through dissolution apparatus: Comparison of hydrodynamic conditions to those of common dissolution techniques. Pharm Dev Technol 16(1):75-87.

Hibler S, Wagner C, Gieseler H. 2012. Vial freeze-drying, part 1: New insights into heat transfer characteristics of tubing and molded vials. J Pharm Sci 101(3):1189-201.

Hsu CC, Walsh AJ, Nguyen HM, Overcashier DE, Koning-Bastiaan H, Bailey RC, Nail SL. 1996. Design and application of a low-temperature peltier-cooling microscope stage. J Pharm Sci 85(1):70-4.

Jameel F and Khan M. 2009. Quality-by-design as applied to the development and manufacturing of a lyophilized protein product. Am Pharm Rev 12(7).

Jansco G, Pupezin J, Van Hook WA. 1970. The vapor pressure of ice between 10– 2 and– 10 2◦ C. J Phys Chem 74:2984-9.

Kasper JC and Friess W. 2011. The freezing step in lyophilization: Physico-chemical fundamentals, freezing methods and consequences on process performance and quality attributes of biopharmaceuticals. European Journal of Pharmaceutics and Biopharmaceutics 78(2):248-63.

Kobayashi M, Harashima K, Ariyama H, Yao A. 2011. Inter-vial variance of the sublimation rate in shelf freeze-dryer. Transactions of the Japan Society of Refrigerating and Air Conditioning Engineers 10:135-44.

Kochs M, Körber C, Heschel I, Nunner B. 1993. The influence of the freezing process on vapour transport during sublimation in vacuum-freeze-drying of macroscopic samples. Int J Heat Mass Transfer 36(7):1727-38.

Koganti VR, Shalaev EY, Berry MR, Osterberg T, Youssef M, Hiebert DN, Kanka FA, Nolan M, Barrett R, Scalzo G. 2011. Investigation of design space for freeze-drying: Use of modeling for primary drying segment of a freeze-drying cycle. AAPS PharmSciTech 12(3):854-61.

Konstantinidis AK, Kuu W, Otten L, Nail SL, Sever RR. 2011. Controlled nucleation in freeze-drying: Effects on pore size in the dried product layer, mass transfer resistance, and primary drying rate. J Pharm Sci 100(8):3453-70.

Krishnan S, Pallitto MM, Ricci MS. Development of formulations for therapeutic monoclonal antibodies and fc fusion proteins. Formulation and Process Development Strategies for Manufacturing Biopharmaceuticals :383-427.

Krishnan S, Pallitto M, Nagle S, Crampton SL, Ricci MS, Cao W, Lin H, Xie Y. 2007. Concentrated protein lyophilates, methods and uses.

Kuu WY, Nail SL, Sacha G. 2009. Rapid determination of vial heat transfer parameters using tunable diode laser absorption spectroscopy (TDLAS) in response to step-changes in pressure set-point during freeze-drying. J Pharm Sci 98(3):1136-54.

Liao X, Krishnamurthy R, Suryanarayanan R. 2007. Influence of processing conditions on the physical state of mannitol-implications in freeze-drying. Pharm Res 24(2):370-6.

Ling W. 2015. Using Surface Heat Flux Measurement to Monitor and Control a Freeze Drying Process .

Liu Y, Zhao Y, Feng X. 2008. Exergy analysis for a freeze-drying process. Appl Therm Eng 28(7):675-90.

Martin A. 1993. Physical pharmacy: Physical chemical principles in the pharmaceutical sciences. BI Waverly. Pvt Ltd.

Milton N, Pikal MJ, Roy ML, Nail SL. 1997. Evaluation of manometric temperature measurement as a method of monitoring product temperature during lyophilization. PDA Journal of Pharmaceutical Science and Technology 51(1):7-16.

Mockus LN, Paul TW, Pease NA, Harper NJ, Basu PK, Oslos EA, Sacha GA, Kuu WY, Hardwick LM, Karty JJ. 2011. Quality by design in formulation and process development for a freeze-dried, small molecule parenteral product: A case study. Pharm Dev Technol 16(6):549-76.

Nail SL and Searles JA. 2008. Elements of quality by design in development and scale-up of freeze-dried parenterals. BioPharm International 21(1).

Nail SL. 1980. The effect of chamber pressure on heat transfer in the freeze drying of parenteral solutions. J Parenter Drug Assoc 34(5):358-68.

Patel SM, Chaudhuri S, Pikal MJ. 2010. Choked flow and importance of mach I in freeze-drying process design. Chemical Engineering Science 65(21):5716-27.

Patel SM, Doen T, Pikal MJ. 2010. Determination of end point of primary drying in freeze-drying process control. AAPS PharmSciTech 11(1):73-84.

Patel SM, Bhugra C, Pikal MJ. 2009. Reduced pressure ice fog technique for controlled ice nucleation during freeze-drying. AAPS PharmSciTech 10(4):1406-11.

Pikal MJ. 2002. Freeze drying. Encyclopedia of Pharmaceutical Technology, Marcel Dekker, New York 1299:1326.

Pikal MJ. 1995. Freeze-Drying of proteins. process, formulation, and stability. ChemInform 26(4).

Pikal M, Rambhatla S, Ramot R. 2002. The impact of the freezing stage in lyophilization: Effects of the ice nucleation temperature on process design and product quality. American Pharmaceutical Review 5:48-53.

Pikal M, Shah S, Roy M, Putman R. 1990. The secondary drying stage of freeze drying: Drying kinetics as a function of temperature and chamber pressure. Int J Pharm 60(3):203-7.

Pikal M, Shah S, Senior D, Lang J. 1983. Physical chemistry of freeze-drying: Measurement of sublimation rates for frozen aqueous solutions by a microbalance technique. J Pharm Sci 72(6):635-50.

Pikal MJ. 1985. Use of laboratory data in freeze drying process design: Heat and mass transfer coefficients and the computer simulation of freeze drying. J Parenter Sci Technol 39(3):115-39.

Pikal MJ, Roy ML, Shah S. 1984. Mass and heat transfer in vial freeze-drying of pharmaceuticals: Role of the vial. J Pharm Sci 73(9):1224-37.

Pisano R, Fissore D, Barresi AA, Brayard P, Chouvenc P, Woinet B. 2013. Quality by design: Optimization of a freeze-drying cycle via design space in case of heterogeneous drying behavior and influence of the freezing protocol. Pharm Dev Technol 18(1):280-95.

Rambhatla S and Pikal MJ. 2004. Heat and mass transfer issues in freeze-drying process development. Lyophilization of Biopharmaceuticals :75-109.

Rambhatla S, Ramot R, Bhugra C, Pikal MJ. 2004. Heat and mass transfer scale-up issues during freeze drying: II. control and characterization of the degree of supercooling. Aaps Pharmscitech 5(4):54-62.

Rambhatla S and Pikal MJ. 2003. Heat and mass transfer scale-up issues during freeze-drying, I: Atypical radiation and the edge vial effect. AAPS PharmSciTech 4(2):111-20.

Rasetto Valeria, Marchisio Daniele L., Fissore Davide and Barresi Antonello A. 2008. Model-based monitoring of a non-uniform batch in a freeze-drying process. Proceedings of 18th european symposium on computer aided process Engineering–ESCAPE18 (edited by B. braunschweig, X. joulia). 1 p.

Rasetto V, Marchisio DL, Fissore D, Barresi AA. 2010. On the use of a dual-scale model to improve understanding of a pharmaceutical freeze-drying process. J Pharm Sci 99(10):4337-50.

Ratti C. 2001. Hot air and freeze-drying of high-value foods: A review. J Food Eng 49(4):311-9.

Rowe T., Greiff D. and Monrow J. 1979. Rate distribution in shelf freeze drying: Preliminary studies. 15th international congress of refrigeration.

Rowe TD. 1990. A technique for the nucleation of ice. International symposium on biological product freeze-drying and formulation.

Roy ML and Pikal MJ. 1989. Process control in freeze drying: Determination of the end point of sublimation drying by an electronic moisture sensor. PDA Journal of Pharmaceutical Science and Technology 43(2):60-6.

Sane P, Agarabi C, Pikal M, Bogner R. a. Quantifying the variation in product temperature and drying time within a lyophilized batch during primary drying. Manuscript in Preparation .

Sane P, Pikal M, Nail S, Bogner R. b. Measurement of heat transfer to vials on a freeze-dryer shelf during primary drying. Manuscript in Preparation .

Schersch K, Betz O, Garidel P, Muehlau S, Bassarab S, Winter G. 2010. Systematic investigation of the effect of lyophilizate collapse on pharmaceutically relevant proteins I: Stability after freeze-drying. J Pharm Sci 99(5):2256-78.

Schneid SC, Gieseler H, Kessler WJ, Pikal MJ. 2009. Non-invasive product temperature determination during primary drying using tunable diode laser absorption spectroscopy. J Pharm Sci 98(9):3406-18.

Schober C and Fitzpatrick J. 2005. Effect of vortex formation on powder sinkability for reconstituting milk powders in water to high solids content in a stirred-tank. J Food Eng 71(1):1-8.

Searles JA, Carpenter JF, Randolph TW. 2001a. The ice nucleation temperature determines the primary drying rate of lyophilization for samples frozen on a temperature-controlled shelf. J Pharm Sci 90(7):860-71.

Searles JA. 2000. Heterogeneity phenomena in pharmaceutical lyophilization. .

Searles JA, Carpenter JF, Randolph TW. 2001b. Annealing to optimize the primary drying rate, reduce freezing-induced drying rate heterogeneity, and determine tg' in pharmaceutical lyophilization. J Pharm Sci 90(7):872-87.

Sharma VK, Chih H, Mrsny RJ, Daugherty AL. 2009. The formulation and delivery of monoclonal antibodies. Therapeutic Monoclonal Antibodies: From Bench to Clinic :673-709.

Shire SJ, Shahrokh Z, Liu J. 2004. Challenges in the development of high protein concentration formulations. J Pharm Sci 93(6):1390-402.

Shittu T and Lawal M. 2007. Factors affecting instant properties of powdered cocoa beverages. Food Chem 100(1):91-8.

Short SM, Cogdill RP, Drennen III JK, Anderson CA. 2011. Performance-based quality specifications: The relationship between process critical control parameters, critical quality attributes, and clinical performance. J Pharm Sci 100(4):1566-75.

Sundaram J, Hsu CC, Shay YM, Sane SU. 2010. Design space development for lyophilization using DOE and process modeling. BioPharm International 23(9).

Tang XC, Nail SL, Pikal MJ. 2005. Freeze-drying process design by manometric temperature measurement: Design of a smart freeze-dryer. Pharm Res 22(4):685-700.

Tchessalov S, Kantor A, Li L, Luksha N, Warne N. 2010. Slow Dissolution Method For Reconstitution of Lyophilized Material.

Varma N, Ganguly A, Sane P, Bogner R, Pikal M, Alexeenko A. Variation of pressure in lyophilization product chamber part 1: Computational modeling. Manuscript Submitted to AAPS PharmSciTech .

Washburn EW. 1921. The dynamics of capillary flow. Physical Review 17(3):273.

Zhang S and Liu J. 2012. Distribution of vapor pressure in the vacuum freeze-drying equipment. Mathematical Problems in Engineering 2012.

Zografi G and Tam SS. 1976. Wettability of pharmaceutical solids: Estimates of solid surface polarity. J Pharm Sci 65(8):1145-9.

Chapter 2

Measurement of Heat Transfer to Vials on a Freeze-Dryer Shelf During Primary Drying

1 ABSTRACT

Determination of the vial heat transfer coefficient (K_v) is one of the prerequisites to successful designing of a freeze-drying cycle at a laboratory-scale and scale-up to manufacturing freeze-dryers. The focus of this work was to develop best practices in determination of vial heat transfer coefficients using pure ice sublimation experiments. Previously established gravimetric procedure and tunable diode laser absorption spectroscopy (TDLAS) were used to determine the batch average and individual vial K_v's. A maximum deviation of 12% was observed in the batch average K_v when determined using the gravimetric procedure versus TDLAS at a chamber pressure of 50 mTorr and several shelf temperatures. An efficient method for rapid determination of K_v at several chamber pressures and shelf temperatures using TDLAS demonstrated that K_v is a stronger function of the chamber pressure than the shelf temperature. Further, individual K_v was determined for each vial at a chamber pressure of 50 mTorr and several shelf temperatures (-35 to +20 °C) using the gravimetric procedure. A reversal of typical edge to center vial behavior was observed at +20 °C leading to 29% higher K_v for the center vial. No significant effect of using actual product versus pure ice or different fill volumes in case of pure ice on batch average K_v was observed at least at a chamber pressure of 60 mTorr and shelf temperature of -20 °C. The overall conclusion was that there is not one correct way of measuring K_v. Selection of the measurement technique will depend on the purpose of the K_v value.

2 INTRODUCTION

Freeze-drying or lyophilization is a preferred method of drying labile bio-therapeutics primarily because of the low processing temperatures that inhibit degradation, the ability to dry to very low moisture contents, and assurance of sterility by filling filtered solutions into sterile vials (Pikal 1995). The process consists of three key steps: freezing, primary drying and secondary drying. During primary drying, frozen water undergoes sublimation, leaving behind the solute and any unfrozen water associated with it, in its glassy, amorphous state. Primary drying is the longest and most energy intensive step in the process (Flink 1977; Liu, Zhao, Feng 2008). An objective of freeze-drying process development is to minimize the drying time by optimization of the heat and mass transfer during primary drying without compromising the quality of the product.

During sublimation of the frozen water, if the temperature of the remaining amorphous phase exceeds its glass transition temperature, the product can undergo collapse, which is unacceptable for a variety of reasons (Pikal 1995). Additionally, when the temperature exceeds the eutectic temperature for any crystalline solute and water, melt-back of the product occurs and is similarly unacceptable. In an optimized cycle, the temperature of the product is often maintained just below the collapse or eutectic temperature during primary drying. However, in cases for which the critical temperature and/or heat transfer are not well-characterized, the use of excessively conservative conditions to achieve a low product temperature leads to unnecessarily prolonged primary drying times.

The temperature of the product in the vial during primary drying is manipulated by controlling the chamber pressure and the shelf temperature. Ideally, the majority of heat required for sublimation is transferred from the temperature-controlled shelf to the product. Other

surfaces such as the walls of the chamber and the door are not temperature controlled, so their contribution of heat to the product is less well defined. Focusing, for the moment, on heat transferred from the shelf (*s*) to the product (*p*), the rate of heat transfer, dQ_{sp}/dt (cal·s^{-1}), is proportional to i) the horizontal cross sectional area of the vial, A_v(cm^2) and ii) the difference in temperature of the surface of the shelf, T_s (°C or K), and the product, T_p, through a coefficient often referred to as a vial heat transfer coefficient, $K_{v,sp}$ (cal·s^{-1}·cm^{-2}·K^{-1}) (Equation 1).

$$\frac{dQ_{sp}}{dt} = A_v K_{v,sp}(T_s - T_p) \qquad \text{Equation 1}$$

The temperature of the product is not uniform throughout the frozen layer. In Equation 1, the relevant product temperature is measured at the inside bottom center of the vial in contact with the product (Pikal, Roy, Shah 1984; Pikal 1985). Due to the slow rate at which the sublimation boundary recedes into the cake, heat flow into and vapor flow away from the product can be treated as quasi-steady state processes. At that steady state, heat from the shelf continues to flow by conduction through the frozen product from the bottom of the product to the sublimation interface, which can be expressed as Equation 2,

$$\frac{dQ_{sp}}{dt} = \frac{A_v K_I (T_p - T_0)}{l_I(t)} \qquad \text{Equation 2}$$

where K_I is the effective thermal conductivity of the frozen product given by 5.9×10^{-3} cal·s^{-1}·cm^{-1}·K^{-1}(Pikal, Roy, Shah 1984), T_o is the temperature of the sublimation interface, and l_I is the thickness of the ice in the frozen product that decreases with time, *t*, as sublimation proceeds.

During the quasi-steady state transfer of heat to the sublimation interface, the temperature of the frozen product at each axial position in the vial is constant[1] or relatively constant, and the rate of heat, dQ/dt (cal·s^{-1}), supplied to the product is equal to the heat removed due to sublimation (Equation 3),

$$\frac{dQ_{sp}}{dt} = \frac{dm}{dt} \cdot \Delta H_s \qquad \text{Equation 3}$$

where dm/dt (g·s^{-1}) is the sublimation rate, and ΔH_s is the heat of sublimation of water, (680 cal·g^{-1}).

Equation 3 couples the quasi-steady state heat transfer from the shelf to the product in the vial (Equation 1) or through the frozen product to the sublimation interface (Equation 2) to the sublimation rate of ice (or mass flow of water vapor) during primary drying. As sublimation proceeds, the sublimation front ideally moves down from the top of the frozen product leaving porous "dry"[2] product through which the vapor leaving the sublimation front must pass. The porous product provides resistance to the mass transfer of vapor that increases with time as the path length increases. The sublimation rate is driven by the difference in pressure at the sublimation interface, P_0 (Torr), and the drying chamber, P_c, and is impeded by the resistance of the porous dry layer above the sublimation interface that increases with time, $R_p(t)$ (cm^2·hr·Torr·g^{-1}) (Pikal, Roy, Shah 1984) as described in Equation 4,

$$\frac{dm}{dt} = \frac{A_p(P_0 - P_c)}{R_p(t)} \qquad \text{Equation 4}$$

[1] If the temperature is not constant, but rather is changing slowly, Equations 1 and 2 also hold for each value of T_p as it changes with time and Equation 1 and 2 provide an excellent approximation.
[2] The "dry" product layer mentioned here refers to the section of the vial contents, which is devoid of any ice but still contains the unfrozen water, which is removed further by secondary drying.

where A_p (cm^2) is the horizontal cross-sectional area of the frozen product, usually calculated from the inner diameter of the vial. The pressure at the sublimation interface is approximated by the vapor pressure of ice at the interface. The vapor pressure of ice is a well-characterized function of its temperature (Equation 5) (Jansco, Pupezin, Van Hook 1970)

$$P_0 = 2.698\times10^{10}\times e^{-6144.96/T_0} \qquad \text{Equation 5}$$

where P_0 is expressed in Torr and T_0, the temperature of ice at the sublimation interface is expressed in K. Combination and rearrangement of Equations 1-5, assuming all of the heat supplied for sublimation (Equation 3) comes from the shelf (Equation 1), yields an equation that can be solved for T_0 using numerical methods (Pikal, Roy, Shah 1984).

$$\frac{3600 \cdot \frac{A_v}{A_p} \cdot K_V \cdot R_p(t) \cdot (T_0 - T_s)}{\Delta H_s} + \left((2.698\times10^{10}\times e^{-6144.96/T_0}) - P_c\right)\left(1 + \frac{K_V \cdot l_I(t)}{K_I}\right) = 0 \qquad \text{Equation 6}$$

Once T_0 is found from Equation 6 for a given combination of P_c, T_s, R_p, K_v with A_v and A_p as constants, the corresponding sublimation rate *(dm/dt)* can be calculated from Equations 4 and 5. The temperature of the product at the bottom center of the frozen product, T_p, which is the highest product temperature during primary drying[3], can then be found from Equations 2 and 3. In practice, this set of equations is solved for each of several horizontal sections of the frozen product in series as sublimation proceeds. Summing the time to remove the ice from each horizontal section yields the total time required for primary drying. Determining the warmest

[3] The highest product temperature during primary drying is in the center at the bottom of the vial assuming all of the heat comes from the shelf through the bottom of the vial, heat conduction up the walls of the vial is negligible, and the sublimation front remains parallel to the shelf.

product temperature, T_p, based on the ice thickness corresponding to each horizontal section allows one to avoid exceeding any critical temperature that would result in either collapse or melt-back of the product. This model (Pikal 1985) has been used successfully to establish the optimal conditions to maximize sublimation rate (thereby minimizing primary drying times), while maintaining a product temperature below a critical temperature. Characterization of the heat flowing to the product is key to using the model successfully.

Accurate determination of the vial heat transfer coefficient, K_v, to characterize the heat flowing to the product allows better predictions using Equations 1-6[4]. Vial heat transfer coefficient can be expressed as the sum of three contributions:

$$\boldsymbol{K_v = K_c + K_r + K_g(P_c)} \qquad \text{Equation 7}$$

where K_c is the coefficient for direct conduction through the points of contact between the vials and shelf[5], K_r is the coefficient for radiative heat transfer and K_g is the coefficient for gas conduction between the shelf and bottom of the vial. (Pikal 1985) Both K_c and K_r are independent of chamber pressure. However, K_g, often the largest contributor to K_v, increases non-linearly with pressure (Nail 1980; Pikal 1985).

Typically, vials are classified as edge or center vials in the vial array on the shelf due to the difference in heat transfer based on their position. Radiative heat transfer generally contributes more to the vials at the edge of the array that have a more direct view of the door and the walls (Pikal, Roy, Shah 1984; Rambhatla and Pikal 2004; Rambhatla and Pikal 2003; Rowe, Greiff, Monrow 1979; Searles 2000). Pikal et al (Pikal, Roy, Shah 1984) reported 15% faster

[4] Accurate determination of the $R_p(t)$ is also a prerequisite for optimization of primary drying.
[5] Ideally, the vials are in a hexagonal array where each vial is in contact with 6 others. Assuming, for the moment, that the product in all vials has the temperature profile, there is insignificant heat flow through vial-to-vial contacts.

sublimation in an average edge vial when compared to an average center vial at 200 mTorr. Another study by Rambhatla et al (Rambhatla and Pikal 2003) concluded the existence of atypical radiation in the case of edge vials by comparing sublimation rates for clear vials characterized by an emissivity, $\varepsilon \approx 0.9$, with gold-coated vials, $\varepsilon \approx 0.4$, in the extreme front row of the array. The ratio of sublimation rates from clear and gold coated vials was 1.37 when the shelf temperature as -25 °C, but only 1.17 for a shelf temperature of 0 °C, both at a chamber pressure of 150 mTorr. The data demonstrated that the relative contribution from radiation is greater at lower shelf temperatures.

Other studies focused on reducing the heterogeneity in sublimation rates within a batch, which is essentially equivalent to addressing the differences in local heat transfer to the product in vials. Kobayashi et al (Kobayashi et al. 2011) proposed that the inter-vial variance in sublimation rate (which is due to variance in K_v) could be minimized and primary drying rates could be increased by controlling the temperature of the drying chamber wall. Further, Gan et al (Gan et al. 2005) found that a uniform sublimation rate with similar final residual moisture contents could be obtained across a batch of vials when trays without edges were used along with controlled chamber wall temperatures. Any vial-to-vial variation in K_v (or sublimation rates) leads to a variation in the product temperature and/or drying time during primary drying, potentially leading to non-uniform quality of the product from vial-to-vial.

This manuscript describes the use of different methodologies for determining the vial heat transfer coefficient, K_v. Different types of K_v measurements and calculations are required based on the ways in which the K_v values will be used. Factors such as i) the shelf temperature, ii) chamber pressure, iii) position of the vial on the shelf and iv) the nature of the pre-

lyophilization solution and v) its height in the vial are shown to affect the value of K_v. The sensitivity of K_v to each of these factors is compared.

3 MATERIALS AND METHODS

3.1 Experimental details for sublimation experiments

Sucrose, mannitol, and sodium chloride (analytical grade, Sigma Aldrich, St. Louis, MO) were used as received. House distilled water was further purified by reverse osmosis (Barnstead GenPure™, Thermo Scientific, Waltham MA). All solutions were filtered through a 0.22μm membrane filter prior to filling into 20 ml tubing glass vials (20 mm finish, Schott, Elmsford, NY). When filling only water, a 10 ml fill volume was used unless otherwise noted. All freeze-drying and sublimation cycles were carried out using a hexagonal, closest-packed arrangement of vials on the bottom-most shelf of a laboratory-scale freeze-dryer, LyoStar II (SP Scientific, Warminster, PA) in a three-shelf configuration (shelf-to-shelf distance of 7.1 cm). The protocol for a sublimation cycle, unless otherwise noted, was:

- Freezing: Cool to +5° C at 1° C/min, hold for 15 mins (for thermal equilibration); cool to -5° C at 1° C/min, hold for 15 min (for thermal equilibration); cool to -45° C at 1° C/min, hold for 8 hours (to reduce the contribution of any previous thermal history of band, walls and door).
- Primary drying/sublimation: Evacuate the chamber to the target chamber pressure, increase shelf temperature to set point at 5° C/min (or as fast as possible). Hold at the set point to allow 20-25% of ice to sublime in the center vials.

3.2 Simulated Data Set of Sublimation Rates

Average sublimation rate versus time data sets for 3 mL of either water or 5% of a mannitol-like solute were simulated using a web-based "LyoCalculator" (LyoTools, SP Scientific) developed using the quasi-steady state heat and mass transfer model described in the introduction above. The heat transfer coefficient was set to a higher value, 4.0 x 10^{-4} cal·cm^{-2}·sec^{-1}·K^{-1}, for 1/3 of the vials (edge vials) and to a lower value, 2.8 x 10^{-4} cal·cm^{-2}·sec^{-1}·K^{-1} for the remaining 2/3 of the vials (center vials). A fill volume of 3 ml (fill depth of 0.57 cm) in a 20 cc vial (outer area of vial = 6.93 cm^2, inner area = 5.72 cm^2), chamber pressure of 60 mTorr and shelf temperature of -20 °C were assumed. For the data set corresponding to pure water, the mass transfer resistance, R_p, was set to a constant value of 1.25 cm^2·hr·Torr·g^{-1}. For the data set corresponding to 5% mannitol-like solute, the resistance was set to $R_p = \left(1.4 + 16 \cdot l_{dry}\right)$ cm^2·hr·Torr·g^{-1},where l_{dry} is the thickness of the dried cake.

4 RESULTS AND DISCUSSION

4.1 Considerations in the Calculation of K_v

4.1.1 Fundamentals of K_v Calculation

The vial heat transfer coefficient, K_v (cal·s^{-1}·cm^{-2}·K^{-1}), can be calculated from the sublimation rate, $\frac{dm}{dt}$ (g·s^{-1}), and product temperature at the inside bottom center of the vial, T_p (°C), by combining Equation 1 and 3 to yield Equation 8,

$$K_v = \frac{\left(\frac{dm}{dt}\right) * \Delta H_s}{3600 * A_v * (T_s - T_p)} \qquad \text{Equation 8}$$

where the factor, 3600, is included to convert hours (typically used to express the sublimation rate) to seconds (the time unit used for K_v in much of the literature). ΔH_s (680 cal/g) and A_v

(which can be measured or found in vial specification information) are constants. Shelf temperature, T_s, can be measured using self-adhesive thermocouples on the shelf surface near the shelf fluid inlet and outlet. The values of T_p and dm/dt require careful experimental measurement.

Measurement of product temperature (T_p)

During primary drying, sublimation proceeds predominantly from top to bottom of the frozen cake, which neglects the usually small contribution of radial sublimation from outer-edge to the center of the vial. Due to the axial (i.e., top to bottom) and radial sublimation, the inside bottom-center of the vial is typically the position of the warmest product during primary drying from where the last traces of ice are removed resulting in a sharp increase in product temperature, T_p, at the end of sublimation. Thermocouples placed in the bottom-center provide the value of T_p as used in Equation 8. Misplacement of the thermocouple away from the center of the bottom of a vial may lead to erroneous measurement of product temperature.

Another indirect method for determining product temperature, T_p, is Manometric Temperature Measurement (MTM) (Milton et al. 1997). In this technique, the isolation valve in the duct connecting the drying chamber and condenser is closed abruptly for about 25 secs, and the pressure rise in the chamber is recorded with time. Several parameters in an equation are fitted to the pressure rise data to obtain the water vapor pressure at the sublimation interface from which the temperature of the ice at that location can be calculated (Equation 5). The temperature of product at the bottom of the vial can be obtained from Equations 2 and 3 (Milton et al. 1997). The temperature measured from MTM is a batch-average temperature. A point to note is that, the calculation of K_v becomes less precise as the product temperature (measured by any method)

approaches the shelf temperature, due to the increased error of subtracting close temperature values (Equation 8).

Often K_v is determined using water rather than product in the vials for several reasons. Product is usually expensive or obtained in limited quantities when a cycle is being developed. In addition, the temperature of water undergoing sublimation remains relatively constant due in part to the relative constancy of the resistance to vapor flow out of the vial. Thus, an average product temperature is easily identified. In contrast, for product that forms a high resistance cake, as sublimation proceeds, the product temperature can rise significantly; in this case, the time over which the product temperature is averaged can influence the value of K_v.

Measurement of sublimation rate (dm/dt)

The measurement of sublimation rate can be complicated by the nature of the freeze-drying process itself. For example, there is "flash off" or rapid sublimation of frost that may have formed on chamber surfaces. This occurs when the chamber pressure is reduced and the shelf temperature is increased to achieve the set point to initiate primary drying. Some methods of measuring sublimation rate will include the "flash off", when it should be ignored. Additionally, as the shelf temperature increases to reach the set point, there is a non-linear increase in sublimation rate until the quasi-steady state value is reached. Identifying the correct start time of sublimation can be challenging. However, waiting until the steady state sublimation rate is reached often allows substantial mass loss, leading to calculation of a higher value of sublimation rate and K_v. In our experience, there is a lag time of 20-30 minutes from the time the target vacuum level is attained (and a rapid increase in the shelf temperature is initiated) to the time to reach the quasi-steady state sublimation rate.

There are several approaches for determining the steady state sublimation rate, *dm*/*dt*, some of which are susceptible to the complications described above. A time-averaged sublimation rate can be determined for an individual, group or batch of vials by abruptly breaking vacuum when an estimated 20-25% of ice in the center vials has undergone sublimation. The individual, group or batch of vials is re-weighed to determine the loss of water gravimetrically over a well-defined time period ending when the vacuum is released (Pikal, Roy, Shah 1984). (The identification of the start time for sublimation is discussed in detail later in section 4.2.1.1.) This approach is often referred to as the gravimetric method of determination of *dm*/*dt*; its value is an average over the time allowed for sublimation. Alternatively, an instantaneous sublimation rate that reflects an average over the entire batch of vials in a freeze-dryer (the so-called, batch-average sublimation rate) can be determined using methods such as Tunable Diode Laser Absorption Spectroscopy (TDLAS), (Gieseler et al. 2007; Schneid et al. 2009) or heat flux sensors installed on the shelf (Ling 2015). Details of the procedures for determining the sublimation rate by gravimetry and TDLAS are discussed in Section 4.2. Manometric Temperature Measurement (MTM) has also been used to determine the sublimation rate periodically during a freeze-drying cycle (Milton et al. 1997). When both the vapor pressure of ice at the sublimation interface and the batch-average product resistance (R_p) can be obtained from MTM data, Equation 4 can be used to calculate an instantaneous batch-average sublimation rate.

4.1.2 Average K_v

There are three basic types of average K_v: time-averaged, batch-averaged and batch-and-time-averaged. The methods for measuring sublimation rate, *dm*/*dt*, and product temperature, $T_{p,}$

largely define the type of K_v that can be calculated. The most appropriate type of K_v depends on how it will be used. For instance, if the aim were to design a freeze-drying cycle for a new formulation, a new freeze-dryer or a new vial type or vial manufacturer, determination of a batch-averaged K_v value at the expected process conditions would be a good starting point. Furthermore, a batch-average K_v for the same set of vials can be determined at a range of shelf temperatures and chamber pressures to characterize sensitivity of K_v to any deviation in process conditions. When using a batch average K_v to optimize a freeze-drying cycle, the calculated time to complete primary drying will be less than that in the center vials and greater than that in the vials toward the edge of a hexagonal, closest-packed array. Often a "soak time" of about 20% of the calculated primary drying time is added to assure all vials have completed primary drying (Pikal 2002).

A time-averaged K_v can be calculated for an individual vial using the gravimetric method of determining the sublimation rate. In contrast, a batch-averaged instantaneous K_v can be determined as a function of time using TDLAS and MTM for measuring the sublimation rate. The heat flux sensor can be used to measure the heat input to a group of vials above the sensor and hence calculate the instantaneous K_v for that group of vials. However, there is currently no method to measure a useful K_v as a function of time for an individual vial in a lab- or manufacturing-scale drying chamber. Product temperature measurement also contributes to the calculation of K_v. The location of the vial(s) in which T_p is measured can influence the value of K_v. For example, when K_v is calculated from the batch-average sublimation rate and the product temperature measured only in center vials, the value of K_v will be lower than if an average temperature is determined proportionately from edge and center vials. This is due to the higher temperature of product in vials toward the edge of the array, at least for process conditions

typically employed in freeze-drying[6]. The simulated data sets of sublimation rates and product temperatures (as described in Section 3.2) are used to explore the difference in the three types of average K_v values in the next sections.

4.1.2.1 Time-averaged K_v for a single vial

Sublimation rates and product temperatures for ice or 5% of a mannitol-like solute undergoing sublimation were calculated using a K_v values of 2.8×10^{-4} and 4.0×10^{-4} cal·cm^{-2}·sec^{-1}·K^{-1} for the 2/3 of center vials and 1/3 of edge vials, respectively. A linear batch-average K_v of 3.2×10^{-4} cal·cm^{-2}·sec^{-1}·K^{-1}was calculated using the mentioned K_v's for the edge and center vials. The K_v value calculated for a vial in the center of the array determined from the start of sublimation to 75, 50, 25 and 0% ice remaining were all 2.81×10^{-4} cal·cm^{-2}·sec^{-1}·K^{-1} in case of pure ice, which is expected since at any instant during the sublimation period, the *dm*/*dt* and T_p are constant. However, ideally when determining K_v based on sublimation of pure ice, it is best to sublime no more than 20-25% ice in the center vials in order to avoid erroneous K_v determination due to the additional radial sublimation not accounted for in the calculation.

When using the parameters corresponding to 5% mannitol instead of pure ice during sublimation run, a decrease in *dm*/*dt* over the period of sublimation (due to formation of dry layer) led to an increase in T_p (due to decreased evaporative cooling). These two counteracting effects also produce no change in the calculated K_v during the course of sublimation with a value of 2.81×10^{-4} cal·cm^{-2}·sec^{-1}·K^{-1} observed at 75, 50, 25 and 0% ice remaining. It should also be noted that in the presence of product, particularly those that produce high resistance cakes, radial

[6] However, it was observed that the product temperature and K_v for the center vial was higher than that of an edge vial at a shelf temperature of +20 °C and a chamber pressure of 50 mTorr (Section 4.3.2)

sublimation is less significant due to the resistance of the porous layer that impedes radial vapor loss.

4.1.2.2 Batch-averaged instantaneous K_v (TDLAS)

TDLAS measures the rate of loss of water from the drying chamber in real-time. This instantaneous measurement can be divided by the number of vials to obtain a batch-averaged *dm/dt*. Using this batch-averaged instantaneous *dm/dt* and instantaneous T_p from thermocouple measurement, a value for K_v can be calculated at each minute. Note that the batch-averaged K_v calculated by this method is highly dependent on the location of the vials that are selected for temperature measurement.

Using simulated data sets, the batch-averaged instantaneous values of K_v were calculated using the T_p measured from I) only center vial(s), II) an average weighted by the proportion of edge and center vials, and III) a linear average (1:1) of edge and center vials (Table I). Values of batch-averaged K_v calculated using these three methods are reported at 75, 50, 25 and 0% ice remaining for both pure ice and 5% mannitol simulated data sets.

For pure ice, the K_v values calculated from the three cases of product temperature were within 5% of each other. The K_v values reported at the end of the cycle (0% ice remaining) were found to be 40% lower when measuring only center vial T_p, 12% lower when using a proportional T_p, and 14% higher when T_p is taken as the average of edge and center vials as compared to the values shown at 75 -25% ice remaining. The differences in the calculated K_v was due to the increase in the edge vial T_p (assumed to be equal to the shelf temperature (-20 °C) when sublimation was complete in those vials ($dm/dt = 0$ g·s^{-1}).

The K_v values calculated from the data set based on 5% of a mannitol-like solute and monitoring only the temperatures in the center vials are lower than those based on pure ice (but still within what is expected for experimental error in K_v measurement). Since the heat transfer coefficients were the same (2.8×10^{-4} and 4.0×10^{-4} $cal\cdot cm^{-2}\cdot sec^{-1}\cdot K^{-1}$, respectively for center and edge vials) as those used in the pure ice example above, the lower calculated K_v for the 5% solute case must be due to the reduced sublimation rate (owing to the formation of dry layer) when compared to pure ice. In all other respects, the K_v values for the solute and pure ice example follow the same trends.

4.1.2.3 Batch-averaged, time-averaged K_v

A value for K_v can be calculated from the total water loss over a well-defined time, yielding a time-averaged value for K_v. When the water loss is obtained for the entire batch, by for example, TDLAS, the K_v is both batch-averaged and time-averaged. The batch-averaged, time-averaged K_v values calculated from the total water loss and the time to remove all water from the simulated data sets are shown in Table I. When temperature is monitored proportionately in edge and center vials, the value for the batch-averaged, time-averaged K_v is remarkably close (3% lower) to the linear average of the K_v values used for the simulation. Instead if only the center vial temperature or equally weighted temperature from the edge and center vials is used, the resulting batch-averaged, time-averaged K_v is about 13% lower or 5% higher, respectively. An estimation of 13% lower K_v using the center vial product temperature can lead to underestimation of the amount of heat being transferred to the product during primary drying. Higher product temperature because of the higher K_v can lead to a structural collapse of the product especially in the edge vials if one is operating at the edge of failure.

4.2 Experimental Measurement of Several Average Vial Heat Transfer Coefficients

4.2.1 Time-averaged K_v for an Individual Vial

4.2.1.1 Characterizing Vial-to-vial Variation in K_v

Determination of the batch-average K_v provides an overall picture of heat transfer to the batch. However, it does not provide the vial-to-vial distribution in K_v within a batch of vials. Time-averaged individual vial K_v values can supplement the overall understanding of heat transfer by providing the vial-to-vial distribution that may be needed to truly optimize the primary drying cycle. The vial heat transfer coefficient, K_v that relates heat flow into product to the difference between T_p and T_s, in a given vial, can be evaluated by using a gravimetric procedure (Pikal, Roy, Shah 1984). In this work, the individual vial *dm/dt* was determined from the weight loss during a well-defined period of steady state sublimation. The position of each vial was tracked by row and column number.

4.2.1.1.1 Measuring *dm/dt*

Each vial was filled with deionized water to a predetermined fill height (i.e., the same fill as the proposed product) and completely stoppered with a stopper having a precision cut metal tube (2 cm in length, 0.46 cm i.d.) (Figure 1) inserted in the center of the stopper (Pikal, Roy, Shah 1984; Pikal 1985). As shown by Hibler et al (Hibler, Wagner, Gieseler 2012), nearly identical K_v values were observed when stainless steel tubes were used in fully stoppered vials instead of conventionally used semi-stoppered closures. The stainless steel tubes in the stoppers allowed calculation of the mass transfer from the vapor flow rate through the tube and removed any variation in resistance due to the position of partially stoppered closures. Freeze-drying/sublimation was carried out as described in Section 3.1. Hibler et al (Hibler, Wagner, Gieseler 2012) showed that for K_v calculations, the initial ramp time (non-steady state conditions)

minimally affected the results over the entire sublimation test at least at the process conditions (chamber pressure 50 to 400 mTorr and shelf temperature of -5 or -10 °C) they studied aiming for 30-50 % of total sublimation. However, they indicated that this bias could increase if one were to aim for less than 30% removal of total mass of water. Hence, the shelf temperature in our experiments was increased as fast as possible to the set point for primary drying only after achieving the target chamber pressure at the end of the final freezing step. Using this procedure, the initial ramp time spent in achieving the set point for primary drying conditions to get to a steady-state sublimation phase was kept to a minimum.

When approximately 20-25% of ice underwent sublimation, the cycle was abruptly stopped by breaking vacuum and increasing the shelf temperature to +10 °C so as not to allow further water loss due to evaporation. The initial mass of the stoppered vials (m_i) was recorded before initiation of the experiment and after sublimation (m_f) to determine the amount of water loss ($dm = m_i - m_f$). The sublimation period, dt, was the difference between the abrupt stop and the start time, identified as the time at which the driving force for sublimation ($P_0 - P_c$, Equation 4) became substantial (i.e., about 300 mTorr), where the vapor pressure of ice, P_0 is estimated by approximating T_0 as T_p (Equation 5). For each vial the sublimation rate was calculated as dm/dt in $g \cdot hr^{-1}$.

4.2.1.1.2 Evaluation of the individual vial heat transfer coefficient for vials fitted with standardized stoppers

The calculations in this section have been adapted from previous work (Pikal, Roy, Shah 1984). The vial heat transfer coefficient, K_v ($cal \cdot s^{-1} \cdot cm^{-2} \cdot K^{-1}$) for each thermocoupled vial can be calculated directly from its average T_p (°C), and its weight loss which is used to find the sublimation rate, dm/dt ($g \cdot s^{-1}$) (Equation 8).

The product temperature is not directly measured in each non-thermocoupled vial *i*. However, it is still possible to determine vial heat transfer coefficients for each non-thermocoupled vial, $K_{v,non\text{-}TC,i,}$, but less directly as described here. Though the sublimation rate, *dm/dt* is proportional to K_v and the temperature difference between the shelf and the product, (T_s - T_p), an increase in K_v can also lead to an increase in T_p, thereby reducing the value of (T_s-T_p), resulting in a net relative increase in the *dm/dt*, which is less than proportional to K_v. The value of K_v in a vial in which T_p is unknown can be determined from the relationship between the relative deviation in $K_{v,}$ RD_{K_v}, and the relative deviation in *dm/dt*, $RD_{\left(dm/dt\right)}$ (Equation 10).

$$\frac{RD_{K_v}}{RD_{\left(dm/dt\right)}} = \frac{\frac{dK_v}{\langle K_v \rangle_{TC}}}{\frac{d\left(dm/dt\right)}{\langle dm/dt \rangle_{TC}}} = \frac{d \ln K_v}{d \ln\left(dm/dt\right)} \qquad \text{Equation 10}$$

where, dK_v and $d\left(dm/dt\right)$ are deviations from the average values determined in thermocouple vials, $\langle K_v \rangle_{TC}$ and $\langle dm/dt \rangle_{TC}$, respectively. The value of Equation 10 for 20 cc vials containing a 3 ml fill of deionized water and fitted with stoppers containing tubes described above is shown in Equation 11 for pure ice.

$$\frac{d \ln K_v}{d \ln\left(dm/dt\right)} = 1 + (855 \cdot K_v) \qquad \text{Equation 11}$$

The factor 855 is a function of the resistance (stopper and tube) to vapor flow, fill depth, average sublimation rate and the area of the vial and product (Pikal, Roy, Shah 1984). The general form of Equation 11 is shown in Appendix I (at the end of this paper). Calculations for pure ice and an example of product (5% w/v sodium chloride) are also given in Appendix I. The deviation in

each non-thermocoupled vial, $\left(dm/dt\right)_{non-TC,i}$, from the average sublimation rate for the thermocoupled (monitored) vials, $\langle dm/dt\rangle_{TC}$, can be approximated as a differential,

$$d\left(dm/dt\right)_i \approx \left(dm/dt\right)_{non-TC,i} - \langle dm/dt\rangle_{TC} \qquad \text{Equation 12}$$

Similarly, the corresponding deviation from average K_v, $\langle K_v\rangle_{TC}$, determined in thermocouple vials can be written as

$$dK_{v,i} \approx K_{v_{non-TC,i}} - \langle K_v\rangle_{TC} \qquad \text{Equation 13}$$

where $K_{v_{non-TC,i}}$ is the K_v of any particular non-thermocoupled vial. The small difference in K_v, $dK_{v,i}$, in each non-thermocoupled vial from the average, $\langle K_v\rangle_{TC}$, can be evaluated from the value of the derivative, $\frac{d\ ln\ K_v}{d\ ln\left(\frac{dm}{dt}\right)}$ (Equation 11). On rearranging Equations 11 through 13, the value of K_v for each non-thermocoupled vial i, $K_{v_{non-TC,i}}$, in the case of pure ice (fill depth of 0.57 cm) is given by Equation 14.

$$K_{v_{non-TC,i}} = \langle K_v\rangle_{TC} \cdot \left\{1 + \left(\frac{\left(dm/dt\right)_{non-TC,i}}{\langle dm/dt\rangle_{TC}} - 1\right) \cdot (1 + (855 * \langle K_v\rangle_{TC}))\right\} \qquad \text{Equation 14}$$

4.2.1.2 Vial Heat Transfer by Category of Vials Based on Position

Conventionally, for the purposes of describing heterogeneous heat transfer patterns in freeze-dryers, vials have been classified as edge and center depending on their positions (Figure 2a). However, using 20 cc vials in a LyoStar II, the vials on the shelf were re-categorized as: front row (9 vials), back row (9 vials), outer edge vials in contact with the stainless steel band (16 vials, excluding those in the back and the front rows) and inner edge vials (18 vials) not in contact with the band (Figure 2b). For this set of experiments, 3 ml deionized water was used in 20 ml vials fitted with the standardized stoppers and weighed before the experiment. Sublimation

was carried out as per the protocol in Section 3.1 at a chamber pressure of 60 mTorr and shelf temperature of -20 °C for 5 hours. Product thermocouples were placed in representative 4 center, 1 front row, 1 back row, 2 right outer edge and 2 right inner edge vials (Figure 2b).

Based on the category of a non-thermocoupled vial, K_v for that vial was calculated from Equation 14 using $dm/dt_{TC,avg}$ (determined by gravimetric procedure) and $K_{v,TC\,avg}$ specific for that particular category of vial. Average K_v for each category was then calculated once the individual vial K_v's for each vial from each category were known. Average K_v across each category using this method of calculation was compared to average K_v calculated using the $dm/dt_{TC,avg}$ and $K_{v,TC\,avg}$ corresponding to the center vials only irrespective of which category the non-thermocoupled vial belonged to (Pikal, Roy, Shah 1984).

A plot of K_v values for the five categories of vials calculated using product temperature from only center vials as well as that from the individual category vials is shown in Figure 3. K_v values calculated for the non-center vials by using only center vial temperature under-predicted the K_v by 10%. The lower T_p in the center vials (-39 °C) as compared to the non-center vials (-37 °C) (Figure 2b) contributed to the difference in K_v calculations. Moreover, when 5 categories of vial locations are employed, the standard deviations in the K_v values for each category are reduced.

4.2.2 Batch-averaged, time-averaged K_v measurements

Batch-averaged K_v can be determined by averaging the individual vial K_v over a batch of vials as obtained by the gravimetric procedure and by using TDLAS (Gieseler et al. 2007; Schneid et al. 2009). TDLAS, installed in the duct connecting the drying chamber and condenser

chamber[7], measures the mass flow rate of water from the drying chamber. TDLAS utilizes two beams of laser light, directed diagonally across the duct – one beam toward the flow and the other against the flow of vapor through the duct. Water vapor absorbs the light, producing a signal that corresponds to the concentration, or number density, N (molecules·cm^{-3}), of water vapor. The Doppler shift of the upstream- and downstream-directed beams provides the linear flow velocity, u (cm·s^{-1}) of the vapor. The sublimation rate (dm/dt) is the product of the number density of the water vapor, the cross-sectional area of the duct through which it flows, A (cm^2), and the vapor flow velocity, u (cm·s^{-1}) according to the Equation 15 (Gieseler et al. 2007; Schneid et al. 2009).

$$\frac{dm}{dt} = N \cdot A \cdot u \qquad \text{Equation 15}$$

Substituting Equation 15 into Equation 8, this approach makes it possible to calculate K_v values over a batch of vials.

In this section, batch-averaged, time-averaged K_v was compared by gravimetry and TDLAS. For this set of experiments, 10 ml deionized water was filled in vials, fitted with the standardized stoppers. Sublimation experiments to determine K_v were performed as per the protocol in Section 3.1 at different shelf temperatures ranging from -20 to +20 °C and chamber pressure of 50 mTorr using gravimetric method. Sublimation was carried out for variable times in order to remove 20-25% of initial amount of ice from the vials during different experiments employing different shelf temperatures. Product temperatures from six center vials were monitored. K_v for each individual vial was calculated using Equation 8 for thermocoupled vials and Equation 16 for non-thermocoupled vials based on the $\langle K_v \rangle_{TC}$ and $\langle {}^{dm}/_{dt} \rangle_{TC}$ from the center

[7] Freeze-dryers with the condenser in the same area as the shelves, or separated only by a plate, rather than a duct, cannot utilize TDLAS for measuring the sublimation rate of water.

thermocoupled vials. Note that the factor 1080 is different than the one used in Equation 14 due to a higher fill depth (1.9 cm) corresponding to 10 ml fill of deionized water.

$$K_{v_{non-TC,i}} = \langle K_v \rangle_{TC} \left\{ 1 + \left(\frac{\left(dm/dt \right)_{non-TC,i}}{\langle dm/dt \rangle_{TC}} - 1 \right) * (1 + (1080 * \langle K_v \rangle_{TC})) \right\} \quad \text{Equation 16}$$

TDLAS was also used to determine the batch-averaged, time-averaged *dm/dt* simultaneously during the gravimetric experiments. At the end of freezing (-45 °C), once the chamber was evacuated to 50 mTorr, a velocity "offset" was determined by closing the isolation valve between the drying chamber and condenser to ensure a zero flow condition. Even with a zero flow condition, a small non-zero average velocity was detected and subsequently subtracted from all the further readings during the sublimation period. Once the offset was determined, the sublimation experiment was continued by increasing the shelf temperature to the set point for primary drying as fast as possible. The batch-averaged instantaneous *dm/dt* obtained from TDLAS over all the 160 vials was then time-averaged and the average product temperature from six center vials was used in Equation 8 to determine the batch-averaged, time-averaged K_v.

The batch-averaged, time-averaged K_v as determined by using gravimetric procedure and TDLAS at a chamber pressure of 50 mTorr is plotted as a function of shelf temperature in Figure 4. Since the determination of K_v by both the methods (TDLAS and gravimetry) was conducted during the same experiment, a two-sample paired t-test was used to compare the average K_v at each shelf temperature. There was no significant difference observed in the batch-averaged, time-averaged K_v at an α level of 0.05 (n=2). Change in the shelf temperature did not seem to affect the batch-averaged, time-averaged K_v at least from -20 to +5 °C. A 20-25% increase in the

batch-averaged, time-averaged K_v was observed as the shelf temperature was increased to +20 °C. In detail discussion about this increase in K_v is given in Section 4.3.1.

4.2.3 K_v as a function of time

Using the sublimation rate (from TDLAS) and the difference between the shelf and product temperature (T_s - T_p) at every minute it is possible to calculate the batch-averaged K_v per minute using Equation 8. Data obtained from the experimental set up as described in Section 4.2.2. were analyzed to compute the instantaneous batch-averaged K_v. A plot of K_v as a function of time excluding the first half hour to reach steady state for sublimation (Figure 5) was plotted at different shelf temperatures of -20, -5, +5 and +20 °C. Since the sublimation time was restricted to allow only 20-25% of initial ice to sublime there is a difference in the sublimation times for the shelf temperatures investigated. There is only a nominal change in K_v using water at a chamber pressure of 50 mTorr and shelf temperature of -20, -5 and +5 °C. However, at +20 °C shelf temperature a 10% increase in K_v was observed within 2 hours. The significant increase in K_v can be attributed to the increased sublimation both axially and radially in the absence of a dry product layer in case of pure ice.

4.3 Factors that affect Vial Heat Transfer Coefficient, K_v

4.3.1 Chamber Pressure

According to Equation 7, K_v has three contributions, one of them being K_g which is the coefficient for gas conduction between the shelf and bottom of the vial (Pikal 1985). The gas conduction term, K_g can be written as (Pikal 1985)

$$K_g = \frac{\propto \Lambda_0 P}{1 + l\left(\frac{\propto \Lambda_0}{\lambda_0}\right) P} \qquad \text{Equation 17}$$

where Λ_0 is the free molecular conductivity of the gas at 0 °C, P is the gas pressure, λ_0 is the heat conductivity of the gas at ambient pressure, and α is a function of the energy accommodation coefficient, a_c and the absolute temperature of the gas, T as given by Equation 18 (Pikal 1985)

$$\alpha = \frac{a_c}{2 - a_c}\sqrt{\frac{273.2}{T}} \qquad \text{Equation 18}$$

The non-linear relationship between chamber pressure and K_v has been extensively discussed in the existing published literature (Hibler, Wagner, Gieseler 2012; Pikal 1985). In this section, a previously established method (Kuu, Nail, Sacha 2009) was adapted to efficiently determine batch-averaged, time-averaged K_v at several conditions of shelf temperature and chamber pressure using TDLAS. The freezing protocol was the same as described in Section 3.1. Vials were filled with 10 ml of de-ionized water and partially capped with two-legged stoppers. Two sets of experiments were performed at several shelf temperatures ranging from -20 to +20 °C:

a) Ascending experiments: Chamber pressure was increased from 50 to 200 mTorr (in increments of 25 mTorr) at each shelf temperature.

b) Descending experiments: Chamber pressure was decreased from 200 to 50 mTorr (in decrements of 25 mTorr) at each shelf temperature.

Product temperature in 5 center vials and 2 edge vials was recorded. At the end of the final freezing step, the chamber was evacuated to the initial pressure set point (for e.g.; 50 mTorr in case of ascending experiments) and a zero velocity offset was determined for TDLAS. At each

chamber pressure, sublimation data was obtained for at least 20 minutes once the steady-state is reached (constant sublimation rate as noted from TDLAS).

Batch-averaged, time-averaged K_v calculated as a function of shelf temperature at different chamber pressures is shown in Figure 6. K_v is a strong function of the chamber pressure. The non-linear dependence between the K_v and the chamber pressure is shown by the decreasing difference between the K_v values at each subsequent chamber pressure at a constant shelf temperature. The total water loss at the end of the sublimation experiment (ascending and descending) was about 35% of the initial at shelf temperatures from -20 to +5 °C. However, at a shelf temperature of +20 °C greater than 35% of initial amount of ice had already sublimed before the chamber pressure was increased to 175 mTorr for ascending experiments or decreased to 75 mTorr during descending experiments. The higher amount of water loss from the vials led to the formation of a non-uniform ice surface. As a result, K_v measurements determined at shelf temperature of +20 °C with 175 mTorr (ascending experiment) or 75 mTorr (descending experiment) as the chamber pressure are susceptible to errors. A two-sample t-test assuming unequal variances was conducted to compare the average K_v values at each condition of chamber pressure and shelf temperature using the ascending and the descending methods. There was no significant difference in the average K_v values observed at an α level of 0.05 (n=3).

4.3.2 Shelf Temperature

Existing literature on vial heat transfer coefficient does not exclusively describe the dependence of the K_v value on the shelf temperature. In this section, gravimetric experiments were performed using a 10 ml fill volume of deionized water in 20 ml vials fitted with the standardized stoppers. Sublimation experiments were performed at chamber pressure of 50 mTorr and several shelf temperatures (-35, -20, -5, +5 and +20 °C). Sublimation was carried out

for variable times depending on the shelf temperature set point during the experiment in order to remove 20-25% of initial amount of ice from the vials. Product thermocouples were placed in six center vials (and two edge vials in some experiments). Several surface temperatures such as that of the stainless steel band and inner wall were also recorded using the self-adhesive thermocouples. K_v for each individual vial was calculated using Equation 8 for thermocoupled vials and Equation 16 for non-thermocoupled vials based on the $\langle K_v \rangle_{TC}$ and $\langle {dm}/{dt} \rangle_{TC}$ from the center thermocoupled vials.

A comparison of time-averaged K_v values separated for edge and center vials along with a linear batch-averaged, time-averaged K_v at chamber pressure of 50 mTorr and several shelf temperatures have been plotted in Figure 7. The batch-averaged, time-averaged K_v is a weak function of the shelf temperature. As expected, the edge vials have the highest time-averaged K_v followed by the batch average and the center vials, at least at shelf temperatures from -35 to +5 °C. The difference in K_v values between the edge and the center vials decreases from 34% to 13% with the increase in the shelf temperature. While the center average K_v is not significantly affected by the shelf temperature, the edge vial K_v decreases by 33% from 5.32 to 3.58×10^{-4} cal·cm^{-2}·sec^{-1}·K^{-1} as the shelf temperature is increased from -35 to +5 °C. The so-called "edge vial effect" (Rambhatla and Pikal 2003) was found to be maximum at the lowest shelf temperature of -35 °C due to the additional heat transfer to the edge vials from the warmer surfaces in the chamber such as the stainless steel band (-27 °C), shelf support and the door. At a shelf temperature of +20 °C, a reversal of edge to center vial behavior was observed where the average K_v for the center vials (3.98×10^{-4} cal·cm^{-2}·sec^{-1}·K^{-1}) was 13% higher than that of the edge vials (4.49×10^{-4} cal·cm^{-2}·sec^{-1}·K^{-1}). This difference in the edge and the center vial K_v was not evident when a batch-averaged K_v is determined using TDLAS.

In order to better understand the variation of K_v values over a shelf of vials, a plot depicting the individual vial time-averaged K_v across the entire shelf of vials at extremes of shelf temperature studied (-35 and +20 °C) is shown in Figure 8. The x-axis denotes the position of the vial in a particular row. Typically, alternating rows of 8 and 9 vials (20cc capacity) can be arranged in a closest packing of hexagonal array in a full load on one shelf of Lyostar II. However, for the purpose of constructing the surface plot for K_v data, values for at least 1 vial per row was deleted carefully, not affecting any patterns in the K_v values across a batch of vials at -35 °C (Figure 8a.) leading to a total of 19 rows of vials arranged from front to back with 7 vials in each row. In case of +20 °C shelf temperature, 19 rows of vials arranged from front to back with 8 or 9 vials in each row have been shown at (Figure 8b.). At -35 °C there is a gradual decrease in K_v from the outermost edge vials (side edges as well as the front and back rows) towards the extreme center which can be designated as the "valley" pattern. A secondary effect of radiation from the warmer surfaces (side walls and the band) was observed on the vials immediately adjacent to the edge vials. However, at +20 °C there is a distinct "mountain" pattern observed in the K_v values across the shelf. The outer and inner edge vials exhibit a K_v of 2.0 -3.0 $\times 10^{-4}$ cal·cm^{-2}·sec^{-1}·K^{-1}. However, a drop in K_v below 2.0 $\times 10^{-4}$ cal·cm^{-2}·sec^{-1}·K^{-1} is observed for the 2nd and 3rd vial from the edge in each row on both the sides and then a dramatic increase to 12.0 $\times 10^{-4}$ cal·cm^{-2}·sec^{-1}·K^{-1} is noted for the extreme center vials.

At any particular condition of shelf temperature and chamber pressure, the center and the edge vial can be assumed to get the similar amount of heat due to gas conduction and contact conduction. The difference in the K_v pattern at shelf temperature of -35 °C and +20 °C can be explained based on the differences in the radiative heat transfer to the vials (Figure 9). At -35 °C, the source of radiation for the center vials is only the shelf (-35 °C) however an edge vial gets

additional heat from other warmer surfaces such as the band (-29 °C) and the inner wall (-25 °C). This leads to a 3 °C difference between the edge (-39 °C) and the center vial (-42 °C). At +20 °C, the center vial has a view of only the upper shelf (+20 °C) whereas the edge vial has a view of the relatively colder surfaces such as the band (-10 °C) and the inner wall (+4 °C). The radiative heat transfer to the edge vial is hence less than that compared to the center vial leading to a -25 °C product temperature in the center vial and a -29 °C product temperature in the edge vial.

4.3.3 Fill volume

To investigate the effect of fill volume on the vial heat transfer coefficient, K_v values were obtained from two fill volumes (3 and 10 ml) of deionized water. K_v was determined by gravimetric method in 20 ml vials with standardized stoppers at a chamber pressure of 60 mTorr and shelf temperature of -20 °C with a sublimation time of 5 hours. Product thermocouples were placed in the five categories of vials as explained in Section 4.2.1.2. Time-averaged K_v for individual thermocoupled vials was calculated using Equation 8. Based on the category a non-thermocoupled vial, K_v for that vial was calculated from Equation 14 and 16 for 3 ml and 10 ml fill respectively, using $\langle K_v \rangle_{TC}$ and $\langle {}^{dm}/_{dt} \rangle_{TC}$ specific for that particular category of vial. The individual vial time-averaged K_v were averaged for every category of vials.

Table II shows the time-averaged K_v values for the 5 categories of vials and batch-averaged, time-averaged K_v using a fill volume of 3 and 10 ml. No significant effect of fill volume on the batch-averaged, time-averaged K_v value at least at the process conditions studied in this experiment was noted. A maximum of 13% increase in K_v for the vials in the front row was observed as the fill volume was increased from 3 to 10 ml. A surface plot for the time-averaged K_v values is shown in Figure 10. A higher variation in K_v was observed across the batch of vials at a fill volume of 10 ml versus at 3 ml. An edge vial containing 10 ml has a higher fill

depth of ice (1.89 cm) than that of 3 ml (0.57 cm). The increased variation in K_v in case of higher fill depth is probably due to an uneven radiation heat transfer from the warmer surfaces to the ice in the vial leading to more radial sublimation.

4.3.4 Product versus water

For determining the effect of using product versus water on the vial heat transfer coefficient, aqueous solutions of several excipients such as sucrose, mannitol and sodium chloride at 5% w/w were prepared. Vials were filled with 3 ml of deionized water or excipient solutions and capped with the standardized stoppers. The freezing protocol used was same as earlier. In case of mannitol, an annealing step (at -25 °C for 5 hours) was added to crystallize mannitol before decreasing the shelf temperature to the final set point of -45 °C. Sublimation/primary drying was performed at a chamber pressure of 60 mTorr and a shelf temperature of -20 °C for 5 hours. Product temperature was recorded for the five vial categories according to Section 4.2.1.2. Time-averaged K_v for individual thermocoupled vials was calculated using Equation 8. Based on the category of a non-thermocoupled vial, K_v for that vial was calculated from Equation 14 for water using $\langle K_v \rangle_{TC}$ and $\langle {dm}/{dt} \rangle_{TC}$ for that category of vial. For sucrose, mannitol and sodium chloride Equations 19, 20 and 21 were derived similar to the derivation in Appendix I. $\langle K_v \rangle_{TC}$ and $\langle {dm}/{dt} \rangle_{TC}$ used in each of these equations were specific for that particular category of vial.

$$\boldsymbol{K_{v_{non-TC,i}} = \langle K_v \rangle_{TC} \left\{ 1 + \left(\frac{\left({dm}/{dt} \right)_{non-TC,i}}{\langle {dm}/{dt} \rangle_{TC}} - 1 \right) * (1 + (2624 * \langle K_v \rangle_{TC})) \right\}} \qquad \text{Equation 19}$$

$$K_{v_{non-TC,i}} = \langle K_v \rangle_{TC} \left\{ 1 + \left(\frac{\left(dm/dt \right)_{non-TC,i}}{\langle dm/dt \rangle_{TC}} - 1 \right) * (1 + (4130 * \langle K_v \rangle_{TC})) \right\} \quad \text{Equation 20}$$

$$K_{v_{non-TC,i}} = \langle K_v \rangle_{TC} \left\{ 1 + \left(\frac{\left(dm/dt \right)_{non-TC,i}}{\langle dm/dt \rangle_{TC}} - 1 \right) * (1 + (1992 * \langle K_v \rangle_{TC})) \right\} \quad \text{Equation 21}$$

Table III shows the time-averaged K_v values for the 5 categories of vials and batch-averaged, time-averaged K_v using water and different solutes. No significant effect of using solute versus water on the K_v values was noted.

Figure 11 shows the time-averaged K_v map across a shelf of vials for water and sucrose constructed as explained previously. On comparing the K_v map for water versus sucrose, the "valley effect" as discussed earlier where the K_v decreases with position from edge to center can be observed in both cases. However, the variation in K_v across the batch is higher for sucrose when compared to water. The higher variation in K_v across the batch in case of sucrose can be explained due to a higher variation in sublimation rates resulting from differences in dry layer thickness that poses a resistance for vapor flow.

4.3.5 Additional factors affecting K_v measurements

a) Vials loaded with or without trays

Traditionally, vials were loaded on to the freeze-dryer shelves along with the trays which added an extra barrier to heat conduction between the bottom of the vial and the shelf thus, lowering the K_v. Current practice in freeze-drying involves direct placement of the vials on the shelves. In some of the laboratory freeze-dryers the vials are loaded with a tray such that the bottom of the tray can be pulled out once the vials are on the shelf leaving behind a stainless steel band (or a railguard) around the vial array that prevents the vials from falling off the shelf.

The presence or absence of steel bands will alter the edge vial effect depending on the process conditions.

b) Vial size/type and stoppers

The height of the vial with respect to the band (which confines the vials on a shelf used in case of some freeze-dryers such as the LyoStar II) affects the heat transfer by radiation to the product and hence the sublimation rate depending on the temperature of the band with respect to the product and the shelf. Moreover, the exact same type of vial from two different manufacturers can vary in its bottom contour, thus, causing a variation in the contribution of contact and gas conduction in the heat transfer to a vial. It is hence, advisable to determine the heat transfer coefficient for the exact final container the product is intended to be freeze-dried in.

Use of either partially placed stoppers or specialized stoppers fitted with precision cut stainless steel tubes or no stoppers affects the resistance to the vapor flow and hence the K_v. Partially placed stoppers can introduce variation in the mass transfer resistance over a batch of vials due to the variation in the placement of stoppers at different heights. In order to circumvent this problem, Pikal et al used stoppers fitted with precision cut stainless steel tubes (Pikal, Roy, Shah 1984). Complete stoppering of vials with these specialized stoppers assured that the closure resistance was fixed by the geometry of the tube and the chamber pressure, and was not subjected to any variations arising from improper placement of stoppers. The thermocouple vials should be fitted with the same stoppers as the non-thermocoupled vials to avoid any bias in sublimation rate and hence K_v.

c) Shelf configuration

The distance between the shelves of the freeze-dryer affects the view factor between the vials on the shelf and the warmer surfaces such as the chamber walls and the door thus affecting the radiation heat transfer. Figure 12 shows the three-shelf configuration versus a one-shelf configuration for a laboratory-scale freeze-dryer, LyoStar II. Since all the vials (center as well as the edge) in the one-shelf configuration have a direct view of the warmer surfaces, the batch average K_v is higher but the variation in K_v across the batch is lower than in the three-shelf configuration.

d) Shelf load

The ratio of center to edge vials changes depending on the use of a full-shelf or partial-shelf load. This affects the batch average K_v based on the magnitude of K_v, the number of center to edge vials and the processing conditions.

e) Type of freeze-dryer

Radiation from the warmer surfaces in the chamber to the vials depends on their surface temperatures, view factors and emissivities of the various surfaces in the freeze-dryer chamber. Radiation from a Plexiglas® door (emissivity of 0.94) is higher than that of a polished stainless steel door (emissivity of 0.28) (Costantino and Pikal 2004). Moreover, structural variation in the built of the side walls (Figure 13) in the chamber between different dryers as well as the placement of the heating and the cooling elements in the drying chamber affects the temperature of the different surfaces and hence the radiation heat transfer to the vials.

f) Presence or absence of band/railguard

Presence of a stainless steel band/railguard in order to confine the vials on the shelf can alter the radiation heat transfer to the edge vials. The view factor between the edge vials and the band is also dependent on the position of the vial. Moreover, when arranged in a hexagonal array, some of the outermost edge vials touch the band thus, altering the contribution of contact conduction.

g) Freeze-drying cycle parameters

Though the shelf temperature of a freeze-dryer can be controlled within a degree, most of the other surface temperatures in the chamber cannot be controlled. On monitoring the temperatures of the walls, the door and the band, an increase of about 10 - 15 °C over a period of 5 hours was observed at a shelf temperature of -20 °C and chamber pressure of 60 mTorr when using pure ice for sublimation experiments. This increase in the surface temperature affects the overall radiation contribution to the vials on a shelf. It is hence advisable to use the exact same final cycle (same cooling rate, same intermediate steps before the final freeze and same equilibration hold times at different temperatures) as the product. If the final product requires an annealing hold at a particular shelf temperature, the same temperature and time hold should also be included when determining the K_v since that will affect the surface temperatures in the chamber.

5 CONCLUSIONS

The vial heat transfer coefficient, K_v, is a very important parameter, which determines the amount of heat transferred to a product at a particular combination of shelf temperature and chamber pressure. Knowledge of heat transfer through a vial to the product is important in case

of designing a freeze-drying cycle for a new product, optimizing an already existing cycle or for scale-up from laboratory-scale to manufacturing-scale.

The value of K_v depends on the source of sublimation rate and product temperature. The type of K_v, whether batch-averaged instantaneous, time-averaged for a single vial or batch-averaged time-averaged, to be determined is governed by the final use of the K_v value. While in case of designing a freeze-drying cycle for a new product a batch-averaged K_v is sufficient, it could be necessary to understand the variation in K_v across a batch when optimizing a cycle. This study discusses two methods of determining the K_v values using TDLAS and gravimetric approach. While TDLAS provides a rapid method of determining the batch-averaged K_v value, the gravimetric approach gives a better understanding of the variation in K_v across a batch at a given combination of process conditions. No significant differences in batch-averaged K_v determined using either of the two methods was observed at several process conditions. The batch-averaged K_v is a strong function of chamber pressure and is only slightly affected by the shelf temperature. However, the difference between the K_v values based on vial positions – edge versus center can be greatly affected by the shelf temperature. No significant effect of fill depth or using a solute versus pure ice was noted on the batch-averaged K_v values at the process conditions studied. The authors propose the use of the exact final cycle using the same input parameters such as fill volume, vial size, stopper type and so on for the determination of K_v as will be used for the final product.

Accurate determination of K_v is important for developing and optimizing a freeze-drying cycle with an ultimate aim of achieving a quality product consistently.

6 ACKNOWLEDGEMENTS

This work was funded by Baxter BioPharma Solutions, Bloomington, IN.

7 REFERENCES

Costantino HR and Pikal MJ. 2004. Lyophilization of biopharmaceuticals. Springer Science & Business Media.

Flink J. 1977. Energy analysis in [food] dehydration processes. Food Technol 31.

Gan KH, Bruttini R, Crosser OK, Liapis AI. 2005. Freeze-drying of pharmaceuticals in vials on trays: Effects of drying chamber wall temperature and tray side on lyophilization performance. Int J Heat Mass Transfer 48(9):1675-87.

Gieseler H, Kessler WJ, Finson M, Davis SJ, Mulhall PA, Bons V, Debo DJ, Pikal MJ. 2007. Evaluation of tunable diode laser absorption spectroscopy for in-process water vapor mass flux measurements during freeze drying. J Pharm Sci 96(7):1776-93.

Hibler S, Wagner C, Gieseler H. 2012. Vial freeze-drying, part 1: New insights into heat transfer characteristics of tubing and molded vials. J Pharm Sci 101(3):1189-201.

Jansco G, Pupezin J, Van Hook WA. 1970. The vapor pressure of ice between 10− 2 and− 10 2◦ C. J Phys Chem 74:2984-9.

Kobayashi M, Harashima K, Ariyama H, Yao A. 2011. Inter-vial variance of the sublimation rate in shelf freeze-dryer. Transactions of the Japan Society of Refrigerating and Air Conditioning Engineers 10:135-44.

Kuu WY, Nail SL, Sacha G. 2009. Rapid determination of vial heat transfer parameters using tunable diode laser absorption spectroscopy (TDLAS) in response to step-changes in pressure set-point during freeze-drying. J Pharm Sci 98(3):1136-54.

Ling W. 2015. Using Surface Heat Flux Measurement to Monitor and Control a Freeze Drying Process .

Liu Y, Zhao Y, Feng X. 2008. Exergy analysis for a freeze-drying process. Appl Therm Eng 28(7):675-90.

Milton N, Pikal MJ, Roy ML, Nail SL. 1997. Evaluation of manometric temperature measurement as a method of monitoring product temperature during lyophilization. PDA Journal of Pharmaceutical Science and Technology 51(1):7-16.

Nail SL. 1980. The effect of chamber pressure on heat transfer in the freeze drying of parenteral solutions. J Parenter Drug Assoc 34(5):358-68.

Pikal MJ. 2002. Freeze drying. Encyclopedia of Pharmaceutical Technology, Marcel Dekker, New York 1299:1326.

Pikal MJ. 1995. Freeze-Drying of proteins. process, formulation, and stability. ChemInform 26(4).

Pikal MJ. 1985. Use of laboratory data in freeze drying process design: Heat and mass transfer coefficients and the computer simulation of freeze drying. J Parenter Sci Technol 39(3):115-39.

Pikal MJ, Roy ML, Shah S. 1984. Mass and heat transfer in vial freeze-drying of pharmaceuticals: Role of the vial. J Pharm Sci 73(9):1224-37.

Rambhatla S and Pikal MJ. 2004. Heat and mass transfer issues in freeze-drying process development. Lyophilization of Biopharmaceuticals :75-109.

Rambhatla S and Pikal MJ. 2003. Heat and mass transfer scale-up issues during freeze-drying, I: Atypical radiation and the edge vial effect. AAPS PharmSciTech 4(2):111-20.

Rowe T., Greiff D. and Monrow J. 1979. Rate distribution in shelf freeze drying: Preliminary studies. 15th international congress of refrigeration.

Schneid SC, Gieseler H, Kessler WJ, Pikal MJ. 2009. Non-invasive product temperature determination during primary drying using tunable diode laser absorption spectroscopy. J Pharm Sci 98(9):3406-18.

Searles JA. 2000. Heterogeneity phenomena in pharmaceutical lyophilization.

8 APPENDIX I

Calculation of $\frac{d \ln K_v}{d \ln\left(\frac{dm}{dt}\right)}$: The relationship between the relative deviation of vial heat transfer coefficient, K_v and sublimation rate, dm/dt

In order to evaluate the derivative, $\frac{d \ln K_v}{d \ln\left(\frac{dm}{dt}\right)}$ it can be assumed that the top radiation to a vial is from a temperature source equal to that of the top shelf temperature. With this assumption the dm/dt ($g \cdot h^{-1}$) may be written as

$$\frac{dm}{dt} = \frac{3600\, A_v K_v (T_s - T_p)}{\Delta H_s} \qquad \text{Equation 22}$$

where the factor of 3600 converts $g \cdot s^{-1}$ to $g \cdot h^{-1}$ and other symbols are as described earlier. The sublimation rate can also be related to the temperature difference between the product measured at the bottom of the vial (T_p) and the temperature of the ice at the sublimation front (T_0) using the approximation

$$\frac{dm}{dt} \cong \frac{3600\, A_v K_I (T_p - T_0)}{\Delta H_s\, l_i} \qquad \text{Equation 23}$$

where l_i is the thickness of ice. The relationship given by Equation 23 is precise only when all heat flow comes through the vial bottom. However, the error introduced by using Equation 23 does not seriously affect the results of this section.

Differentiation of Equation 22 and 23 gives Equations 24 and 25 respectively:

$$\frac{d \ln K_v}{d \ln\left(\frac{dm}{dt}\right)} = 1 + 3600 \frac{A_v K_v}{\Delta H_s} \left(\frac{d(dm/dt)}{dT_0} \cdot \frac{dT_0}{dT_p} \right)^{-1} \qquad \text{Equation 24}$$

$$\left(\frac{dT_0}{dT_p}\right)^{-1} = 1 + \left(\frac{l_i \Delta H_s}{3600 A_v K_i}\right)\left(\frac{d(dm/dt)}{dT_0}\right) \quad \text{Equation 25}$$

Substituting for $\left(\frac{dT_0}{dT_p}\right)^{-1}$ from Equation 25 in Equation 24 then yields

$$\frac{d \ln K_v}{d \ln\left(\frac{dm}{dt}\right)} = 1 + 3600 \frac{A_v K_v}{\Delta H_s}\left(\frac{d(dm/dt)}{dT_0}\right)^{-1} + \frac{K_v l_i}{K_i} \quad \text{Equation 26}$$

Evaluating $\frac{d(dm/dt)}{dT_0}$***:***

Equation 27 shows an alternative way of writing $\frac{d(dm/dt)}{dT_0}$.

$$\frac{d(dm/dt)}{dT_0} = \frac{d(dm/dt)}{dP_0} \cdot \frac{dP_0}{dT_0} \quad \text{Equation 27}$$

Evaluating $\frac{d(dm/dt)}{dP_0}$***:***

Sublimation rate, *dm/dt* is directly proportional to the pressure differential between that at the sublimation front, P_0 and the chamber, P_c and inversely proportional to the total resistance to the water vapor flow from the vial to the chamber as follows:

$$(dm/dt) = \frac{P_0 - P_c}{R_{Total}} \quad \text{Equation 28}$$

Differentiating Equation 28 yields:

$$\frac{d(dm/dt)}{dP_0} = \frac{1}{R_{Total}} \quad \text{Equation 29}$$

In case of pure ice, since there is no formation of dry layer during sublimation, only the resistance of the stainless steel tube in the specialized stopper, R_{TB} contributes to R_{Total}. Hence, Equation 29 becomes:

$$\frac{d(dm/dt)}{dP_0} = \frac{1}{R_{TB}} \qquad \text{Equation 30}$$

However, in case of a product such as sodium chloride R_{total} is the sum of the resistance to vapor flow from the dried product, R_p as well as the tube. Thus for any product, Equation 29 can be expressed as Equation 31 where A_p is the area of the product.

$$\frac{d(dm/dt)}{dP_0} = \frac{1}{R_{TB} + \frac{R_p}{A_p}} \qquad \text{Equation 31}$$

Evaluating R_{TB}:

The theoretical relationship between the resistance (Torr· h·g^{-1}) to vapor flow offered by a tube and pressure is given by:

$$R_{TB}{}^{-1} = \frac{\left[150.A\left(\frac{a}{l}\right)\right]}{\left[1+\frac{8}{3}\left(\frac{a}{l}\right)\right]} + 7965.A\left(\frac{a^2}{l}\right).\bar{P} \qquad \text{Equation 32}$$

where A is the tube cross sectional area, a is the tube radius, l is the tube length and $\overline{P}$ is the mean pressure across the tube (Pikal, Roy, Shah 1984). Substituting l = 2.0 cm and a = 0.23 cm for the tubes used in this study in Equation 32 yields:

$$R_{TB}{}^{-1} = 2.25 + 35.8.\bar{P} \qquad \text{Equation 33}$$

Further, the mean pressure across the tube $\overline{P}$ is the mean of the pressure inside the vial, P_v and the chamber pressure, P_c as given by Equation 34

$$\bar{P} = \left(\frac{P_v + P_c}{2}\right) \quad \text{Equation 34}$$

In case of water and product, pressure in the vial, P_v can be assumed to be equal to the pressure at the sublimation front, P_0 in the absence of dry layer formation. There exists an exponential relationship between P_0 and T_0, the temperature at the sublimation front given by Equation 5. To calculate T_0 Equation 23 can be rearranged as Equation 35.

$$T_0 = T_p - \left(\frac{\frac{dm}{dt}}{A_v . K_I}\right)\Delta H_s \, l_i \quad \text{Equation 35}$$

In case of water, for a 3 ml fill with T_p= -38 °C, (as obtained from thermocouples), the T_0 was calculated as -40 °C using Equation 35. Hence, $P_v \approx P_0$ = 94 mTorr (calculated using Equation 5). At a chamber pressure, P_c = 60 mTorr and P_v = 94 mTorr, R_{TB} = 0.20 Torr· h·g^{-1} (calculated using Equation 33). Substituting for R_{TB} in Equation 30 gives:

$$\frac{d(dm/dt)}{dP_0} = \frac{1}{R_{TB}} = 5 \quad \text{Equation 36}$$

In case of sodium chloride, for a 3 ml fill volume, $P_v \approx P_c$ = 60 mTorr yielding R_{TB} = 0.23 Torr· h·g^{-1}. Substituting for R_{TB} in Equation 31 with R_p = 3.32 cm^2·Torr· h·g^{-1} (unpublished data) and A_p = 5.73 cm^2 for the 20 cc vials used in this study we obtain Equation 37.

$$\frac{d(dm/dt)}{dP_0} = 1.23 \quad \text{Equation 37}$$

Evaluating $\frac{dP_0}{dT_0}$:

Equation 5, the relationship between P_0 and T_0 can also be expressed as:

$$\ln P_0 = \frac{-6144.96}{T_0} + 24.0184 \qquad \text{Equation 38}$$

Differentiating Equation 38 gives:

$$\frac{dP_0}{dT_0} = P_0\left(\frac{6144.96}{T^2}\right) \approx 0.1P_0 \text{ (Verified for } T_0 \text{ from -45 to +20° C)} \qquad \text{Equation 39}$$

Substituting Equations 36 and 39 with P_0 = 94 mTorr for water in Equation 27 yields:

$$\frac{d(dm/dt)}{dT_0} = 0.05 \qquad \text{Equation 40}$$

Substituting Equations 37 and 39 with P_0 = 155 mTorr for sodium chloride in Equation 27 yields:

$$\frac{d(dm/dt)}{dT_0} = 0.02 \qquad \text{Equation 41}$$

Substituting A_v = 6.95 cm^2, ΔH_s = 680 $cal \cdot g^{-1}$, l_i = 0.57 cm for a 3 ml fill and K_i = 5.9 x 10^{-3} $cal \cdot cm^{-1} \cdot K^{-1} \cdot sec^{-1}$ and Equations 40 and 41 in Equation 26 gives Equations 42 and 43 for water and product respectively.

$$\frac{d \ln K_v}{d \ln\left(\frac{dm}{dt}\right)} = 1 + 855K_v \qquad \text{Equation 42}$$

$$\frac{d \ln K_v}{d \ln \left(\frac{dm}{dt}\right)} = 1 + 1992 K_v$$ Equation 43

9 FIGURES

a) **b)**

Figure 1 - (a) Top view of a 20 cc tubing vial fitted with a 2-legged stopper inserted with a small precision cut stainless steel tube (2 cm in length, 0.46 cm i.d.) (b) A lateral view of the standardized stopper.

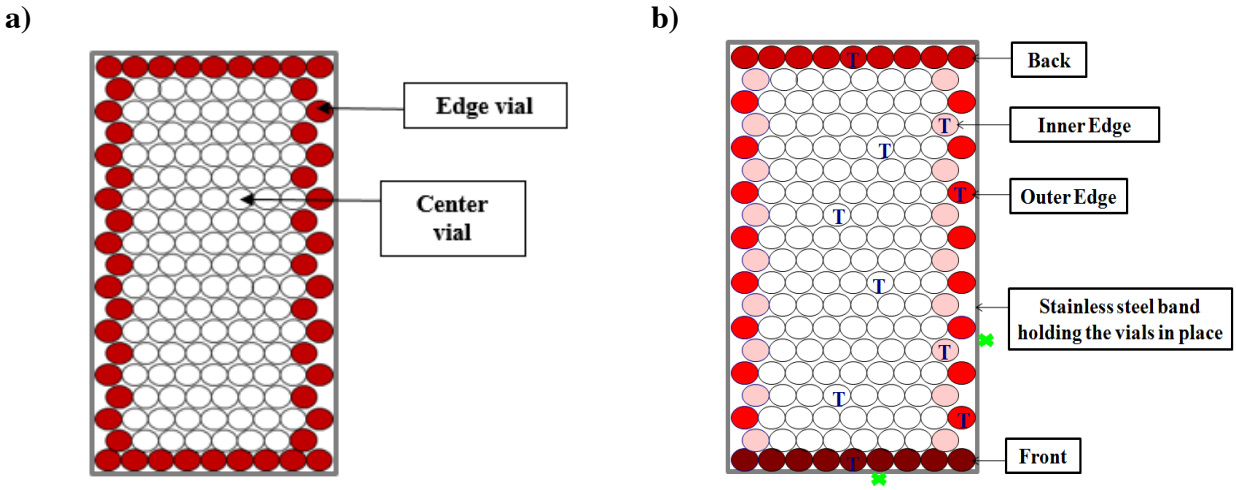

Figure 2 – Classification of vials into a) 2 categories: edge and center b) 5 categories: front row, back row, outer edge, inner edge, and center to better describe the heterogeneity in heat transfer to product in the vials.

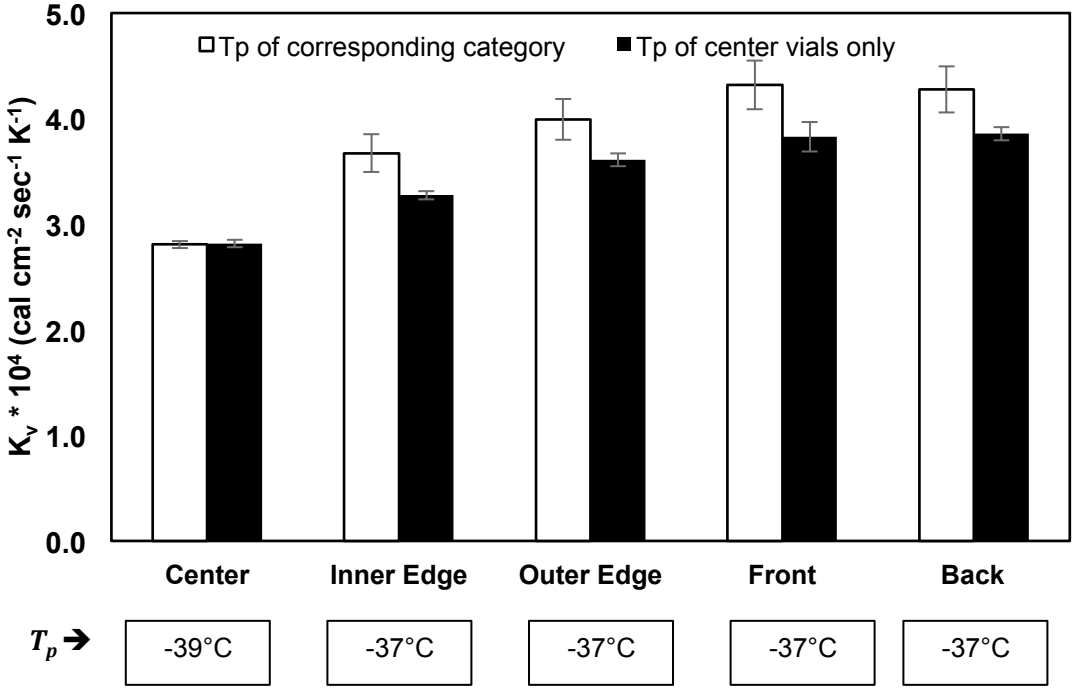

Figure 3 – Average K_v for the categories of vials shown in Figure 2. K_v was determined gravimetrically using 3 mL of water in 20 cc vials hexagonally closest packed. The *dm*/*dt* and T_p of thermocoupled vials from each category were recorded for 5 hrs at a chamber pressure of 60 mTorr and shelf temperature of -20 °C. K_v values for non-thermocoupled vials in each category were determined as described in section 4.2.1.1.2.

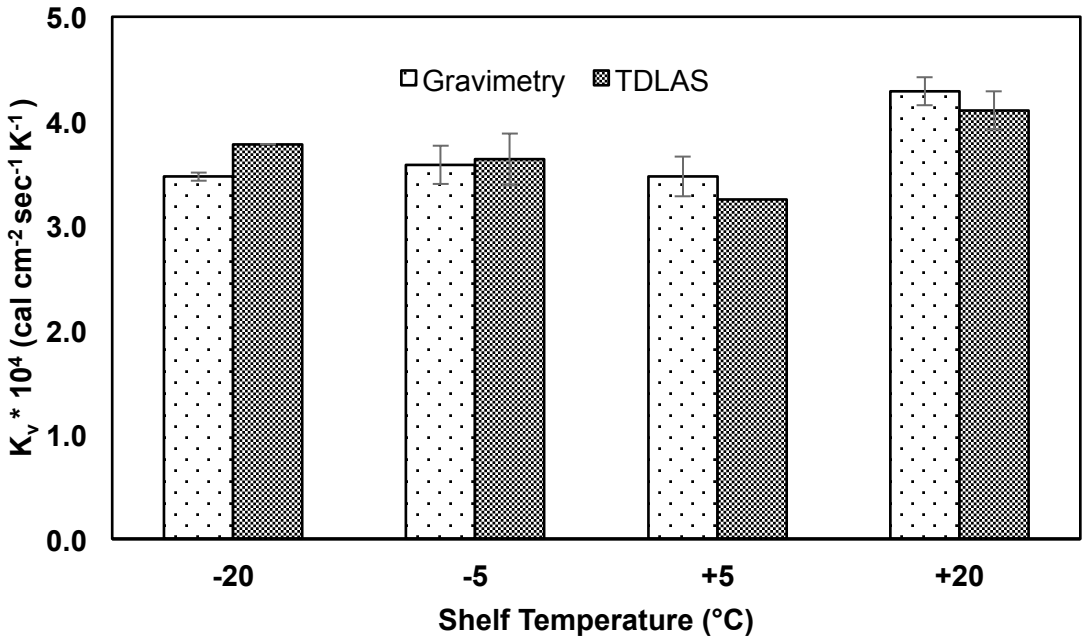

Figure 4 - Comparison between batch-averaged, time-averaged K_v as determined by gravimetric procedure and using TDLAS at a chamber pressure of 50 mTorr and shelf temperatures of -20, -5, +5 and +20 °C.

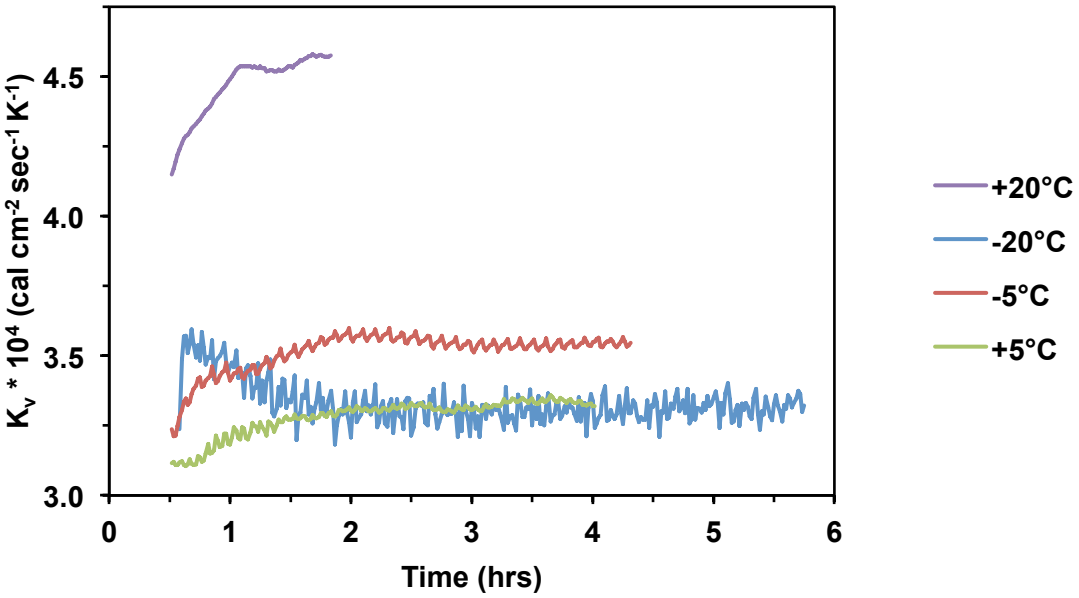

Figure 5 - Batch-averaged instantaneous K_v determined over 160 vials as a function of time. The sublimation rate was measured using TDLAS at a chamber pressure of 50 mTorr and shelf temperatures of -20, -5, +5 and +20 °C.

a)

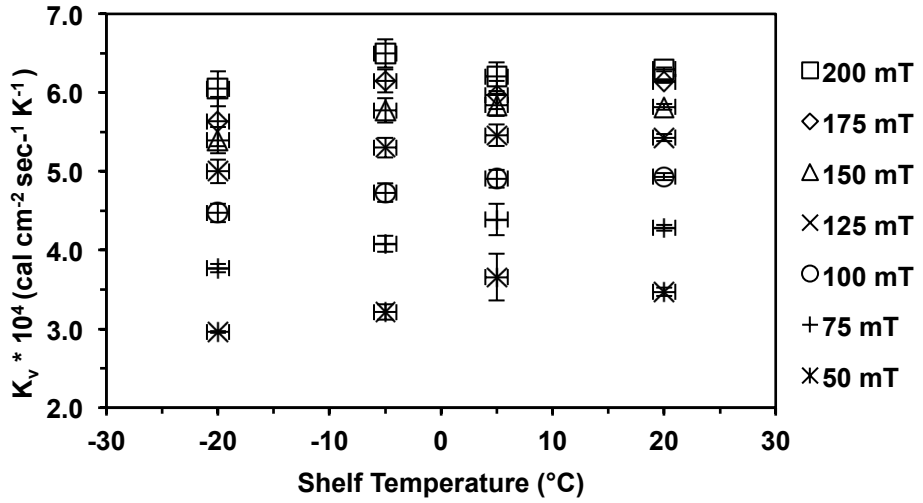

b)

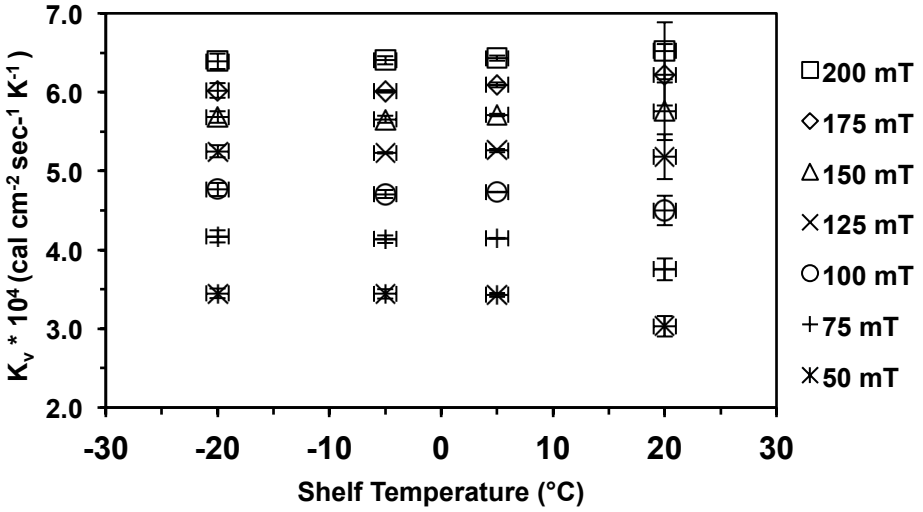

Figure 6 - Batch-averaged, time-averaged K_v determined for 20 cc vials (partially placed 3-legged stoppers) using a 10 ml fill volume of deionized water. Batch-averaged sublimation rate was determined using TDLAS over a range of chamber pressures (50, 75, 100, 125, 150, 175, 200 mTorr) and shelf temperatures (-20, -5, +5 and +20 °C) (a) Ascending experiments where chamber pressure was increased from 50 to 200 mTorr in increments of 25 mTorr at a constant

shelf temperature (b) Descending experiments where chamber pressure was decreased from 200 to 50 mTorr in decrements of 25 mTorr at a constant shelf temperature

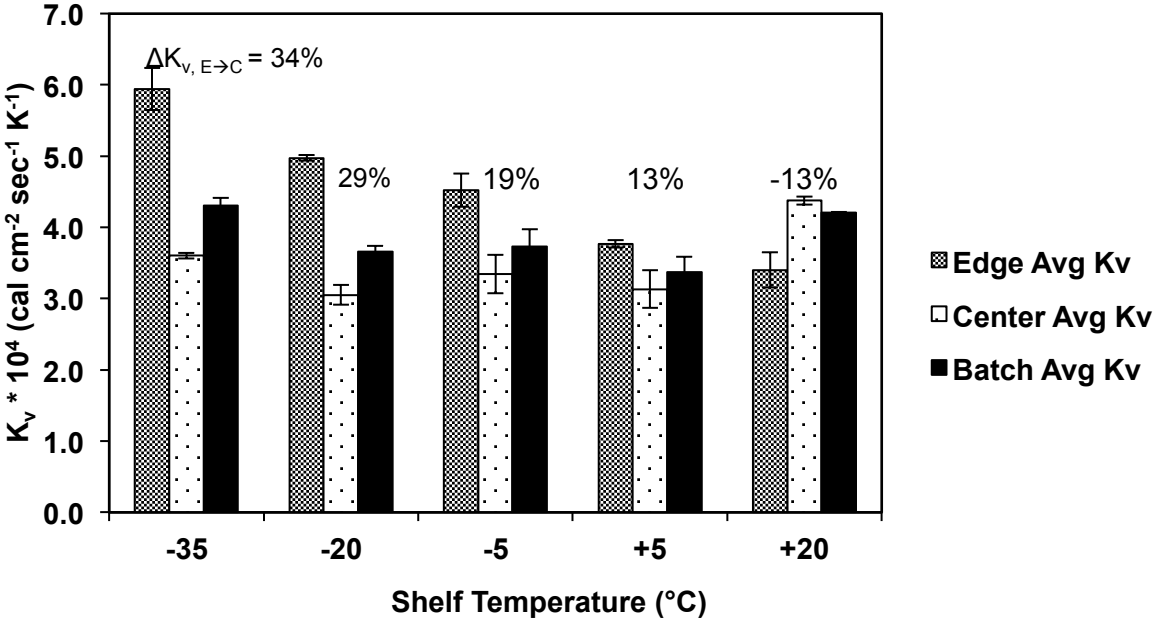

Figure 7 – Comparison between edge, center and batch-averaged, time-averaged K_v values calculated using gravimetric method at chamber pressure of 50 mTorr and shelf temperatures of -35, -20, -5, +5 and +20 °C. Fill volume = 10 ml with standardized stoppers. Individual vial K_v's for non-thermocoupled vials were determined using Equation 16 based on the average T_p, dm/dt and K_v of the center thermocoupled vials.

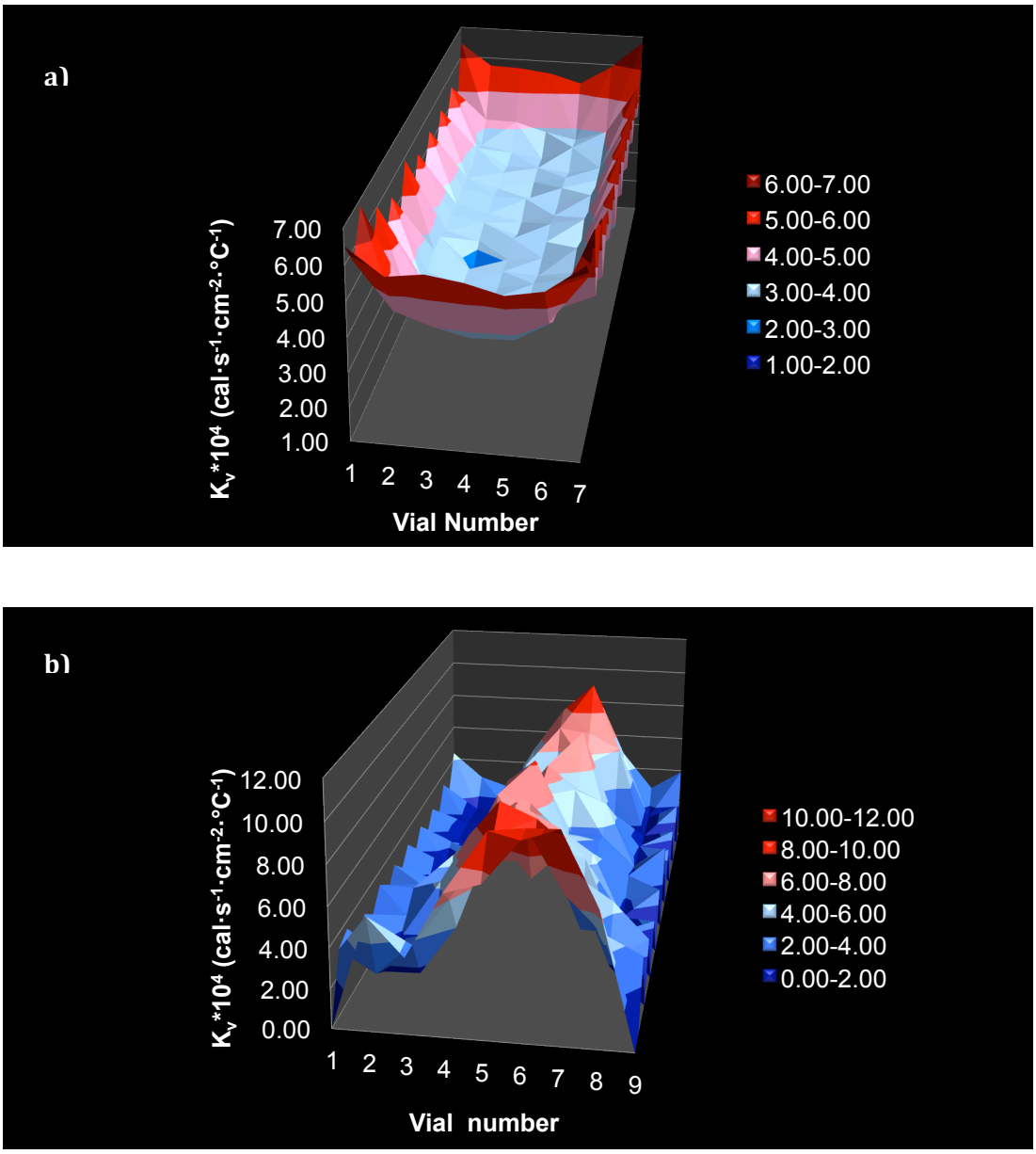

Figure 8 – A surface plot showing time-averaged individual vial K_v over an entire tray of 20cc vials at chamber pressure of 50 mTorr and shelf temperature of a) -35 °C and b) +20 °C.

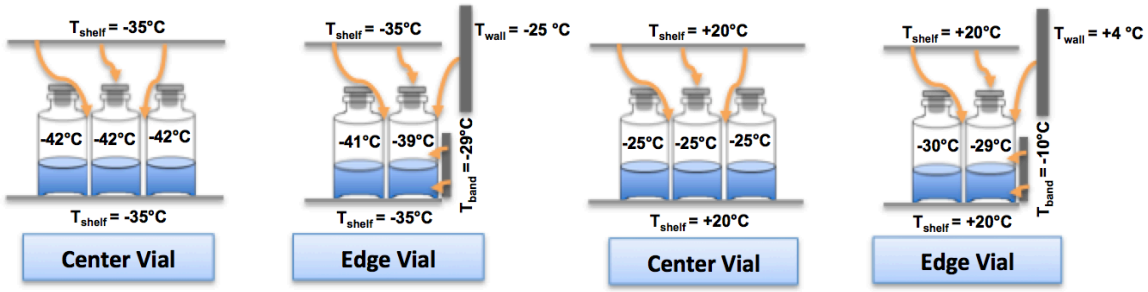

a) Shelf temperature = -35 °C **b) Shelf temperature = +20 °C**

Figure 9 – Comparison of several temperatures from surrounding surfaces for an edge and a center vial at a chamber pressure of 50 mTorr and shelf temperature (T_{shelf}) of **a)** -35 °C and **b)** +20 °C. The ice temperature in the vials, wall temperature (T_{wall}) and band temperature (T_{band}) have been indicated.

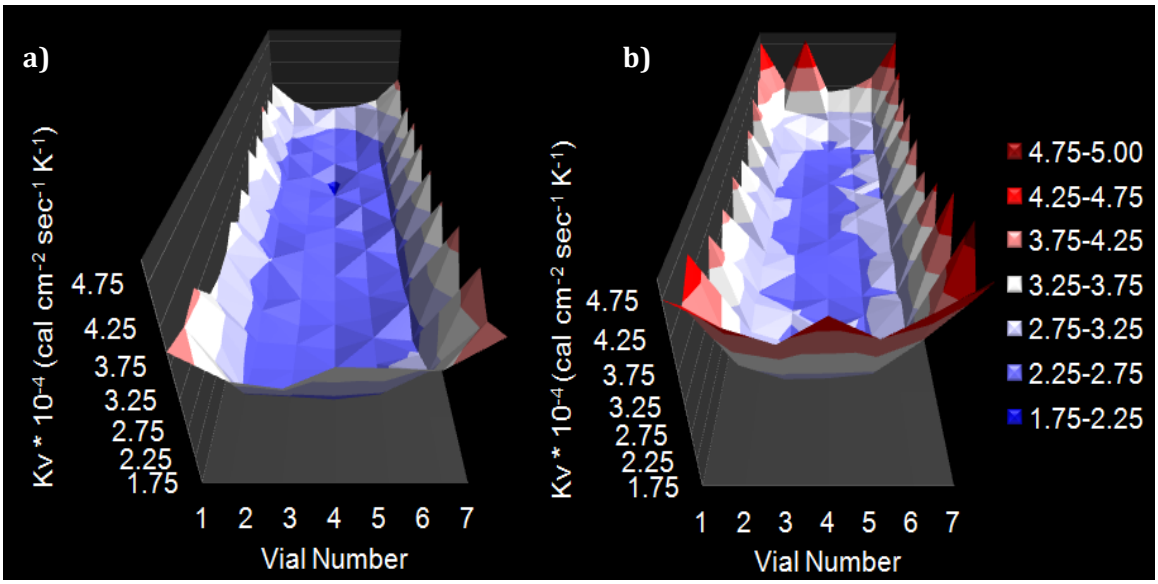

Figure 10 – A surface plot showing time-averaged individual vial K_v over an entire tray of 20cc vials at chamber pressure of 60 mTorr and shelf temperature of -20 °C using a fill volume of a) 3 ml and b) 10 ml.

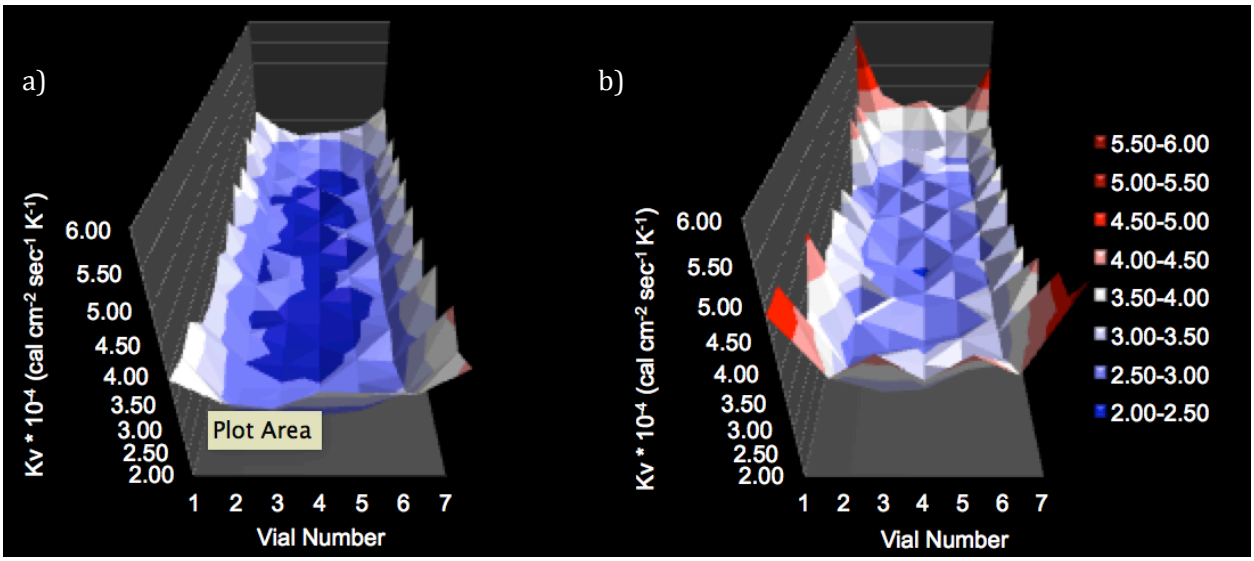

Water 3 ml

Sucrose 3 ml

Figure 11 – Comparison between surface plots showing individual vial K_v over a batch of 20 cc vials at chamber pressure of 60 mTorr and shelf temperature of -20 °C for a) water and b) 5% w/w sucrose at a 3 ml fill volume.

a) 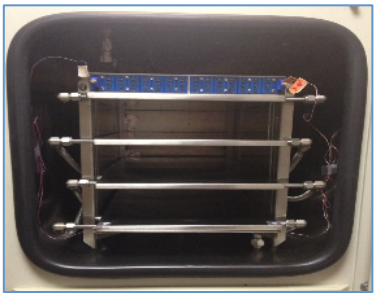 b) 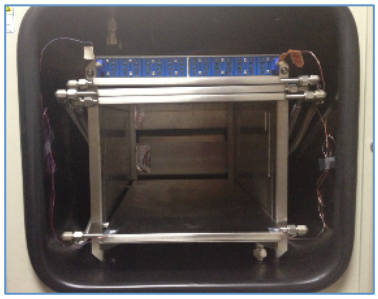

Figure 12 – Placement of shelves in a LyoStar II (a) three-shelf configuration (b) one-shelf configuration

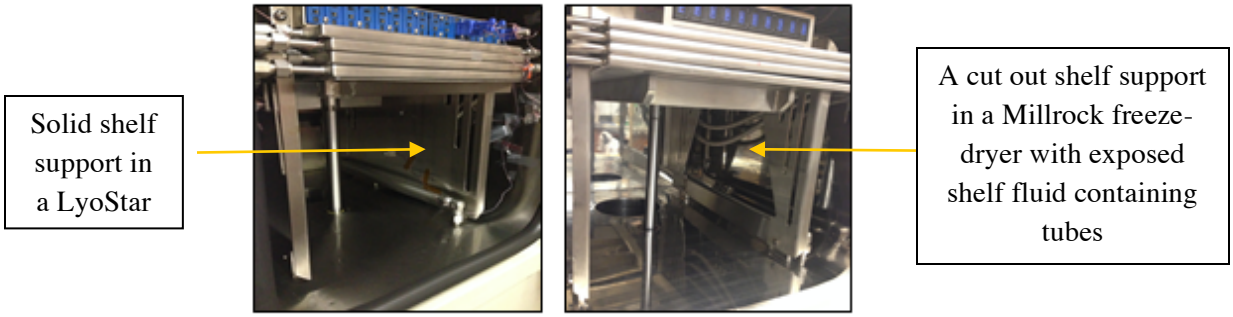

Figure 13 – Examples of different types of sidewalls: a solid shelf support in case of LyoStar freeze-dryer (left panel) and a cut out shelf support in the Millrock freeze-dryer (right panel)

Table I - (a) Batch-averaged instantaneous K_v values in cal·cm^{-2}·sec^{-1}·K^{-1} calculated at 75, 50, 25 and 0% ice remaining during sublimation of pure ice (upper panel) and 5% mannitol (lower panel) using batch averaged *dm*/*dt* and T_p from 3 different cases (I) from only center vials, (II) proportionally weighted from both center and edge vials (2:1) and (III) equally weighted from both center and edge vials. Both *dm*/*dt* and T_p were estimated using a steady-state heat and mass transfer theory based lyo-calculator. (b) Batch-averaged, time-averaged K_v (cal·cm^{-2}·sec^{-1}·K^{-1}) is also shown for both pure ice and mannitol using all the three cases of T_p. Linear average of K_v values is 3.20×10^{-4} cal·cm^{-2}·sec^{-1}·K^{-1}

	K_v x 10^4 cal·cm^{-2}·sec^{-1}·K^{-1} *(for pure ice)*		
	Case I: Center vial T_p	**Case II:** Proportionally weighted (2:1) center to edge vial T_p	**Case III:** Equally weighted (1:1) center to edge vial T_p
(a) Batch-averaged instantaneous K_v at time points corresponding to x% ice remaining			
75%	3.12	3.19	3.23
50%	3.12	3.18	3.22
25%	3.13	3.19	3.23
0% (end of the cycle)	1.87	2.81	3.75
(b) Batch-averaged, time-averaged K_v	2.82	3.10	3.35
	K_v x 10^4 cal·cm^{-2}·sec^{-1}·K^{-1} *(for a mannitol-like product)*		
	Case I: Center vial T_p	**Case II:** Proportionally weighted (2:1) center to edge vial T_p	**Case III:** Equally weighted (1:1) center to edge vial T_p

(a) Batch-averaged instantaneous K_v at time points corresponding to x% ice remaining			
At 75% ice remaining	3.03	3.17	3.25
At 50% ice remaining	2.99	3.16	3.26
At 25% ice remaining	2.97	3.16	3.27
At 0% ice remaining	1.87	2.80	3.74
(b) Batch-averaged, time-averaged K_v	2.76	3.09	3.36

Table II - Comparison between time-averaged K_v values for 5 categories of vials at chamber pressure of 60 mTorr and shelf temperatures of -20 °C at a fill volume of 3 and 10 ml. Standard errors (SE) have also been indicated.

		K_v x 10^4 cal·cm^{-2}·sec^{-1}·K^{-1}					
		Batch-Averaged	**Center Vials**	**Inner Edge Vials**	**Outer Edge Vials**	**Front Row Vials**	**Back Row Vials**
3 ml	Avg	2.99	2.66	3.48	4.08	3.95	3.73
	SE	0.08	0.07	0.12	0.14	0.19	0.14
10 ml	Avg	3.19	2.82	3.67	4.43	4.52	4.00
	SE	0.02	0.01	0.17	0.12	0.01	0.08

Table III – Comparison between time-averaged K_v values for different solutes (at 5% w/v) such as sodium chloride, sucrose and mannitol with water along with their batch-average K_v values. The K_v values were determined at a chamber pressure of 60 mTorr and shelf temperature of -20 °C for different vial categories at a fill volume of 3 ml. Standard errors (SE) have also been indicated.

		Batch Average	**Center Vials**	**Inner Edge Vials**	**Outer Edge Vials**	**Front Row Vials**	**Back Row Vials**
Water	**Avg**	2.99	2.66	4.08	3.48	3.95	3.73
	SE	0.08	0.07	0.14	0.12	0.19	0.14
Sodium chloride	**Avg**	2.68	2.30	3.91	3.13	4.11	3.64
	SE	0.15	0.12	0.15	0.37	0.04	0.17
Sucrose	**Avg**	3.04	2.73	4.03	3.40	4.00	3.81
	SE	0.04	0.08	0.09	0.05	0.07	0.03
Mannitol	**Avg**	2.95	2.62	3.96	3.46	3.84	3.78
	SE	0.04	0.02	0.09	0.06	0.11	0.08

Chapter 3

Quantifying the Variation in Product Temperature and Drying Time within a Lyophilized Batch during Primary Drying

1. ABSTRACT

Product temperature during the primary drying step of lyophilization is implicitly controlled by a judicious choice of shelf temperature and chamber pressure. A conventional method of selecting the final process conditions is by "trial and error" approach, which gets very tedious, expensive and time consuming because of the heterogeneity involved in the freezing and primary drying steps of lyophilization. The need to obtain a high quality stable lyophilized final product at an affordable cost has made it necessary to optimize the freeze-drying process by identifying and quantifying the sources of variation therein.

The aim of this report was to measure variation in key process parameters for a model formulation (5% sodium chloride). Then, using a probability analysis, combined with a first principles model of primary drying, the second aim was to determine the distribution of drying times and maximum product temperatures within a batch using realistic operating conditions.

Frequency distributions of fill volume, vial heat transfer coefficient (K_v), and dry layer resistance to vapor transport (R_p) were experimentally measured. A linear gradient in temperature across the shelf was assumed. To determine fill volume variation, each of 160 20-cc vials (equal to a full shelf in Lyostar II freeze-dryer) were filled with 3 ml water and weighed. Conventional gravimetric method of determining the sublimation rate was used to further calculate the heat transfer coefficient for individual vial. Variation in dry layer resistance to vapor transport, a function of the variation in the ice nucleation temperature was determined by controlling the ice nucleation at several temperatures using ice fog technique. At each nucleation temperature, instantaneous sublimation rates, measured by Tunable Diode Laser Absorption Spectroscopy (TDLAS), were used to determine the corresponding R_p using steady-state heat and

mass transfer equations. Frequency distributions for the four parameters were expressed as 11-level histograms to provide sufficient detail.

A very good agreement was found between the theoretical predictions and experimental results using 5% sodium chloride as the model system. Variation in dry product layer resistance and vial heat transfer coefficients were found to be the dominant contributors to the variation in primary drying times and maximum product temperatures.

2. INTRODUCTION

Freeze-drying (lyophilization) is a well-established process to improve the stability of labile drugs such as therapeutic proteins. In the freeze-dried solid state, chemical or physical degradation reactions are inhibited or sufficiently decelerated, resulting in improved long-term stability (Carpenter et al. 1997). The process of freeze-drying consists of three steps: (a) freezing, (b) primary drying, and (c) secondary drying. During freezing, the pre-lyophilized solution is frozen to sub-ambient temperatures, typically -40 °C, where water is converted to ice, solutes concentrate and crystallize out and/or remain amorphous. During primary drying, the drying chamber is evacuated to pressures below 500 mTorr and the shelf temperature is ramped up to supply energy for the sublimation of ice (Pikal, Roy, Shah 1984). In the next step of secondary drying, the shelf temperature is raised further to desorb the remaining unfrozen water (15-20% of the product at the end of primary drying) to obtain low final residual moisture content (0.5 to 3%) in the final product(Pikal 2002). While the freezing and secondary drying stages typically take a few hours, primary drying can take several days depending on the processing conditions required for the formulation. Moreover, the energy required to remove 1 kg of water during primary drying is nearly double and costs 4-8 times other available drying methods (Liu, Zhao, Feng 2008; Ratti 2001). Thus, in general, freeze-drying is a very time- and energy- intensive process and a current focus of the pharmaceutical industry is process optimization by accounting for the heterogeneity in the overall process to reduce the cycle times as well as to get a quality end product consistently (Fissore, Pisano, Barresi 2011; Gieseler, Kramer, Schneid 2008; Giordano, Barresi, Fissore 2011; Jameel and Khan 2009; Koganti et al. 2011; Mockus et al. 2011; Nail and Searles 2008; Pikal 1985; Pisano et al. 2013; Sundaram et al. 2010; Tang, Nail, Pikal 2005).

Heterogeneity associated with the freezing step has been well documented in the existing literature (Kasper and Friess 2011). Due to the inherent stochastic nature of ice nucleation (Searles, Carpenter, Randolph 2001a), water in vials in the same batch nucleates at different times and temperatures leading to a range of ice crystal sizes. As the ice sublimes during primary drying and leaves behind a porous dry layer, the size of ice crystals determines the (i) shape and size of the pores, (ii) pore size distribution, and (iii) connectivity of the pores (Pikal, Rambhatla, Ramot 2002) (Rambhatla et al. 2004). These characteristics of the porous dry layer (also called the cake) affect process parameters such as primary (Searles, Carpenter, Randolph 2001) and secondary drying (Pikal et al. 1983; Searles, Carpenter, Randolph 2001a) as well as several product attributes such as protein stability (Bhatnagar, Bogner, Pikal 2007; Chang, Kendrick, Carpenter 1996), specific surface area (Konstantinidis et al. 2011) and residual moisture (Awotwe-Otoo et al. 2013).

During primary drying, not all vials dry at the same time and temperature. One of the factors affecting the heat transfer to the product is the vial heat transfer coefficient. In pharmaceutical freeze-drying, the vial heat transfer coefficient has been documented to have three contributions: (i) contact conduction due to the specific points of contact between the vial and the bottom shelf, (ii) gas conduction through the gap between the bottom of the vial and the top of the shelf beneath and (iii) radiation from the warmer surfaces in the chamber (walls, door). (Pikal, Roy, Shah 1984) The inherent variation in the bottom contour of a vial even within the same batch of vials affects the heat transfer due to contact conduction and gas conduction. A typical batch of vials on a single shelf is categorized into edge and center vials based on their positions. At the usual freeze-drying conditions, the outermost edge and the extreme center vials experience the highest and the lowest amount of radiative heat transfer, respectively, with

intermediate values for the remaining vials. All these factors lead to a variation in the product temperatures across a batch of vials on the same shelf. Also, variation in the dry product layer resistance (an effect of the ice nucleation temperature during freezing as discussed above) leads to a difference in the sublimation rates and hence product temperatures over the shelf. Thus, for any lyophilization cycle, "hot" and "cold" areas exist where a few vials tend to exhibit higher and lower temperatures, respectively, than the average vial on the shelf. The "hot" spots in a batch of vials determine the maximum product temperature in primary drying whereas the "cold" spots determine the maximum primary drying time. The partially dried cake can collapse when: (a) the product temperature exceeds the collapse temperature of the formulation (such as "hot" spots during an aggressive cycle) (b) the shelf temperature is increased to the secondary drying temperature prematurely, i.e., before the completion of primary drying (such as vials in the "cold" spots). A conservative cycle (where the product temperature is controlled well below the collapse temperature of the product) can be employed to decrease product loss due to collapse; however, an excessively conservative cycle unnecessarily prolongs the primary drying time. To minimize product collapse during the initial phase of the secondary drying, the primary drying time may be prolonged even further. This can lead to an increase in the overall cost of the product due to increased energy consumption, extended cycle times and less efficient plant utilization. The freeze-drying process is manipulated, often using arbitrary changes in shelf temperature and "operational" primary drying time, resulting in an increase in the time and costs related to getting a product to the patient.

Several case studies exist in the literature highlighting the effect of the variation in the overall freeze-drying process on the quality of the end product with regards to its stability (Chang, Kendrick, Carpenter 1996), cake appearance and reconstitution time (Awotwe-Otoo et

al. 2013). Traditionally, quality has been "tested into the product" at the end of the process by several independent quality control tests, leading to rejection of batches that do not meet quality standards. However, the link between the product quality attributes and their clinical consequence is often not explicitly known (Short et al. 2011). This advocates for the use of a more controlled freeze-drying process by better understanding the underlying physics to create mathematical models, which will accurately predict the critical output parameters responsible for governing the quality of the final product. Current freeze-drying literature describes a few such theoretical models (Fissore, Pisano, Barresi 2011; Gieseler, Kramer, Schneid 2008; Giordano, Barresi, Fissore 2011; Jameel and Khan 2009; Koganti et al. 2011; Mockus et al. 2011; Nail and Searles 2008; Pikal 1985; Pisano et al. 2013; Sundaram et al. 2010; Tang, Nail, Pikal 2005), which allow a systematic approach to designing a successful freeze-drying cycle with minimum number of representative experimental runs.

In this study, a first principles quasi-steady-state heat and mass transfer model for the primary drying step of freeze-drying process was combined with a probability distribution of sources of variation to predict the fraction of out-of-specification vials at a particular set of product and operating conditions. The distribution of product temperatures and primary drying times in a batch of product subject to all the known variations in critical parameters important in determining maximum product temperature and primary drying time.

3. MODEL DEVELOPMENT

3.1. Steady state heat and mass transfer theory

A previous quasi-steady-state heat and mass transfer model (Pikal 1985) was used to link variation in fill volume, shelf temperature, vial heat transfer coefficient and dry product layer

resistance to vial-to-vial distribution in time to complete primary drying (i.e., removal of all ice crystals). During primary drying, the rate of heat transfer only from the shelf to the product, dQ/dt (cal·s^{-1}), is proportional to a vial heat transfer coefficient, K_v, (cal·s^{-1}·cm^{-2}·K^{-1}) (Equation 1),

$$\frac{dQ}{dt} = A_v \cdot K_v \cdot (T_s - T_p) \qquad \text{Equation 1}$$

where A_v (cm^2) is the horizontal cross sectional area of the vial, T_p (°C or K) is the temperature of the product at the inside bottom center of the vial in contact with the product, and T_s (in the same units as T_p) is the shelf surface temperature (Pikal, Roy, Shah 1984; Pikal 1985). Additionally, the heat from the vial bottom continues to flow by conduction through the frozen product to the sublimation interface (Equation 2) where it is consumed by the process of sublimation,

$$\frac{dQ}{dt} = \frac{A_v \cdot K_I \cdot (T_p - T_0)}{l_I(t)} \qquad \text{Equation 2}$$

where K_I is the effective conductivity of the frozen product (i.e., largely due to the ice) 5.9 x 10^{-3} cal·cm^{-1}·K^{-1}·sec^{-1} (Pikal, Roy, Shah 1984), T_o is the temperature at the sublimation interface, and l_I is the thickness of the ice remaining in the frozen product. The value of l_I decreases with time as sublimation proceeds primarily from the top to the bottom of the cake over which a temperature difference ($\Delta T = T_p - T_o$) exists across the cake where $T_p > T_0$. According to the law of conservation of energy, the heat supplied from the bottom of the vial, dQ/dt, is balanced by the sum of mass transfer and the heat utilized in increasing the temperature of the frozen plug as given in Equation 3

$$\frac{dQ}{dt} = \Delta H_s \cdot \frac{dm}{dt} + m \cdot c_v \cdot \frac{\partial T}{\partial t} \qquad \text{Equation 3}$$

where ΔH_s (680 cal·g^{-1}) is the heat of sublimation, dm/dt (g·s^{-1}) is the sublimation rate, $\frac{\partial T}{\partial t}$ is the rate of change in temperature of the frozen product of mass, m, and specific heat, c_v. Except for the initial 10-15 minutes when the shelf temperature is changed from the final freezing set point to the set point for primary drying, the product temperature during the remainder of the primary dying phase is constant (quasi steady-state). Hence, the term $m_s c_v(\partial T/\partial t)$ is very small for majority of primary drying than the heat of sublimation term and can be ignored leading to Equation 4.

$$\frac{dQ}{dt} = \Delta H_s \cdot \frac{dm}{dt} \qquad \text{Equation 4}$$

As primary drying proceeds, the sublimation front moves down from the top of the frozen product thus leaving a porous dry layer of product. This dry layer poses a resistance to mass transfer for the vapor leaving the sublimation front. The sublimation rate, dm/dt, can then be related to the driving force for sublimation, $(P_0 - P_c)$, and the resistance to vapor flow from the frozen product to the drying chamber, $(R_p + R_s)$, by Equation 5

$$\frac{dm}{dt} = \frac{A_p(P_0 - P_c)}{(R_p + R_s)} \qquad \text{Equation 5}$$

where A_p (cm^2) is the horizontal cross-sectional area of the frozen product, P_0 (mTorr) is the vapor pressure of ice at the sublimation interface, P_c (mTorr) is the chamber pressure, R_p (cm^2·hr·Torr·g^{-1}) is the resistance of the porous dry layer above the sublimation interface and R_s (hr·Torr·g^{-1}) is the resistance posed by the stopper. However, resistance posed by the stopper, R_s is negligible as compared to that of the dry product layer, R_p, and can be ignored (Pikal, Roy,

Shah 1984). The vapor pressure of ice at the sublimation interface, P_0 is a well-characterized function of the temperature of ice at the sublimation interface, T_0 (K) given by Equation 6 (Jansco, Pupezin, Van Hook 1970)

$$P_0 = 2.698\times10^{10}\times e^{-6144.96/T_0} \qquad \text{Equation 6}$$

At quasi steady-state conditions, the heat and mass transfer can be coupled by rearranging Equation 1 through 6 to obtain Equation 7

$$\Delta H_s \cdot \left[\frac{A_p \cdot (P_0 - P_c)}{R_p}\right] - A_v \cdot K_v \cdot (T_s - T_p) = 0 \qquad \text{Equation 7}$$

With knowledge of the mass transfer coefficient (R_p) and the vial heat transfer coefficient (K_v), and depending on the process parameters chamber pressure (P_c) and shelf temperature (T_s), Equation 8 can be solved to obtain the product temperature, T_p. Once T_p is known, sublimation rate, *dm*/*dt* can be calculated from Equation 5.

3.2. Critical variables considered and processing variable matrix

Following four input process variables were identified to be critical in determining the process output parameters namely the maximum primary drying product temperature (T_{max}) and primary drying time (t_{dry}):

a) Vial heat transfer coefficient

b) Product dry layer resistance

c) Shelf temperature

d) Fill volume

First variations in the above mentioned input parameters were determined from experimental data and were grouped into different levels to capture 99.999% of the data along with calculating an average value and frequency of occurrence at that level. Individual values for each of the independent critical variables for each distribution were then treated with the heat and mass transfer theory to get a value for T_{max} and t_{dry}.

The experimental details for determining the variations in the input parameters are given in Section 4. Figure 1 shows the processing variable matrix where the input parameters A, B, C, D denote shelf temperature, dry product layer resistance, vial heat transfer coefficient and fill volume, respectively. Data obtained for the four input variables was distributed into 11 levels leading to 11^4 (14,641) combinations of T_{max} and t_{dry}. However, since all combinations were not equally probable and all the input variables were assumed to be independent of each other the probability of each chosen combination can be expressed as the product of individual probabilities as given by Equation 8

$$\boldsymbol{P_n = P_{V_{fill}}.P_{K_v}.P_{R_p}.P_{T_s}} \qquad \text{Equation 8}$$

where P_n represents the probability that each of the four statistical variables has the value chosen in the "n^{th}" calculation. Since T_{max} and t_{dry} depend on the four input variables, P_n also represents the probability that a given vial has that particular T_{max} and t_{dry}. The number of vials whose product temperature exceeds the collapse temperature and those that have not finished with primary drying at any given time can then be calculated.

4. MATERIALS AND METHODS

4.1. Determination of shelf temperature

The surface temperature of the shelf was measured near the shelf fluid inlet of the bottom-most shelf using self-adhesive copper-constantan thermocouples (Omega Engineering Inc., Stamford, CT).

4.2. Determination of fill weight variation

Each of 160, 20 cc vials (Schott, Elmsford NY) was identified based on its position on the shelf (row and column number). Empty vials were weighed and filled with 3 ml of solution containing 5% w/v sodium chloride and 0.1% w/v sucrose using a manual Eppendorf® Repeater™ pipet (50 ml capacity). Filled vials were reweighed. The fill weight was determined from the difference between the initial and final weights for each vial. Four sets of 160 vials were weighed to determine the fill weight variation (n = 640).

4.3. Determination of individual vial heat transfer coefficient

Measurement of vial heat transfer coefficient for individual vials:

The procedure to determine vial heat transfer coefficient by gravimetric method was adapted from previous work (Pikal, Roy, Shah 1984; Pikal 1985). Each of the 160 vials in a batch was tracked using a row and a column number based on its position on the shelf. Vials were filled with 3 ml of deionized water and capped with specialized stoppers inserted with precision cut stainless steel tubes (2 cm in length, i.d. 0.46 cm) to ensure uniformity of mass transfer resistance. Thus, any change in the sublimation rate for vials could solely be attributed to a difference in the heat transfer.

Conventionally, vials are classified as edge and center vials depending on their positions.

However, a 5 category vial classification was used in this study: front row (9 vials), back row (9 vials), side outer edge vials in contact with the stainless steel band (16 vials, excluding the ones accounted in the back and the front rows) and side inner edge vials (18 vials) not in contact with the band (Figure 2). Given the availability of limited thermocouple slots in our lab freeze-dryer (LyoStar II, SP Industries, Warminster, PA) thermocouples were placed in representative 4 center, 1 front row, 1 back row, 2 right outer edge and 2 right inner edge vials (Figure 2). The temperatures of product nearest the bottom center of the vials were measured using 30 gauge copper-constantan (type-T) thermocouples (Omega Engineering Inc., Stamford, CT) with a resolution of ±0.1 °C. The product thermocouples were calibrated for 0.0 °C before each experiment using a mixture of ice and deionized water. The surface temperature of the shelf was measured near the shelf fluid inlet of the bottom most shelf using self-adhesive copper-constantan thermocouples (Omega Engineering Inc., Stamford, CT). Vials were loaded on to the bottom-most shelf of LyoStar II freeze-dryer in a three-shelf configuration (equal spacing between the shelves). Protocol for the sublimation cycle was as follows:

- Freezing: Cool to +5 °C at 1 °C/min, hold for 15 mins (for thermal equilibration); cool to -5° C at 1 °C/min, hold for 15 min (for thermal equilibration); cool to -45 °C at 1 °C/min, hold for 8 hours (to erase previous thermal history for the stainless steel band holding the vials in place, walls and door).
- Primary drying/sublimation: Evacuate the chamber to 60 mTorr, increase shelf temperature to -20 °C at 5 °C/min. Hold at the set point for 5 hours to allow 20-25% of ice to sublime in the center vials.

At the end of 5 hours, sublimation was abruptly stopped by equilibrating the chamber pressure to atmospheric pressure. Ice in the vials was thawed carefully by increasing the shelf temperature to +10 °C without any further loss of water due to evaporation. The stoppered vials were weighed with water before initiation of the experiment (m_i) and after sublimation (m_f) at the end of 5 hours. The total time for sublimation, *dt*, was calculated by carefully analyzing the start time which was determined as the point at which the driving force for sublimation (P_0 - P_c, Equation 6) becomes substantial (about 300 mTorr). The vapor pressure of ice, P_0 was estimated from Equation 6 by assuming $T_0 = T_p$ (since there exists no dry layer as the sublimation of ice proceeds from top to bottom of the vial). From the difference in the weights of the vials before and after sublimation, the amount of water sublimed, *dm*, was determined ($dm = m_i - m_f$). For each vial, the sublimation rate was then expressed as *dm/dt* in $g \cdot hr^{-1}$. Five sublimation experiments were done to determine the variation in vial heat transfer coefficient (n = 800).

Evaluation of the individual vial heat transfer coefficient for vials with specialized stoppers:

The calculations for determining the heat transfer coefficient for each vial were adapted from previous work (Sane et al. b). Since the product temperature, T_p (°C), and sublimation rate, *dm/dt* ($g \cdot s^{-1}$) for the monitored (thermocoupled) vials are measured during the experiment, the vial heat transfer coefficient, K_v ($cal \cdot s^{-1} \cdot cm^{-2} \cdot K^{-1}$), for this set of vials can be calculated directly by rearranging Equation 1 and 4 to obtain Equation 9 with other parameters known.

$$K_{v,TC} = \frac{\left(\frac{dm}{dt}\right) * \Delta H_s}{3600 * A_v * (T_s - T_p)} \qquad \text{Equation 9}$$

For any unmonitored (non-thermocoupled) vial i, where the product temperature is unknown, the vial heat transfer coefficient, $K_{v_{non-TC,i}}$ was calculated indirectly using Equation 10

$$K_{v_{non-TC,i}} = \langle K_v \rangle_{TC} \cdot \left\{ 1 + \left(\frac{\left({}^{dm}/_{dt} \right)_{non-TC,i}}{\langle {}^{dm}/_{dt} \rangle_{TC}} - 1 \right) \cdot (1 + (855 * \langle K_v \rangle_{TC})) \right\} \qquad \text{Equation 10}$$

where $\langle K_v \rangle_{TC}$ is the average K_v of the thermocoupled vials, $\left(\frac{dm}{dt}\right)_{non-TC,i}$ is the sublimation rate of any particular non-thermocoupled vial and $\langle \frac{dm}{dt} \rangle_{TC}$ is the average sublimation rate of the thermocoupled vials (Sane et al. b). Equation 10 holds true for vials fitted with stoppers containing standardized tubes (2 cm in length, i.d. 0.46 cm) and a fill depth of 0.5 cm using deionized water. A detailed derivation for this equation can be found in (Sane et al. b). The factor 855 is a function of the resistance (posed by the product, stopper and tube) to vapor flow, fill depth, sublimation rate and the area of the vial and product. The derivation for Equation 10 is based on the fact that there is a small difference in the *dm*/*dt* and K_v between a thermocoupled and a non-thermocoupled vial and any change in the K_v ultimately causes a net relative change in the *dm*/*dt*, which is less than proportional to K_v. Based on the category of a non-thermocoupled vial, K_v for that vial was calculated from Equation 10 using $\langle \frac{dm}{dt} \rangle_{TC}$ and $\langle K_v \rangle_{TC}$ specific for the thermocoupled vials from the same category of vials.

4.4. Determination of variation in product layer resistance due to variation in degree of super-cooling

Six freeze-drying experiments were performed using FreezeBooster® nucleation technology (Millrock Technology, Kingston, NY) to control ice nucleation at temperatures ranging from -5 °C to -10 °C in a LyoStar II freeze-dryer. A 3 ml fill volume of a solution containing 5% w/v sodium chloride and 0.1% w/v sucrose in a 20 cc vial was used for these experiments. The freezing profile was as follows: cool to +5 °C at 1 °C/min, hold for 15 minutes

for thermal equilibration, cool at 1 °C/min to the temperature at which ice nucleation was to be initiated and followed by a hold for 30 minutes. The ice nucleation was initiated using FreezeBooster® and the cooling was further continued to the final freezing set point of -40 °C at 1 °C/min with a hold time of 2 hours. Following freezing, primary drying was initiated by ramping up the shelf temperature at 1 °C/min to -20 °C and a chamber pressure of 60 mTorr. Instantaneous sublimation rate, *dm/dt,* was measured using Tunable Diode Laser Absorption Spectroscopy (TDLAS) (Gieseler et al. 2007) over 160 vials. Using this instantaneous *dm/dt*, product dry layer resistance R_p and dry layer thickness, l_{dry} were calculated as shown below.

Calculation of R_p:

Equations 2 and 4 were rearranged to determine the instantaneous temperature at the sublimation interface, T_0 followed by the vapor pressure at the sublimation interface, P_0 using Equation 6. The instantaneous product dry layer resistance R_p was then calculated using Equation 5 and the resistance due to stopper R_s was ignored since it is negligible as compared to R_p (Pikal 1985).

Calculation of l_{dry}:

For each time interval during primary drying (per minute), the amount of ice sublimed, Δm_i, was calculated as the product of the mean sublimation rate over the interval and the time step over that interval, $(t_i - t_{i-1})$given by Equation 11

$$\Delta m_i = 0.5 \cdot \left[\left(\frac{dm}{dt}\right)_i + \left(\frac{dm}{dt}\right)_{i-1}\right] \cdot (t_i - t_{i-1}) \qquad \text{Equation 11}$$

The total amount of ice sublimed over time t_n, $\Delta m(t)$, was calculated as the sum of all Δm_i from the beginning of primary drying, $i = 0$ mins, to the time of interest, $i = n$ mins by

$$\Delta m(t) = \sum_{i=0}^{n} \Delta m_i \qquad \text{Equation 12}$$

The thickness of the frozen layer, l_{ice}, was then calculated using Equation 13

$$l_{ice} = l_{max} \cdot \left[1 - \left(\frac{\Delta m(t)}{\Delta m_{H_2O}}\right)\right] \qquad \text{Equation 13}$$

where l_{max} is the maximum thickness of the frozen layer (and maximum thickness of the dry layer, at the end of primary during), and Δm_{H_2O} is the total amount of water per vial. For each time point (every minute) in primary drying, an average thickness of the dry layer was computed using Equation 14

$$l_{dry} = l_{max} - l_{ice} \qquad \text{Equation 14}$$

The product resistance as a function of the dry layer thickness, was then fitted by the empirical relationship:

$$R_p = \left[R_o + \frac{A_1 \cdot l_{dry}}{1 + A_2 \cdot l_{dry}}\right] \qquad \text{Equation 15}$$

where R_p is the measured dry layer product resistance to the water vapor leaving the ice surface through the dried cake of thickness, l_{dry} (Pikal 1985). The parameters, R_o, A_1, and A_2, were used to fit the shape of the R_p versus l_{dry} curve.

4.5. Model system

Sodium chloride at a concentration of 5% w/v (eutectic temperature of -21 °C) with 0.1% w/v sucrose was used as a model system to compare the experimental data to the theoretical calculations. Sucrose was added in very small quantities to the sodium chloride solution to prevent blow out of crystalline sodium chloride at the initiation of primary drying due to the high

sublimation rate in the absence of any dry product layer at the beginning. Fill volume of 3 ml in a 20 cc vial was used. Primary drying was carried out at a shelf temperature of -20 °C and chamber pressure of 60 mTorr. Two vials in the extreme sides of the front row (2 front corner vials) were left empty since they were placed on the thermocouples affixed to the shelves to monitor the shelf surface temperature during the experiment.

5. RESULTS AND DISCUSSION

5.1. Variation in shelf temperature

The shelf surface temperature as measured using the self-adhesive thermocouples during a freeze-drying cycle for a solution containing 5% w/v sodium chloride and 0.1% w/v sucrose was found to be -20 ± 1 °C during primary drying. The variation in shelf temperature was approximated as a linear distribution within 1 °C between the warm spot near the inlet of the heat transfer fluid and the cold spot near the outlet of the heat transfer fluid as shown in Figure 3. In our experience, at least at low to moderate thermal loads, variation in shelf surface temperature does not appear to be a major source of variation in heat transfer.

5.2. Variation in fill volume

The variation in fill volume was determined from the distribution of the weight of water over 640 vials. The most significant data are at the higher end of the range, since the material in those vials will take longer to complete primary drying. The porous cake in the vials that have not completed primary drying and still contain ice crystals will collapse when the remaining ice melts as the shelf temperature is increased to secondary drying set point. Figure 4 shows a frequency distribution of fill weights over 640 vials using a fill volume of 3 ml containing 5% w/v sodium chloride with 0.1% w/v sucrose. The “outliers” at 3.06 g in Figure 4 are important

data points as the product in those vials are more likely to undergo collapse if not completely dried.

5.3. Variation in vial heat transfer coefficient

Vial heat transfer coefficient, K_v is one of the important parameters needed for designing a freeze-drying cycle for a new product or to scale-up an already existing cycle from laboratory scale to manufacturing scale. According to Equation 1, at any shelf temperature the heat transferred to the product from the shelf only is proportional to the K_v value for that vial. K_v, can be expressed as the sum of three contributions as given by Equation 16:

$$\boldsymbol{K_v = K_c + K_r + K_g(P_c)} \qquad \text{Equation 16}$$

where K_c is the coefficient for direct conduction through the points of contact between the vials and shelf, K_r is the coefficient for radiative heat transfer and K_g is the coefficient for gas conduction between the shelf and bottom of the vial (all coefficients with the units of $cal \cdot s^{-1} \cdot cm^{-2} \cdot K^{-1}$) (Pikal 1985). Both K_c and K_r are independent of chamber pressure. However, K_g, often the largest contributor to K_v, increases non-linearly with pressure (Pikal 1985). A position-based heterogeneity in heat transfer rates for a vial will lead to different thermal profiles for the product in the vials on the same shelf. In general, vials at the edge of the shelf get a view of the warmer surfaces in the freeze-drying chamber such as the chamber walls and the door. At lower shelf temperatures, the edge vials receive additional heat due to atypical radiation from these warm surfaces leading to a higher product temperature and faster drying time (Brülls and Rasmuson 2002; Pikal, Roy, Shah 1984; Rambhatla and Pikal 2003). Alternatively, vials closer to the condenser chamber lose some energy due to radiation to the condenser plate leading to a lower product temperature and hence slower drying behavior of the product in those vials.

Figure 5 shows a combined distribution of the vial heat transfer coefficients over 800 vials determined using Equations 9 and 10 for 20 cc vials containing 3 ml fill of deionized water at a shelf temperature of -20 °C and chamber pressure of 60 mTorr. The distribution is skewed with a long tail depicting existence of edge vials with the higher K_v values and other remaining vials with intermediate K_v values. The average K_v was found to be 3.17×10^{-4} cal·cm^{-2}·sec^{-1}·K^{-1} with a standard deviation of 0.65×10^{-4} cal·cm^{-2}·sec^{-1}·K^{-1}. If the primary drying step is set using the average K_v, the vials with K_v value lower than that, especially the ones at the data point 2.38×10^{-4} cal·cm^{-2}·sec^{-1}·K^{-1} will not be completely devoid of ice when transitioning from primary to secondary drying. This would lead to a loss of product cake structure in these vials due to exceeding the critical temperature, the primary reason being the presence of remaining ice. Alternatively, the product temperature for the vials with K_v values higher than the average will be higher at any given shelf temperature. If an aggressive primary drying shelf temperature is being used for a product with the knowledge of the average K_v value, care needs to be taken to not exceed the critical temperature in the vials with K_v's higher than the average (especially at the data point 5.578×10^{-4} cal·cm^{-2}·sec^{-1}·K^{-1}).

5.4. Variation in dry product layer resistance

During the freezing step of lyophilization, pure water does not freeze spontaneously at the equilibrium freezing point and remains in the liquid state well below 0 °C (even 10 to 15 degrees) which is termed as supercooling (Rambhatla et al. 2004). The onset of ice nucleation is a stochastic process, which depends on the properties of the solution and the process conditions (Pikal, Rambhatla, Ramot 2002). The degree of supercooling affects the size of the ice crystals formed thus, affecting the resulting pore structure in the dry cake, which forms during primary drying. This consequently changes the resistance posed to the vapor flow by the dry product

layer, R_p, when moving from the sublimation front to the empty space in the vial (Searles, Carpenter, Randolph 2001a). For example, lower degree of supercooling in a vial (nucleation at higher temperatures) results in larger size ice crystals during freezing, larger pores during primary drying leading to a lower resistance of the dry product layer and hence a shortened primary drying time.

In our experience at laboratory scale, a range of ice nucleation temperatures from -10 °C to -20 °C over a batch of vials during freeze-drying experiments using 5% w/v sodium chloride with 0.1% w/v sucrose was observed. In a typical Class 100 environment in the pharmaceutical manufacturing areas, the degree of supercooling can be even higher (Rambhatla et al. 2004). This range of ice nucleation temperatures leads to a range in dried layer resistance for vials within a batch.

In order to determine the dependence of average R_p on the nucleation temperature (T_{nuc}), ice nucleation was controlled during lyophilization experiments using FreezeBooster® nucleation technology (as described in Section 4.4.). Instantaneous R_p and l_{dry} were calculated during the experiments at one-minute intervals and fitted to Equation 15. A linear relationship between R_p and l_{dry} was observed at all nucleation temperatures for the sodium chloride system. A representative plot of R_p versus l_{dry} at an ice nucleation temperature of -9.3 °C is shown in Figure 6 where R_o, A_1, and A_2 were found to be 1.3, 7.6 and 0, respectively. The fitting parameters R_o, A_1, and A_2 were obtained for all the six controlled nucleation experiments. Absolute nucleation temperatures (T_{nuc}) were then plotted with R_p obtained from the experimental data (Figure 7). Natural log dependence between average R_p and absolute T_{nuc} was observed. Using y = 1.2687ln(x) + 0.2291 obtained from Figure 7, average R_p was calculated for nucleation temperatures ranging from -5 to -17 °C (range of nucleation temperatures observed during a

regular freeze-drying experiment without controlled nucleation). The resistance was related to nucleation temperature by an ice nucleation temperature-dependent factor, F_{Tnuc}, specific for that material (sodium chloride) as described in Equation 17.

$$R_{p,nuc} = \mathrm{F}_{T_{nuc}} \cdot \left[R_o + \frac{A_1 \cdot l_{dry}}{1 + A_2 \cdot l_{dry}} \right] \qquad \text{Equation 17}$$

The temperature-dependent factor allowed maintaining the general shape of R_p versus l_{dry} curve simultaneously accounting for an increase in resistance as ice nucleation temperature decreased. In order to determine $F_{T,nuc}$, -5 °C was used as the reference point and a value of 1.0 for $F_{T,nuc}$ was assumed at -5 °C. For any other nucleation temperature below -5 °C, $F_{T,nuc}$ was calculated as a ratio between the R_o at that nucleation temperature to that of R_o at -5 °C . A plot of $F_{T,nuc}$ versus nucleation temperatures is shown in Figure 8. Using the relationship from Figure 8, $F_{T,nuc}$ was calculated for nucleation temperatures ranging from -10 to -20 °C that were observed during spontaneous ice nucleation during an uncontrolled freeze-drying cycle. Distribution for $F_{T,nuc}$ values is shown in Figure 9.

It should be noted that due to the difficulty in effectively controlling the ice nucleation below -10 °C over the entire shelf of vials, the controlled nucleation experiments were performed within a range of -5 to -10 °C. However, the spontaneous nucleation temperatures usually observed during uncontrolled freeze-drying experiments is outside this range of control nucleation experiments. This is one of the limitations of the model to be considered.

5.5. Comparison between theoretical and experimental data

Frequency distributions for the four input variables (Figures 3-5, 9) were used to calculate the probabilities of all their possible combinations. For each of the combinations of

input variables, the primary drying times and maximum product temperatures were calculated using the model developed and are shown in Figure 10. The full range of drying times and product temperatures as predicted from the model is much wider than will be experienced by the product in the majority of vials. The total primary drying time ranges from 9.7 hours to 21.8 hours and the maximum product temperature from -35.2 to -30.0 °C. However, most of the product in the vials experiences a much lower range.

Table I shows data at selected values of cumulative frequency extracted from Figure 10. The values corresponding to cumulative frequency of 0.05 and 0.95 can be used to produce a 90% confidence interval, given by -34.1 to -31.4 °C for maximum product temperature, and 11.5 to 16.6 hours for time to complete primary drying. These ranges still seem unacceptably large for real variation in a batch of lyophilized product. However, low product temperatures do not result in product defects; more often, those vials containing product that exceeds a temperature will undergo product collapse, resulting in an unacceptable product appearance, higher reconstitution time, and higher residual moisture. (Of course, none of these is true for 5% NaCl, but this formulation was simply used as a model formulation that undergoes primary drying only and does not proceed to secondary drying.) Similarly, a short time to complete primary drying does not result in product defects; more often, those vials containing product that takes a long time to complete primary drying may not in fact complete sublimation of all ice before the temperature is raised for the secondary drying cycle. In those cases, product collapse may occur and high residual moisture content is likely.

If one uses the batch average, the maximum product temperature is calculated to be -33.3 °C and the time to complete primary drying is calculated to be 12.3 hours. However, if one were to set the primary drying cycle time to 12.3 hours, only half the vials would be dry. More often,

a safety margin of about an additional 30% is used and perhaps 16 hours would be set for the primary drying cycle time. However, according to Table I, even 16 hours would not be sufficient to dry the vials which have the lowest product temperature on the shelf which would lead to a potential cake collapse in those colder vials. Thus, instead of an arbitrary or rule-of-thumb safety margin, the data on variation (Figure 10) allows the primary drying cycle time to be set according to the tolerance for incomplete drying. For example, in this case, there is a 10% probability (from cumulative frequency of 0.9 in the above table) of a vial to contain crystalline water at 15.3 hours; there is a 1% probability (from cumulative frequency of 0.99) of a vial containing crystalline water at 19.6 hours; at 21.7 hours, we have better than six sigma assurance. The accuracy of the frequency distribution, particularly in the tails of the distribution, is critical to obtain a true measure of the vials where product will exceed a certain maximum product temperature or not have completed primary drying within a certain cycle time.

In order to verify the calculations, a solution of 5% w/v sodium chloride and 0.1% w/v sucrose was used since it showed clear noticeable loss of structure when the temperature exceeded the critical temperature. A eutectic system was chosen for this study since the loss in the cake structure could be observed more readily when the critical temperature was exceeded as compared to an amorphous system. Also, eutectic system posed another advantage of absence of any unfrozen water on freezing that avoided complications due to use of the secondary drying step. Several freeze-drying experiments using conservative shelf temperatures during primary drying such that all the vials are maintained below the eutectic temperature (-21 °C for sodium chloride) were performed. However, during these experiments the primary drying was stopped abruptly and the product temperature was increased to room temperature after various times in primary drying. These times span the range from few to significant numbers of vials projected

(by the calculations) to be still in primary drying at the point of increasing the product temperature. The loss in structure was due to exceeding the eutectic temperature, however, the actual reason being incomplete removal of water due to shortened primary drying time from the vials that tend to dry slowly. High solubility of sodium chloride made it possible to analyze 160 vials in less than 20 minutes due to an immediate loss of structure as sodium chloride dissolved in the residual water.

The calculated and observed percentage of vials not dried was then compared (Figure 11). There is a very good agreement between the predicted and the observed primary drying times. Figure 12 shows the distribution of dried vials at various primary drying times as obtained from experimental data. The increasing number of vials with dry product can be seen as the cycle time increases from 14.4 to 18.0 hours. As expected, the edge vials generally dry before center vials. However, this is not always the case, since there is a difference in product resistance depending on the temperature of ice nucleation in each vial. The random nature of ice nucleation is evident from the pattens above. The "collapse" or melt-back, in this case, is not simply position dependent.

6. CONCLUSIONS

In this study, variation in four input parameters namely; fill volume, shelf temperature, vial heat transfer coefficient and dry layer product resistance were obtained from experimental data. Protocols for accurate measurement of variation in the input parameters were identified. All the possible combinations of these input variables together with their frequency distributions obtained from the experiments, were treated with previously established steady-state heat and mass transfer theory to obtain maximum primary drying temperatures and primary drying times.

Such a prediction would allow economic analysis of the cost of process changes, where cost is determined by the cost of product rejects plus the cost of extended cycles designed to reduce such rejects.

Variation in maximum product temperature was relatively small for the examples studied here, but that may not be a perfectly general result. In general, variation in maximum product temperature would be expected to be most serious with a low collapse temperature product where the resistance versus dry layer thickness dependence is strong and linear. Variation in drying time appeared to be of greater practical significance, at least for the sodium chloride system studied. A good quantitative agreement between average drying time predicted from the model and that observed experimentally was observed. It was found that variations in the vial heat transfer coefficient and product resistance were the dominant contributors to the variation in the primary drying time and maximum product temperature. Product resistance was the least well characterized parameter since it could be determined only for controlled nucleation temperatures less than -10 °C and needed to be extrapolated to lower nucleation temperatures from -10 °C to -19 °C (observed nucleation temperatures in the laboratory scale with spontaneous nucleation) using natural log dependence. This dependence of the product resistance on the nucleation temperature will change with formulation.

Future studies will focus on extending the use of the model to other pharmaceutical materials at different concentrations, which will pose a range of mass transfer resistances.

7. ACKNOWLEDGEMENTS

The authors would also like to thank Dr. Ken Qian, Charlie Jones, and Johanna Rivera for helping with a few of the early on studies and Dr. Steve Nail for the in-depth discussions on measurement of vial heat transfer coefficient. This work was funded by # FDA-09-1062623-SS.

8. REFERENCES

Awotwe-Otoo D, Agarabi C, Read EK, Lute S, Brorson KA, Khan MA, Shah RB. 2013. Impact of controlled ice nucleation on process performance and quality attributes of a lyophilized monoclonal antibody. Int J Pharm 450(1):70-8.

Bhatnagar BS, Bogner RH, Pikal MJ. 2007. Protein stability during freezing: Separation of stresses and mechanisms of protein stabilization. Pharm Dev Technol 12(5):505-23.

Brülls M and Rasmuson A. 2002. Heat transfer in vial lyophilization. Int J Pharm 246(1):1-16.

Carpenter JF, Pikal MJ, Chang BS, Randolph TW. 1997. Rational design of stable lyophilized protein formulations: Some practical advice. Pharm Res 14(8):969-75.

Chang BS, Kendrick BS, Carpenter JF. 1996. Surface-induced denaturation of proteins during freezing and its inhibition by surfactants. J Pharm Sci 85(12):1325-30.

Fissore D, Pisano R, Barresi AA. 2011. Advanced approach to build the design space for the primary drying of a pharmaceutical freeze-drying process. J Pharm Sci 100(11):4922-33.

Gieseler H, Kramer T, Schneid S. 2008. Quality by design in freezedrying: Cycle design and robustness testing in the laboratory using advanced process analytical technology. Pharm Technol 10:88-95.

Gieseler H, Kessler WJ, Finson M, Davis SJ, Mulhall PA, Bons V, Debo DJ, Pikal MJ. 2007. Evaluation of tunable diode laser absorption spectroscopy for in-process water vapor mass flux measurements during freeze drying. J Pharm Sci 96(7):1776-93.

Giordano A, Barresi AA, Fissore D. 2011. On the use of mathematical models to build the design space for the primary drying phase of a pharmaceutical lyophilization process. J Pharm Sci 100(1):311-24.

Jameel F and Khan M. 2009. Quality-by-design as applied to the development and manufacturing of a lyophilized protein product. Am Pharm Rev 12(7).

Jansco G, Pupezin J, Van Hook WA. 1970. The vapor pressure of ice between 10– 2 and– 10 2◦ C. J Phys Chem 74:2984-9.

Kasper JC and Friess W. 2011. The freezing step in lyophilization: Physico-chemical fundamentals, freezing methods and consequences on process performance and quality attributes of biopharmaceuticals. European Journal of Pharmaceutics and Biopharmaceutics 78(2):248-63.

Koganti VR, Shalaev EY, Berry MR, Osterberg T, Youssef M, Hiebert DN, Kanka FA, Nolan M, Barrett R, Scalzo G. 2011. Investigation of design space for freeze-drying: Use of modeling for primary drying segment of a freeze-drying cycle. AAPS PharmSciTech 12(3):854-61.

Konstantinidis AK, Kuu W, Otten L, Nail SL, Sever RR. 2011. Controlled nucleation in freeze-drying: Effects on pore size in the dried product layer, mass transfer resistance, and primary drying rate. J Pharm Sci 100(8):3453-70.

Liu Y, Zhao Y, Feng X. 2008. Exergy analysis for a freeze-drying process. Appl Therm Eng 28(7):675-90.

Mockus LN, Paul TW, Pease NA, Harper NJ, Basu PK, Oslos EA, Sacha GA, Kuu WY, Hardwick LM, Karty JJ. 2011. Quality by design in formulation and process development for a freeze-dried, small molecule parenteral product: A case study. Pharm Dev Technol 16(6):549-76.

Nail SL and Searles JA. 2008. Elements of quality by design in development and scale-up of freeze-dried parenterals. BioPharm International 21(1).

Pikal MJ. 2002. Freeze drying. Encyclopedia of Pharmaceutical Technology, Marcel Dekker, New York 1299:1326.

Pikal M, Rambhatla S, Ramot R. 2002. The impact of the freezing stage in lyophilization: Effects of the ice nucleation temperature on process design and product quality. American Pharmaceutical Review 5:48-53.

Pikal M, Shah S, Senior D, Lang J. 1983. Physical chemistry of freeze-drying: Measurement of sublimation rates for frozen aqueous solutions by a microbalance technique. J Pharm Sci 72(6):635-50.

Pikal MJ. 1985. Use of laboratory data in freeze drying process design: Heat and mass transfer coefficients and the computer simulation of freeze drying. J Parenter Sci Technol 39(3):115-39.

Pikal MJ, Roy ML, Shah S. 1984. Mass and heat transfer in vial freeze-drying of pharmaceuticals: Role of the vial. J Pharm Sci 73(9):1224-37.

Pisano R, Fissore D, Barresi AA, Brayard P, Chouvenc P, Woinet B. 2013. Quality by design: Optimization of a freeze-drying cycle via design space in case of heterogeneous drying behavior and influence of the freezing protocol. Pharm Dev Technol 18(1):280-95.

Rambhatla S, Ramot R, Bhugra C, Pikal MJ. 2004. Heat and mass transfer scale-up issues during freeze drying: II. control and characterization of the degree of supercooling. Aaps Pharmscitech 5(4):54-62.

Rambhatla S and Pikal MJ. 2003. Heat and mass transfer scale-up issues during freeze-drying, I: Atypical radiation and the edge vial effect. AAPS PharmSciTech 4(2):111-20.

Ratti C. 2001. Hot air and freeze-drying of high-value foods: A review. J Food Eng 49(4):311-9.

Sane P, Pikal M, Nail S, Bogner R. Measurement of heat transfer to vials on a freeze-dryer shelf during primary drying. Manuscript in Preparation .

Searles JA, Carpenter JF, Randolph TW. 2001. The ice nucleation temperature determines the primary drying rate of lyophilization for samples frozen on a temperature-controlled shelf. J Pharm Sci 90(7):860-71.

Short SM, Cogdill RP, Drennen III JK, Anderson CA. 2011. Performance-based quality specifications: The relationship between process critical control parameters, critical quality attributes, and clinical performance. J Pharm Sci 100(4):1566-75.

Sundaram J, Hsu CC, Shay YM, Sane SU. 2010. Design space development for lyophilization using DOE and process modeling. BioPharm International 23(9).

Tang XC, Nail SL, Pikal MJ. 2005. Freeze-drying process design by manometric temperature measurement: Design of a smart freeze-dryer. Pharm Res 22(4):685-700.

9. FIGURES

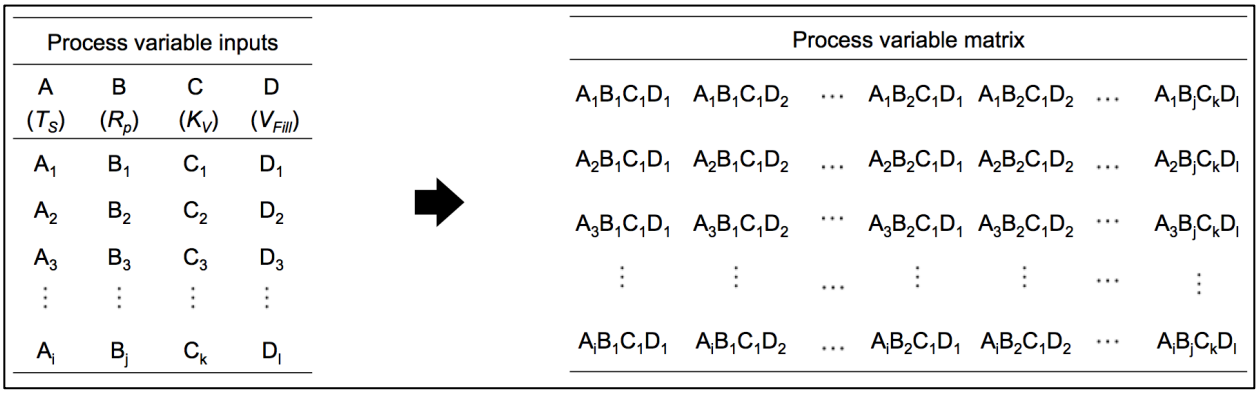

Figure 1- Processing variable matrix denoting the four input variables (A = shelf temperature, T_s, B = dry layer product resistance R_p, C = vial heat transfer coefficient, K_v, D = fill volume V_{fill}) and their combinations used to determine the key output parameters: maximum product temperature, T_{max} and primary drying time, t_{dry}.

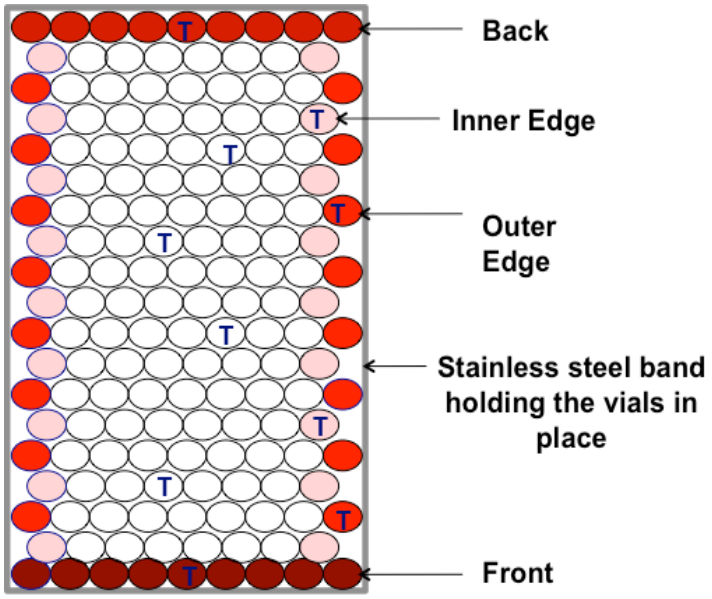

Figure 2 - Hexagonal arrays of 20 cc vials on a single shelf where each circle represents an individual vial. The five-category classification of vials on a shelf has been shown along with the placement of the thermocouples (shown as a "T" in the circle)

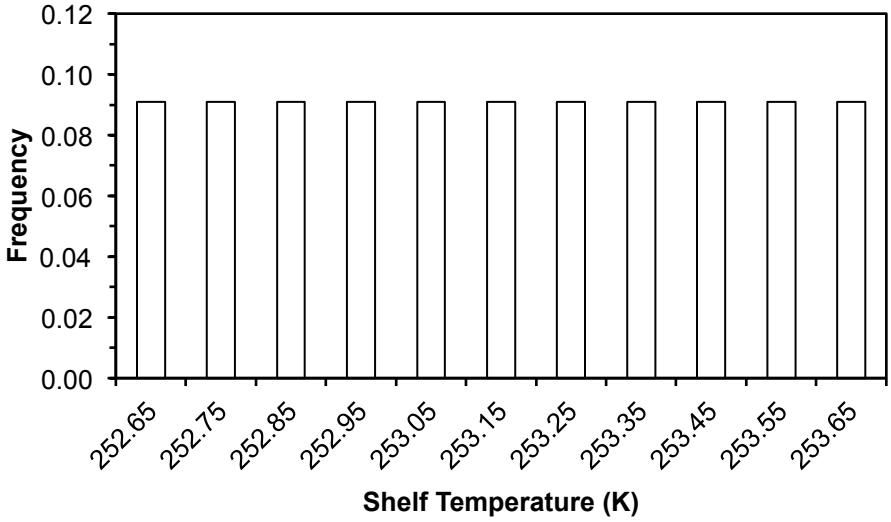

Figure 3 - A linear gradient approximation of the shelf temperature across a -20 °C controlled shelf.

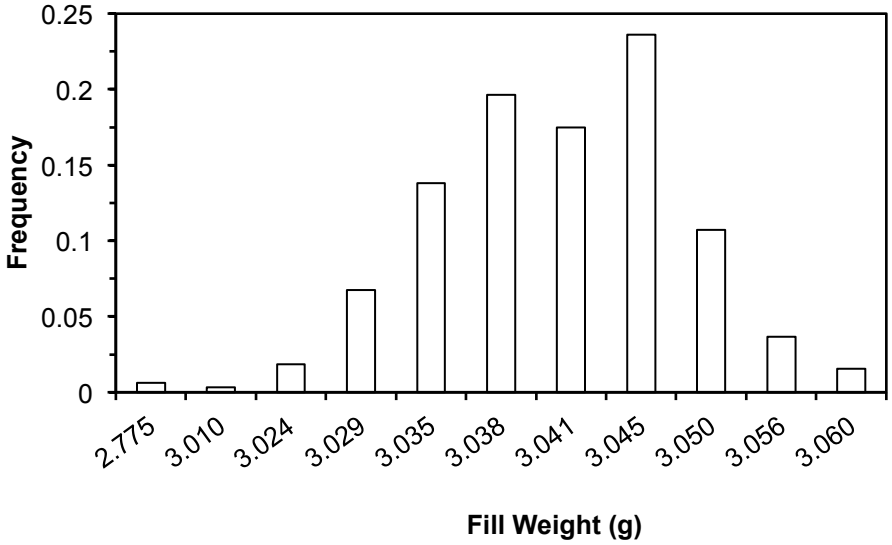

Figure 4 - Variation in fill weight using 3 ml of 5% w/v sodium chloride with 0.1% w/v sucrose (n=640).

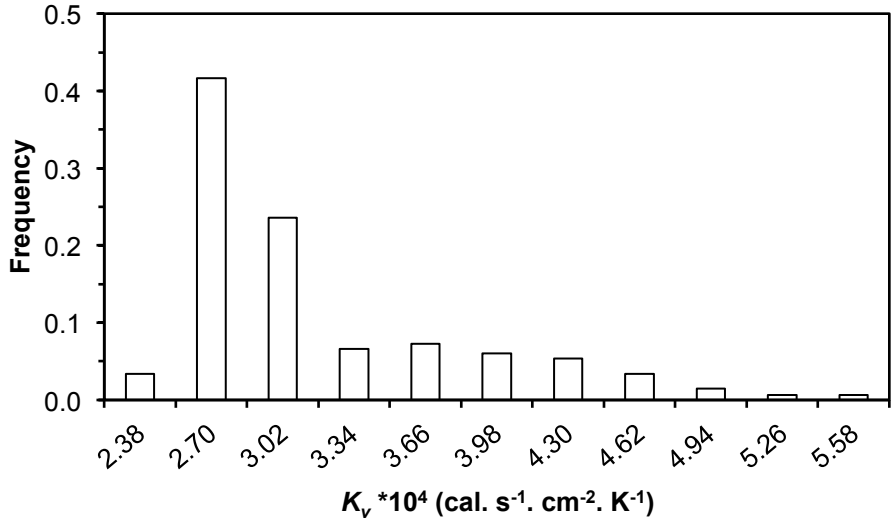

Figure 5 - Frequency distribution of vial heat transfer coefficient using a 3 ml fill volume of deionized water at a shelf temperature of -20 °C and chamber pressure of 60 mTorr (n = 800).

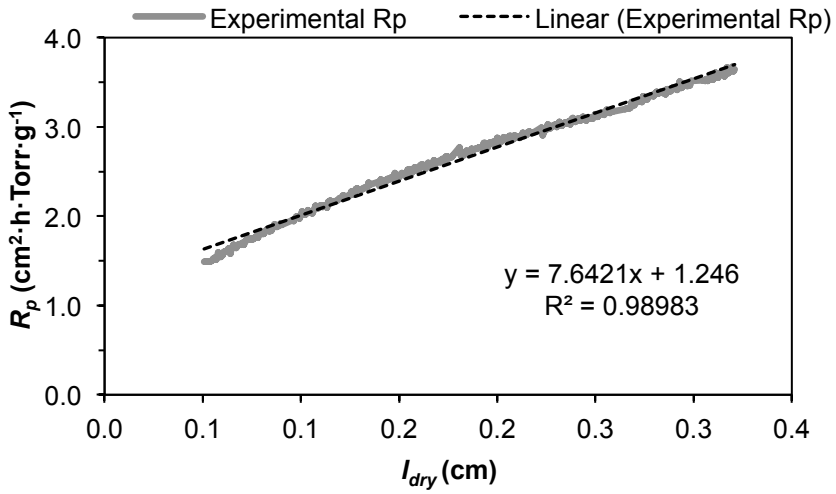

Figure 6 - Linear relationship between R_p versus l_{dry} for formulation containing 5% w/v sodium chloride and 0.1% w/v sucrose obtained by controlling ice nucleation at -9.3 °C.

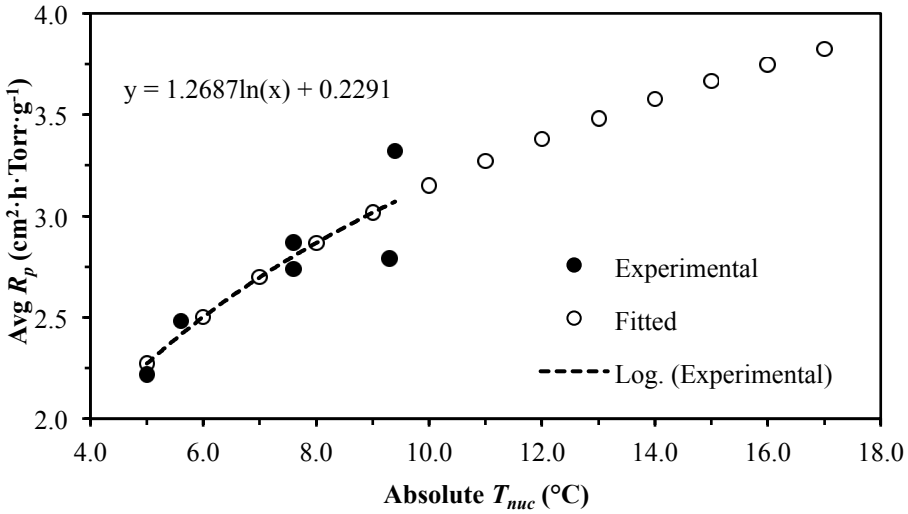

Figure 7 - Experimental average dry product layer resistance (R_p) (closed circles) from six controlled nucleation freeze-drying experiments ranging from -5 to -10 °C and R_p extrapolated using natural log dependence (open circles) for T_{nuc} from -5 to -17 °C.

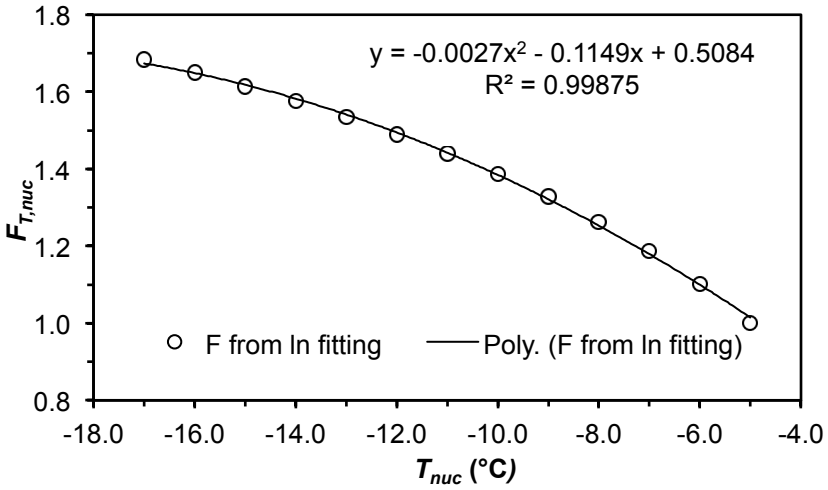

Figure 8 - Plot of $F_{T,nuc}$ versus ice nucleation temperatures ranging from -5 to -17 °C representing the temperatures observed during freeze-drying experiments with uncontrolled ice nucleation.

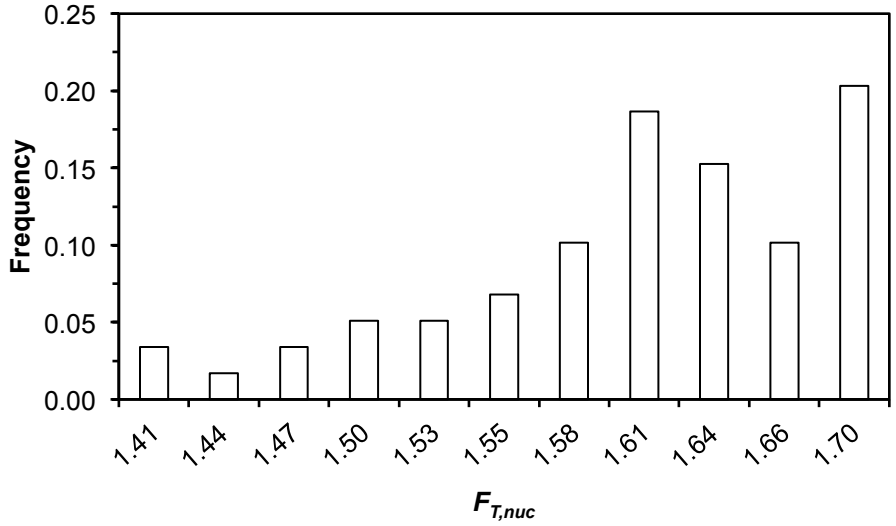

Figure 9 - Histogram for $F_{T,nuc}$ obtained for ice nucleation temperatures from (-10 to -20 °C) observed during spontaneous ice nucleation during an uncontrolled freeze-drying cycle.

a)

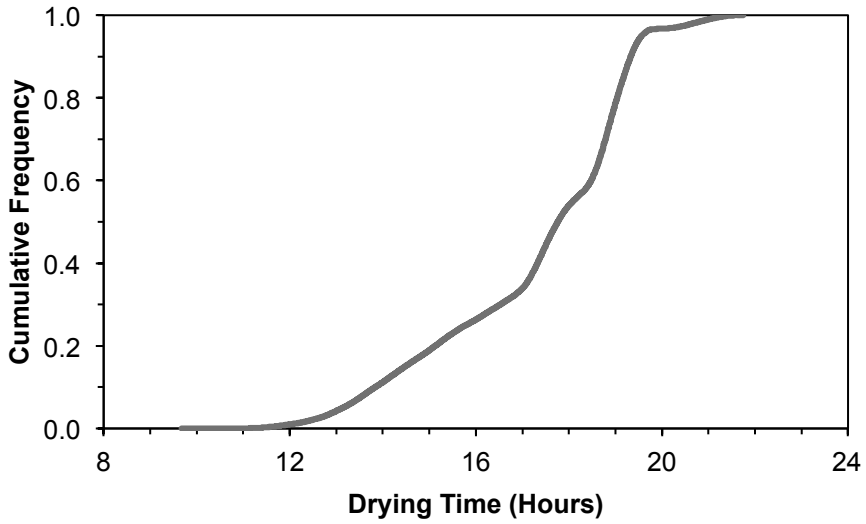

b)

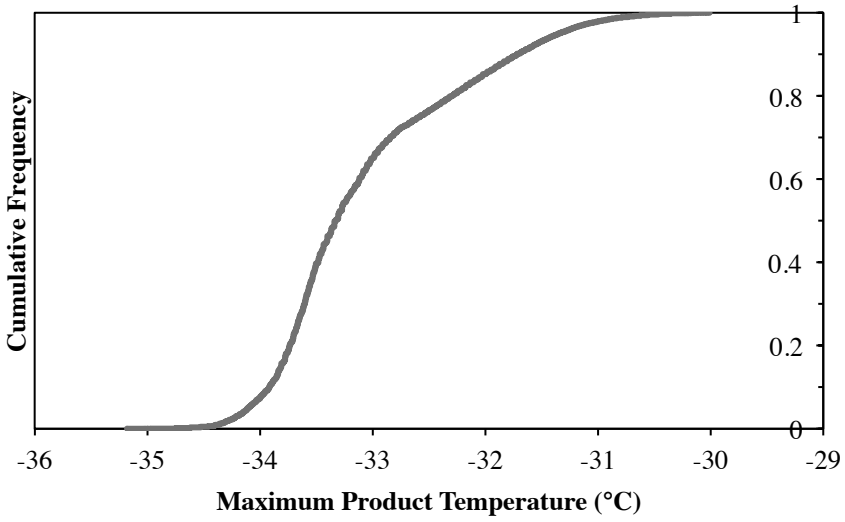

Figure 10 - Distribution of (a) primary drying times and (b) maximum product temperatures obtained by using the frequency distribution for the input variables

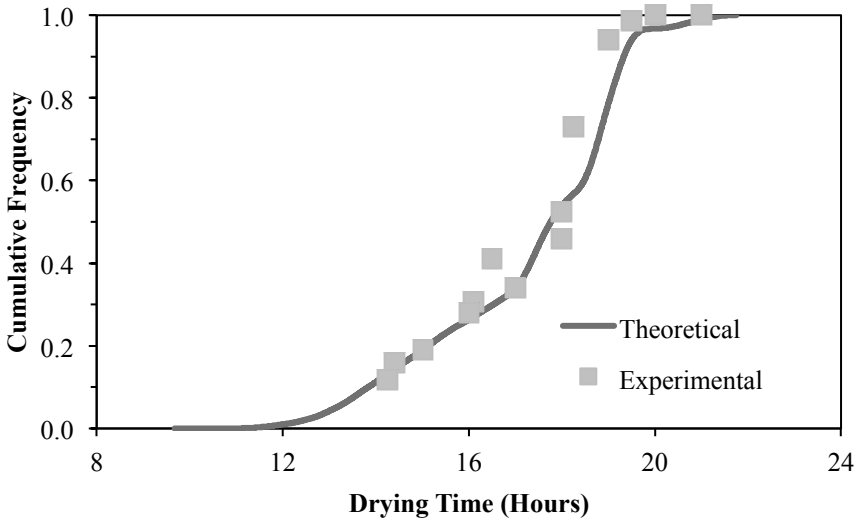

Figure 11 - Comparison between theoretical calculations and experimental results showing cumulative frequency of number of vials that are completely dry at any given primary drying time.

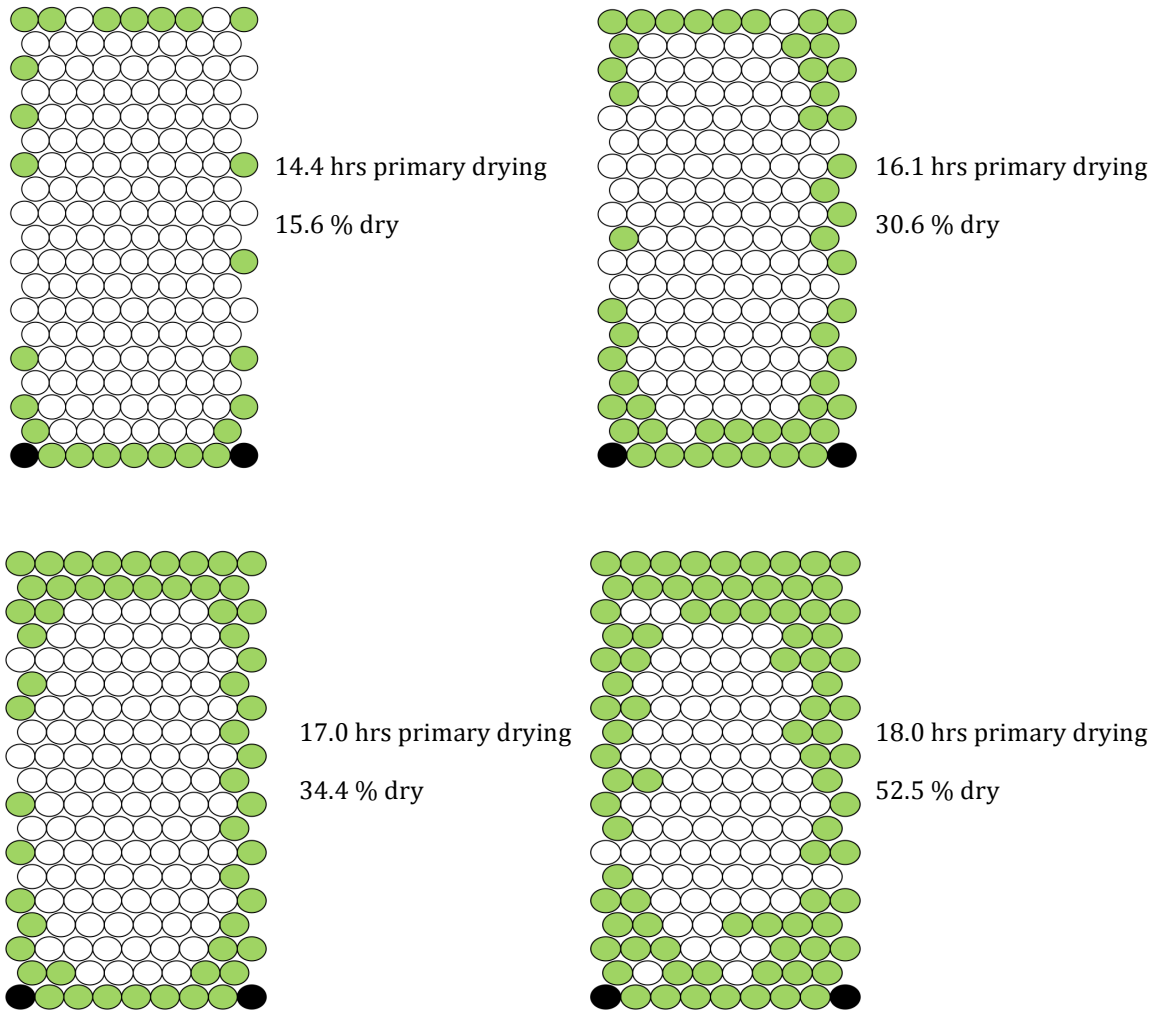

Figure 12 - Distribution of vials containing 5% sodium chloride with 0.1% sucrose that are dry at different primary drying times.

● → vials with collapsed product, ○ → vials completely dry, ● → empty vials

Table I: Data from Figure 10 at selected values of cumulative frequency.

Cumulative Frequency	**Maximum Product Temperature (°C)**	**Primary Drying Time (Hours)**
0.05	-34.1	11.5
0.1	-33.9	11.7
0.25	-33.7	11.9
0.5	-33.3	12.3
0.75	-32.6	13.4
0.9	-31.7	15.3
0.95	-31.4	16.6
0.99	-30.8	19.6
0.999	-30.3	21.2
6σ	-30.0	21.7

Chapter 4

Spatial Variation of Pressure in the Lyophilization Product Chamber: Experimental Measurements and Implications For Scale-up and Batch Uniformity*

*This manuscript was first published in AAPS Pharm Sci Tech (Sane, Pooja, et al. "Spatial Variation of Pressure in the Lyophilization Product Chamber Part 2: Experimental Measurements and Implications for Scale-up and Batch Uniformity." *AAPS PharmSciTech* (2016): 1-12.)

1. ABSTRACT

Product temperature during the primary drying step of freeze-drying is controlled by a set point chamber pressure and shelf temperature. However, recent computational modeling suggests a possible variation in local chamber pressure. The current work presents an experimental verification of the local chamber pressure gradients in a lab-scale freeze-dryer. Pressure differences between the center and the edges of a lab-scale freeze-dryer shelf were measured as a function of sublimation flux and clearance between the sublimation front and the shelf above. A modest 3 mTorr difference in pressure was observed as the sublimation flux was doubled from 0.5 to 1.0 $kg \cdot hr^{-1} \cdot m^{-2}$ at a clearance of 2.6 cm. Further, at a constant sublimation flux of 1.0 $kg \cdot hr^{-1} \cdot m^{-2}$, an 8-fold increase in the pressure drop was observed across the shelf as the clearance was decreased from 4 to 1.6 cm. Scale-up of the pressure variation from lab- to a manufacturing-scale freeze-dryer predicted an increased uniformity in drying rates across the batch for two frequently used pharmaceutical excipients (mannitol and sucrose at 5% w/w). However, at an atypical condition of shelf temperature of +10 °C and chamber pressure of 50 mTorr, the product temperature in the center vials was calculated to be a degree higher than the edge vial for a low resistance product, thus reversing the typical edge and center vial behavior. Thus, the effect of local pressure variation is more significant at the manufacturing-scale than at a lab-scale and accounting for the contribution of variations in the local chamber pressures can improve success in scale-up.

2. INTRODUCTION

Freeze-drying (lyophilization) continues to be the preferred method of drying for the increasing number of biotherapeutic products in the pharmaceutical market. Though it is one of the most expensive unit operations in the manufacturing of pharmaceutical products, drying at low temperatures reduces degradation of therapeutic proteins. Moreover, freeze drying offers excellent sterility assurance and freedom from foreign particles as well as low moisture and low headspace oxygen in the final container (Brülls and Rasmuson 2002; Carpenter et al. 1997).

Product temperature during the primary drying step is controlled through a combination of chamber pressure and shelf temperature appropriate for a particular product. The pressure in the drying chamber has potentially two opposing effects on the product temperature.

i. Heat transfer to the vial increases with increasing pressure. The heat transfer rate, dQ/dt ($cal \cdot s^{-1}$) from shelf to product is proportional to the vial heat transfer coefficient, K_v ($cal \cdot s^{-1} \cdot cm^{-2} \cdot K^{-1}$),

Equation 1

$$\frac{dQ}{dt} = A_v \cdot K_v \cdot (T_s - T_p)$$

where A_v (cm^2) is the cross sectional area of the vial, T_p (°C or K) is the temperature of the product at the inside bottom center of the vial, and T_s (using the corresponding temperature scale) is the temperature of the shelf surface (Pikal, Roy, Shah 1984; Pikal 1985). The vial heat transfer coefficient, K_v, is the sum of three contributions:

Equation 2

$$\boldsymbol{K_v = K_c + K_r + K_g(P_c)}$$

where the coefficients, K_c, K_r, and K_g (P_c) are associated with heat conduction through the points of contact between the vials and shelf, radiative heat transfer, and gas conduction between the shelf and bottom of the vial, respectively (Pikal 1985). Both K_c and K_r are independent of chamber pressure (P_c). However, K_g (P_c), often the largest contribution to K_v, increases non-linearly with pressure (Pikal 1985). At low to moderate pressures (25 to 100 mTorr), K_g, increases sharply with chamber pressure, and becomes less sensitive to changes in chamber pressures above 200 mTorr.

ii. The sublimation rate per vial, dm/dt ($g \cdot s^{-1}$), during primary drying is governed by the difference in the vapor pressure of ice at the sublimation interface, P_o, and the chamber pressure, P_c, in Torr.

Equation 3

$$\frac{dm}{dt} = A_p \cdot \frac{P_o - P_c}{R_{p,s}}$$

where $R_{p,s}$ ($cm^2 \cdot hr \cdot Torr \cdot g^{-1}$) is the resistance of the dry layer and stopper to vapor transfer; contribution of the stopper to the resistance is normally minimal and can be disregarded.

Equation 3 at first seems to suggest that an increase in the chamber pressure will decrease the driving force for sublimation, $(P_o - P_c)$. However, an increase in chamber pressure also results in an increase in the heat transfer rate to the product (Equations 1 and 2), which can increase the product temperature, including the temperature at the ice sublimation interface, T_o. Due to the exponential relationship between vapor pressure and the temperature at the sublimation interface (Jansco, Pupezin, Van Hook 1970), an increase in T_o results in a much larger increase in the vapor pressure of ice, P_o, and often

an increase in the driving force (P_o - P_c) for sublimation (Equation 3). Thus, an increase in chamber pressure generally increases the sublimation rate, but at high chamber pressure may slow sublimation.

The pressure in a freeze-drying chamber is ideally controlled to within a few mTorr by feedback from a single capacitance manometer. Any local variations in pressure in the chamber during primary drying can affect the local heat and mass transfer to the product and potentially lead to variation in product temperatures within a batch. In extreme cases, variation in product temperature can lead to a portion of the batch with collapsed product or having higher moisture content.

Recent studies using computational fluid dynamics (CFD) modeling have suggested spatial pressure variations in the drying chamber, particularly across the vial array on the shelf. Rasetto et al (Rasetto et al. 2008) modeled the vapor flow dynamics in a laboratory and a manufacturing scale freeze-dryer with chamber volumes of 0.2 and 10.3 m^3, respectively. In the manufacturing-scale dryers, their model suggested that the local pressure varied as much as 3.4 Pa (25 mTorr) over the shelf. Another study that added heat transfer to the CFD model to describe the drying of the product in each vial, found higher pressures in the center of the shelves when compared to the edges (Rasetto et al. 2010). At a clearance of 8.5 cm between shelves (corresponding to a 2.7 cm gap between the top of a typical 20 ml vial and the upper shelf), the model showed a pressure difference of 3.7 Pa (28 mTorr) during primary drying at a sublimation rate of 1 $kg \cdot hr^{-1} \cdot m^{-2}$. Zhang and Liu (Zhang and Liu 2012) derived a set of elegant equations to describe the vapor pressure in a manufacturing scale freeze-dryer based on a planar Couette flow with subliming boundary. Calculations for two example freeze-dryers indicated variable vapor concentrations within the drying chamber. The authors suggested that the variation in pressure

could be mitigated by increasing the distance between the shelves and adjusting the position of the duct that leads from the drying chamber to the condenser chamber. Similar results were also obtained by Varma et al (Varma et al.) from their model of the vapor flow field in the drying chamber of a laboratory scale dryer, at various chamber pressures, sublimation rates and clearances between the sublimation front and the upper shelf. The pressure variation between the center and edge along the length of the shelf was found to increase with sublimation rate in the range of 0.5 to 1.3 $kg \cdot hr^{-1} \cdot m^{-2}$ and as the clearance was decreased from 9 to 2.6 cm.

While several groups used mathematical models to suggest pressure gradients in the drying chamber during primary drying, there was no experimental evidence corroborating these findings. The goal of this work was to experimentally measure any spatial chamber pressure differences in a laboratory scale freeze-dryer under conditions corresponding to those used in the CFD studies by Varma et al (Varma et al.). In addition, the impact of spatial pressure variation on variation in primary drying time and product temperature was explored for two model systems, 5% sucrose and 5% mannitol, at lab and larger scales. Finally, to place the pressure variation impact on process in perspective, the variation in product temperature history caused by the local variation in chamber pressure was compared to the corresponding variation caused by variations in vial heat transfer coefficient and product resistance.

3. MATERIALS AND METHODS

Measurement of local pressure difference:

A uniform sublimation flux across a freeze-dryer shelf was used as a boundary condition in the CFD model of Varma et al (Varma et al.). In order to closely match this boundary condition experimentally, an ice slab was generated in lieu of product or ice in vials. Briefly, a

stainless steel band (3.5 cm in height; see (f) in Figure 1) that fit around the perimeter of the shelf (51 cm x 28 cm) was lined with thin, deformable black plastic sheeting (0.02 mm thickness; (e) in Figure 1) and placed on the bottom shelf in the drying chamber of a freeze dryer (LyoStar 3, SP Industries, Warminster, PA), where the upper shelves were in the topmost position (Figure 1). Distilled water was added to the plastic-lined band to a height of 3.2 cm. The thin plastic sheeting took the contour of the shelf when filled with water to provide uniform heat transfer from the shelf to the ice.

A false Plexiglas® shelf ((c) in Figure 1) was installed in the drying chamber just below the factory-installed upper shelf. The false shelf provided a uniform clearance, *h,* between the ice slab and the upper (in this case, false) shelf. The clearance between the ice and upper shelf, *h*, was intended to simulate the gap between the vial opening and upper shelf, since vapor would normally emanate from the vial opening (not from the point at which it leaves the ice within the vial) and flow through the space between the upper shelf and the top of the vials. Thus, h = 2.6 cm above a 20 cc vial would translate to a shelf-to-shelf distance of 3¼ inches (8.3 cm).

The CFD model of Varma et al (Varma et al.) indicated the highest pressure was at the center of the shelf as compared to the back (or front) edge. Thus, the freeze-dryer was outfitted to measure the pressure difference from the center to edge above an ice slab undergoing sublimation. In the LyoStar 3, the shelves are supported by stainless steel plates ((g) in Figure 1) which are solid except for slots to allow the shelves to move up and down. In the CFD model (Varma et al.), the supporting plates were represented as solid walls (i.e., zero mass flux boundary condition). To match the boundary conditions, the side slots in the support plates were taped off during experimental measurements. A differential capacitance manometer (CM), with a full scale range of 0-1000 mTorr (Model 226A, MKS, Andover, MA, see (j) in Figure 1) was

connected to two stainless steel tubes (¼" i.d.) of unequal length ((l) in Figure 1) fed through the Pirani port (a) on LyoStar 3 (Figure 1). The longer tube from the positive side and the shorter tube from the negative side of the differential CM were connected to stainless steel tubes (¼" i.d.) that led to the center ((b) in Figure 1) and the rear (not visible in Figure 1) positions of the false shelf (c), respectively. At each of these terminal positions in the chamber, the tubes were connected by elbow connectors to ports in the Plexiglas® false upper shelf (c) such that the measurement of pressure did not significantly alter the vapor flow in the chamber (Figure 1).

An ice slab was generated from the distilled water in the plastic by cooling the shelf to -40 °C for 30 minutes. The chamber pressure was then reduced to a set point (50, 60, 110, 115, 140, or 200 mTorr) and the zero velocity offset for the Tunable Diode Laser Absorption Spectrometer (Milton et al. 1997; Schneid et al. 2009) (TDLAS; Physical Sciences Inc., Andover, MA,) was determined. The clearance, h, between the ice slab surface and false upper shelf (c) was then set to 2.6 cm. The pressure difference between the center and back edge ports in the false upper shelf ($\Delta P_{c\rightarrow e} = P_{center} - P_{edge}$) was measured during sublimation of ice from the slab. Calibration of the zero point for $\Delta P_{c\rightarrow e}$ was a challenge, which is discussed in detail in Appendix I. The shelf temperature was raised periodically to produce a series of increasing sublimation rates which were measured by TDLAS. At each shelf temperature set point, the center to edge pressure difference ($\Delta P_{c\rightarrow e}$) was recorded after 30 minutes to allow the temperature gradient in the ice slab to reach steady state. Shelf temperature set points ranged from -30 °C to +35 °C. At the highest shelf temperature that could be reached without resulting in choked flow (Patel, Chaudhuri, Pikal 2010), the clearance between the false shelf and the ice slab surface, h, was adjusted to a series of values using the stoppering system and $\Delta P_{c\rightarrow e}$ was recorded 15 minutes after each adjustment of the distance h.

Freeze-drying cycles for representative pharmaceutical materials:

Mannitol (USP) and sucrose (USP) (Sigma Aldrich, St. Louis, MO) were used as representative crystalline and amorphous lyophilized solutes. Aqueous solutions at 5% (w/w) were filtered through a 0.22 μm membrane filter into 20 cc tubing vials (Amcor®, Madison, CT). For each solute, three full shelves (480 vials) were freeze-dried in a laboratory scale freeze-dryer (LyoStar 3, SP Industries, Warminster, PA). The same freezing protocol was used for both materials: using a cooling rate of 0.5 °C/min, the shelf was cooled to +5 °C, held for 30 minutes and cooled to -10 °C, held for 15 minutes. Ice nucleation was initiated at -10 °C using Praxair *ControLyo™ Nucleation on Demand Technology* installed on Lyostar 3. Once ice nucleated the shelves were immediately cooled to -40 °C and held for 2 hours. The remainder of the cycles differed significantly. The cycle specifics were:

5% w/v sucrose

- Fill volume: 3 ml
- Primary Drying: Shelf temperature of -25 °C and chamber pressure set to 65 mTorr for 24 hours.
- Secondary Drying: Shelf heated at 0.2 °C/min to 40 °C and held for 4 hours.

5% w/v mannitol

- Fill volume: 5 ml
- Primary Drying: Shelf temperature of +30 °C and chamber pressure set to 150 mTorr for 12 hours.
- Additional Drying: Shelf heated at 0.2 °C/min to 40 °C and held for 4 hours.

The surface temperature of the shelf was measured near the shelf fluid inlet and outlet of the bottom most shelf using self-adhesive copper-constantan thermocouples (Omega Engineering

Inc., Stamford, CT). The temperatures of other surfaces (i.e., door, walls for the shelf support and the steel band which holds the vials in place on a shelf) were also recorded. The temperatures of product at the bottom center of the vials were measured using 30 gauge copper-constantan (type-T) thermocouples (Omega Engineering Inc., Stamford, CT) with a resolution of ±0.1 °C. The product thermocouples were calibrated for 0.0 °C before each batch was freeze-dried using a mixture of ice and deionized water. In addition, wireless thermocouples, Tempris® (iQ Mobil, Holzkirchen, Bavaria, Germany) were used to record the product temperature in selected center vials. Chamber pressure was measured using the standard capacitance manometer installed in an upper port in the drying chamber. TDLAS was used to monitor the mass flow rate of water vapor through the duct leading to the condenser chamber.

Calculation of consequences of spatial variation in chamber pressure, product resistance and vial heat transfer coefficient

The fourth version of an Excel®-based lyo-calculator using previously established algorithms (Pikal 1985) was used to calculate the product temperature and primary drying time based on input parameters for dry layer product resistance, fill volume, solute concentration, chamber pressure, shelf temperature, vial heat transfer coefficient, and cross-sectional areas of the vial and product. High and low estimates for (i) resistance of dried product layer to water vapor flow for mannitol and sucrose at 5% w/v, (ii) vial heat transfer coefficient based on position of the vial (edge or center) on the shelf and (iii) accounting for local chamber pressure were used in the lyo-calculator to estimate the product temperature and primary drying time for each case. All other input parameters corresponded to a 20 cc vial, and shelf temperature and chamber pressure for each cycle as described in the previous section.

4. RESULTS

Spatial variation in local pressure in the drying chamber has been suggested by CFD models (Rasetto et al. 2008; Rasetto et al. 2010; Varma et al. ; Zhang and Liu 2012). However, to the authors' knowledge, the present report describes the first attempt to experimentally verify any local pressure difference in the drying chamber. The effects of sublimation rate and shelf-to-shelf clearance on experimentally measured local pressure differences are described below.

Local pressure at the center of the shelf was found to be higher than at the back edge of the shelf (Figure 2a). When the clearance between the ice and false upper shelf, h, was 2.6 cm there was a relatively small increase in pressure difference of 3 mTorr at the center as compared to the edge of the shelf when sublimation rate was doubled from 0.5 to 1.0 $kg \cdot hr^{-1} \cdot m^{-2}$. As sublimation flux increased, the concentration of vapor flowing from the sublimation front to the condenser increased. Due to the narrow space between the shelves, the resistance to vapor flow led to a measurable pressure drop from the center to the edge of the shelf (Zhang and Liu 2012). The center-to-edge difference in the pressure, $\Delta P_{c \rightarrow e}$, versus sublimation flux showed no obvious dependence on chamber pressure over the range of 50-200 mTorr at a constant sublimation flux (Figure 2a); the model of Zhang et al. (8) also predicts a pressure independent difference in local pressure across the shelf.

At the highest sublimation rate attainable at each chamber pressure, the center-to-edge pressure difference, $\Delta P_{c \rightarrow e}$, was measured at a series of clearances between the sublimation front and the upper false shelf. The pressure difference was more sensitive to clearance than to the sublimation rate (Figure 2a vs. 2b), with a dependence on clearance raised to the power of -3. When the pressure differences measured at various sublimation rates (Figure 2b) were normalized to a fixed sublimation rate of 1 $kg \cdot hr^{-1} \cdot m^{-2}$, the effect of clearance on $\Delta P_{c \rightarrow e}$ became

even more remarkable, particularly at a clearance in the range of 1.5[8] to 4 cm (Figure 2c). These experimental observations were found to be in good agreement with the corresponding CFD results as shown in Figures 6 and 8 of Varma et al (Varma et al.), but not with the model of Zhang et al. (8), which shows that pressure drop is proportional to the clearance raised to the power of -3/2. The Zhang model makes the assumption that the shelves have an infinite length, which may account for the difference in the dependence of pressure drop on clearance.

5. DISCUSSION

The consequences of local pressure variation on calculated product temperature history are compared to effects of other known variations in a lab-scale freeze-dryer. In a separate section, the consequences of local pressure variation are calculated for a theoretical manufacturing scale dryer for two commonly used pharmaceutical materials.

In a Lab-scale Freeze-dryer

In addition to the local chamber pressure variation over a batch of vials, there is significant vial-to-vial variation in (a) vial heat transfer coefficient, K_v (Pikal, Roy, Shah 1984) and (b) resistance of the dry product to water vapor flow, R_p (Konstantinidis et al. 2011; Searles, Carpenter, Randolph 2001a). Each of these variations contributes to the overall variation in vial-to-vial thermal history of product, which can result in a variation in product quality within a batch. The effect of pressure variation can be compared with the effects of previously documented variations in K_v and R_p using two different representative materials, sucrose and mannitol, that have different optimal cycles. Sucrose and products containing sucrose are often dried at a low shelf temperature to avoid the collapse associated with temperatures above the

[8] Pressure differences at clearances below 1.4 cm could not be measured due to equipment constraints.

glass transition of the sucrose freeze-concentrate (-32 °C) (Pikal 2002). In contrast, mannitol can be aggressively dried at a higher shelf temperature and chamber pressure, because it crystallizes and has a high eutectic temperature (-1.5 °C) (Liao, Krishnamurthy, Suryanarayanan 2007) above which there would be melting of ice causing gross collapse of the cake. In addition to the difference in freeze-drying cycles, the resistance of the dry cakes to vapor transport differs, with 5% w/w mannitol cakes having resistance values about 2-3 times those of 5% w/w sucrose cakes. Variation in each of the three parameters -- chamber pressure, K_v and R_p -- are discussed separately below.

Spatial Pressure Variation

At the sublimation rate of 0.13 $kg \cdot hr^{-1} \cdot m^{-2}$ (measured for a batch of 5% sucrose at a chamber pressure of 65 mTorr and a shelf temperature of -25 °C), the center to edge pressure difference calculated from the plot of $\Delta P_{c \rightarrow e}$ versus sublimation rate (Figure 2a.) is less than 0.5 mTorr[9]. At a nominal chamber pressure of 65 mTorr, the local pressure at the center of the shelf would be between 65 and 65.5 mTorr (Table I). The pressure over a vial (as measured from the port in the false upper shelf; Figure 1) is assumed to be equal to the pressure beneath the vial, since there is no net vapor flow in the vertical direction and no pressure drop. Thus, a 0.5 mTorr increase in the local chamber pressure would be expected to increase the vial heat transfer coefficient for the center vials, but only by about 0.5%[10]. This slight increase in the vial heat transfer coefficient increases the driving force for sublimation (P_o - P_c) by about one mTorr (Table V), leading to a small, but positive, effect on the sublimation rate. Thus, an increase in the local pressure results in a slightly higher product temperature and shorter primary drying time

[9] 0.13 $kg \cdot hr^{-1} \cdot m^{-2}$ x 2.7 mTorr/($kg \cdot hr^{-1} \cdot m^{-2}$) = 0.35 ≈ 0.5 mTorr . The value of 2.7 mTorr/($kg \cdot hr^{-1} \cdot m^{-2}$) taken from Figure 2a.

[10] Based on experience in our lab (Sane et al. b)

(Table I) for 5% sucrose, which has a relatively low dry product resistance. These calculated changes in product temperature and drying time are so small, however, that they are likely not detectible experimentally.

At a sublimation rate of 0.94 $kg \cdot hr^{-1} \cdot m^{-2}$ (7 times that of 5% sucrose), measured during primary drying of three trays of 5% mannitol in vials, the difference in local chamber pressure from the center to the edge of a shelf is calculated to be 2.5 mTorr[11], such that the local pressure for center vials would be 152.5 mTorr when the chamber pressure is set at 150 mTorr. The vial heat transfer coefficient is less sensitive to changes in chamber pressure at higher pressures (Pikal, Roy, Shah 1984). The vial heat transfer coefficient for center vials is calculated to be only 0.02 x 10^{-4} $cal \cdot cm^{-2} \cdot sec^{-1} \cdot K^{-1}$ higher than for the edge vials, assuming a 2.6 clearance between vial and upper shelf. There is no calculated change in the product temperature or drying time due to the 2.5 mTorr increase in pressure (Table I). At constant pressure, no impact of variation in shelf spacing on vial heat transfer coefficient of the edge vial was assumed in these calculations. In the next two sections, the variation in product temperature and primary drying time caused by the higher local pressure for the center vials (Table I) is compared with the influence of other sources of variation.

Vial Position-related Variation in Vial Heat Transfer Coefficient

Typically the vials on a freeze-dryer shelf can be divided into two classes based on position: edge vials (which are the outermost vials on the shelf) and center vials. Additional radiative heat transfer from the warmer surfaces (such as the band, the door and the walls) in the freeze-drying chamber to the cold product in the edge vials is responsible for the higher product temperature and faster drying rate in the edge vials as compared to the center vials (Rambhatla

[11] 0.94 $kg \cdot hr^{-1} \cdot m^{-2}$ x 2.7 mTorr $(kg \cdot hr^{-1} \cdot m^{-2})$ = 2.5 mTorr. The value of 2.7 mTorr/$(kg \cdot hr^{-1} \cdot m^{-2})$ taken from Figure 2a.

and Pikal 2003). Edge vials represent 1/3 of the total batch of 20 cc vials on a LyoStar 3 shelf. The vial heat transfer coefficients for product in 20 cc vials at the edge and in the center of the shelf dried at shelf temperatures and chamber pressures used for 5% w/w sucrose and 5% w/w mannitol are shown in Table II. While data were obtained in LyoStar II (SP Industries, Warminster, PA), the values are expected to apply to the same conditions in a LyoStar 3 due to similarities in the chamber configuration.

In the case of 5% sucrose, both the low chamber pressure and low shelf temperature result in less heat transfer by gas conduction when compared to the mannitol case; radiation of heat (primarily from the band) to the edge vials contributes significantly to the overall heat transfer coefficient of the edge vials (Equation 2). At the primary drying conditions used for sucrose, the edge vials have a 38% higher heat transfer coefficient than the center vials (Table II) resulting in about a degree warmer product temperature and a 4 hour shorter drying time than the center vials. In contrast, the vial heat transfer coefficients at conditions corresponding to the mannitol cycle (primarily due to the higher chamber pressure) are higher than for the sucrose cycle (Table II); at the higher shelf temperature and chamber pressure, there is greater heat transfer due to gas conduction and the relative contribution of radiation from the walls to the edge vials is lower than for the sucrose cycle. At the cycle conditions used for mannitol, the edge vials have a 12% higher heat transfer coefficient than the center vials resulting in about a degree warmer product temperature and a 0.4 hour shorter drying time than the center vials.

Comparison between the effect of local pressure variation in the chamber versus the effect of position of the vial on the vial heat transfer coefficient (Table I vs. II) shows that the latter is much more dominant. The increase in radiation to the edge vial increased the product temperature by about a degree and decreased the primary drying time by 4 hours for sucrose. In

contrast, a 0.5 mTorr increase in the local pressure for the center vials increase the product temperature by 0.3 °C and decrease the drying time only by 0.2 hours. In practice, at the lab-scale, the effect of the increase in local pressure would be imperceptible relative to the radiation-related position effect.

Variation in Resistance of Dry Product Layer to Vapor Flow

Within a batch of product, the temperature at which ice nucleates in each vial can occur over a wide range below the equilibrium freezing point (Kasper and Friess 2011; Kochs et al. 1993; Searles, Carpenter, Randolph 2001a). The ice nucleation temperature affects the size of the resulting ice crystals, with higher nucleation temperatures producing larger ice crystals. Variation in ice nucleation temperatures ultimately causes variation in the resistance to the vapor flow offered by the porous dry cake remaining as the sublimation front recedes into the product. In the absence of ice nucleation control, the variation in product resistance contributes significantly to overall variation in drying time and product temperature within a single batch (Rambhatla et al. 2004; Searles, Carpenter, Randolph 2001a). For example, at the higher end of the range for sucrose resistance (4.42 $cm^2 \cdot hr \cdot Torr \cdot g^{-1}$), corresponding to a lower ice nucleation temperature (-17 °C), an additional 3 hours would be required to complete primary drying (Table III), and the product temperature would increase by about 1.5 °C.[12] In contrast to sucrose, the higher resistance of the 5% mannitol cakes reduces the ability of heat to be removed by sublimation; the result of the variation in ice nucleation temperature (and therefore product

[12] A freeze-drying cycle is ideally optimized for process conditions to target a product temperature 2-3 °C below the product's critical temperature. An increase of 1.5 °C in the product temperature due to the higher product resistance associated with a lower ice nucleation temperature can thus increase the risk of approaching or exceeding the critical temperature, causing loss of product cake structure.

resistance) is a higher variation in product temperature as compared to the sucrose case, and less of a difference in drying times.

In a lab-scale freeze-dryer, the effect of local pressure variation on product thermal history (Table I) is not significant relative to the effect of variation in ice nucleation (Table III) and radiation-related vial position effect (Table II) for either 5% sucrose and 5% mannitol. In the case of 5% sucrose, a change in position from center to edge decreased the drying time by 4 hours due to increased radiation from the walls. Additionally, an increase in the ice nucleation temperature from -17 to -8 °C decreased the drying time by about 3 hours irrespective of the edge or the center vial. However, a change in the local chamber pressure for the center vials caused only a 0.2 hour decrease in the drying time.

At Manufacturing Scale

Scale-up of 5% Sucrose and 5% Mannitol Batches

Scale-up effects of locally higher pressure based on CFD and experimentally verified data can be simulated assuming that the pressure difference scales directly with path length of water vapor from the center to edge, as predicted by the equations of Zhang and Liu and in the models of Varma et al (Varma et al.) and Rasetto et al (Rasetto et al. 2008; Rasetto et al. 2010; Zhang and Liu 2012). Scaling up cycles developed in a lab scale freeze dryer with a 20 inch shelf (i.e., 10 inches from center to front or back edge) to a larger freeze-dryer with a 6 foot shelf (i.e., 36 inches from center to edge) and reducing the clearance (*h*) from 2.6 cm to 1.6 cm to maximize manufacturing capacity, the locally high pressure in the very center of the shelf is expected to be much higher than the chamber pressure at the edge of the shelf or measured at the top of the chamber. The center to edge pressure difference for a 1.6 cm clearance is 3 times that of a 2.6 cm clearance at a sublimation rate of 1 $kg \cdot hr^{-1} \cdot m^{-2}$, or 8 mTorr (Figure 2c). Adjusted for the

increase in center to edge path length from 10 inches to 36 inches, the pressure in the center of the shelf is expected to rise by 28.8 mTorr over nominal chamber pressure for a sublimation rate of 1 $kg \cdot hr^{-1} \cdot m^{-2}$. Given the ice sublimation flux of 0.13 $kg \cdot hr^{-1} \cdot m^{-2}$ for 5% sucrose at a chamber pressure of 65 mTorr and shelf temperature of -25°C, the pressure in the center of a larger scale freeze dryer shelf is expected to be 3.7 mTorr higher than the nominal chamber pressure (i.e, 68.7 mTorr). When drying 5% mannitol at a chamber pressure of 150 mTorr and shelf temperature of +30°C, the sublimation rate is 0.94 $kg \cdot hr^{-1} \cdot m^{-2}$; and the pressure in the center of the larger shelf is calculated to be 27.1 mTorr higher or 177.1 mTorr. Thus, at the larger scale, the product temperatures in the center vials are expected to be much higher (Table IV) than at the laboratory scale (Table I), due to the effect of pressure on the heat transfer coefficient. Surprisingly, because of this effect, the batch temperature becomes more uniform at the larger scale than in the laboratory; that is edge and center vials run closer in temperature and drying time. The effect of locally high pressure is still small compared to the radiation-related position effect (Table II) and ice nucleation temperature effect (Table III) on variation across the batch, but the increased uniformity on scale-up is noteworthy. The vials at the center are not expected to complete primary drying as fast as those at the edge, but center vials are expected to dry faster than at the laboratory scale. So, the batch is becomes more uniform in drying time on scale-up.

It should be noted that the higher local chamber pressure at the center of the shelf does not depress the sublimation due to a reduction in the driving force (P_o - P_c) for mass transfer in center vials (Equation 3). Instead, the locally higher pressure increases the vial heat transfer coefficient (Equation 2) leading to an increase in the product temperature (Equation 1), including at the sublimation interface. Due to the exponential relationship between ice temperature and vapor pressure, the higher product temperature results in a substantial increase in the vapor

pressure at the sublimation interface, P_o. Thus, when local chamber pressure, P_c, is elevated, there is a much higher increase in the vapor pressure of ice, P_o, than local chamber pressure, P_c, resulting in a greater driving force (P_o - P_c) for sublimation (Equation 3). As the pressure increases, in each case explored in this work, the driving force for sublimation, P_o-P_c, increases (Table V).

Scale up of a theoretical product with low resistance and high collapse temperature, freeze-dried at P_c = 50 mTorr and T_s = +10 °C

Using the resistance parameters characteristic of 5% sucrose with a low ice nucleation temperature (i.e., higher resistance), the sublimation rate at a chamber pressure of 50 mTorr and shelf temperature of +10 °C was calculated to be 0.5 $kg \cdot hr^{-1} \cdot m^{-2}$. At this sublimation rate, the local chamber pressures for center vials at lab- and manufacturing-scale were calculated to be 1.3 and 14.4 mTorr higher than at the edge vials, respectively. At the low chamber pressure of 50 mTorr, where the vial heat transfer coefficient is more sensitive to changes in chamber pressure, the increase in local pressure from 50 mTorr to 51.3 mTorr at lab-scale and to 64.4 mTorr at manufacturing-scale increases the vial heat transfer coefficient for the center vials (Table VI). In addition, note that at a shelf temperature of +10°C, the effective contribution of radiation to the edge vials from the band and the chamber walls is low, about 5% (Sane et al. b). This combination of circumstances creates conditions such that at the highest center pressure, 64.4 mTorr, the vial heat transfer coefficient for center vials exceeds that of edge vials (Table VI). At lab scale, where the center pressure is only 1.3 mTorr higher than at edge, the center and the edge vials have comparable K_v values and the same maximum product temperature, making the batch more uniform than would be predicted using a K_v based on the nominal chamber pressure of 50 mTorr. However, if during scale-up the gap is reduced to accommodate more product in

the dryer (and the shelf is larger), heat flow to center vials will be greater than to edge vials and the product in the center vials would be atypically warmer by a degree than product in the edge vials. The product in the center vials could reach the collapse temperature during scale-up. Widening the gap between the shelves can mitigate the temperature inversion and avoid collapse.

Under the right conditions, somewhere between the mannitol, sucrose, and the hypothetical sample examples, scaling up the product can be used to make the batch uniform. Additional modeling can identify the design space within which scaling up can be used to improve batch uniformity.

6. CONCLUSIONS AND SIGNIFICANCE

Product temperature during the freeze-drying process is often a major determinant of the final freeze-dried product quality. For successful scale up from a laboratory to a production scale dryer, a reproducible product temperature profile from vial to vial both intra- and inter-batch is desirable. Previously, radiation from the warmer surfaces such as the chamber walls and the stainless steel band as well as the variation in the dry layer product resistance have been shown to be responsible for the non-uniformity in drying behavior during primary drying (Brülls and Rasmuson 2002; Kasper and Friess 2011; Kobayashi et al. 2011; Kochs et al. 1993; Konstantinidis et al. 2011; Pikal, Rambhatla, Ramot 2002; Pikal, Roy, Shah 1984; Rambhatla et al. 2004; Rambhatla and Pikal 2003). Additionally, recent models using CFD simulations suggest substantial pressure gradients across shelves in the freeze-dryer chamber, which could lead to additional variation within a batch. In this report, we described the use of a differential capacitance manometer fed through a vacuum fitting to two ports in a false shelf to directly measure pressure differences on the order of 1-10 mTorr in a lab-scale dryer. The local pressure was higher in the center of the shelf as predicted by CFD modeling (Varma et al.). The rise in

pressure at the center of the shelf was linearly related to the sublimation flux. Moreover, the locally higher center pressure was remarkably sensitive to the clearance between the sublimation interface (equivalent to the opening of a vial) and the upper shelf, increasing exponentially with decreasing clearance. While the effects of the locally higher center pressure on product temperature and time to complete primary drying were shown to be negligible in the lab-dryer, predictions of scale-up effects indicate a significant impact on drying behavior in a manufacturing environment, which in some cases could make the product quality more uniform, but in other cases could compromise product quality. The effect is dependent on the product resistance and drying conditions. The elevated pressure predicted at the center of a shelf can raise product temperature and/or reduce drying time, making the batch more uniform at large-scale relative to lab-scale. In at least one hypothetical but plausible case, the locally higher center pressure was shown to raise the temperature of product in the center vials sufficiently to exceed that of the usually warmer edge vials, which could result in collapse during scale up.

The contribution of the locally higher pressure to the intra-batch variation in the product temperature during primary drying was shown to be far less than the known the effects of variation in ice nucleation temperatures and the radiation from warmer surfaces to edge vials at the lab-scale. However, at manufacturing scale the relative contributions of each source of variation can change. By carefully accounting for the impacts of local variations in chamber pressure, variation in ice nucleation temperature (or control of ice nucleation), and position dependent heat transfer variation, scale-up of a cycle from lab to manufacturing scale can be significantly de-risked.

7. ACKNOWLEDGMENTS

This work was done in collaboration with Cyrus Agarabi, Mansoor Khan and Rakhi Shah from FDA and was funded by FDA U01-PU002-2012 through the National Institute for Pharmaceutical Technology and Education (NIPTE).

8. REFERENCES

Brülls M and Rasmuson A. 2002. Heat transfer in vial lyophilization. Int J Pharm 246(1):1-16.

Carpenter JF, Pikal MJ, Chang BS, Randolph TW. 1997. Rational design of stable lyophilized protein formulations: Some practical advice. Pharm Res 14(8):969-75.

Jansco G, Pupezin J, Van Hook WA. 1970. The vapor pressure of ice between 10– 2 and– 10 2◦ C. J Phys Chem 74:2984-9.

Kasper JC and Friess W. 2011. The freezing step in lyophilization: Physico-chemical fundamentals, freezing methods and consequences on process performance and quality attributes of biopharmaceuticals. European Journal of Pharmaceutics and Biopharmaceutics 78(2):248-63.

Kobayashi M, Harashima K, Ariyama H, Yao A. 2011. Inter-vial variance of the sublimation rate in shelf freeze-dryer. Transactions of the Japan Society of Refrigerating and Air Conditioning Engineers 10:135-44.

Kochs M, Körber C, Heschel I, Nunner B. 1993. The influence of the freezing process on vapour transport during sublimation in vacuum-freeze-drying of macroscopic samples. Int J Heat Mass Transfer 36(7):1727-38.

Konstantinidis AK, Kuu W, Otten L, Nail SL, Sever RR. 2011. Controlled nucleation in freeze-drying: Effects on pore size in the dried product layer, mass transfer resistance, and primary drying rate. J Pharm Sci 100(8):3453-70.

Liao X, Krishnamurthy R, Suryanarayanan R. 2007. Influence of processing conditions on the physical state of mannitol-implications in freeze-drying. Pharm Res 24(2):370-6.

Milton N, Pikal MJ, Roy ML, Nail SL. 1997. Evaluation of manometric temperature measurement as a method of monitoring product temperature during lyophilization. PDA Journal of Pharmaceutical Science and Technology 51(1):7-16.

Patel SM, Chaudhuri S, Pikal MJ. 2010. Choked flow and importance of mach I in freeze-drying process design. Chemical Engineering Science 65(21):5716-27.

Pikal MJ. 2002. Freeze drying. Encyclopedia of Pharmaceutical Technology, Marcel Dekker, New York 1299:1326.

Pikal M, Rambhatla S, Ramot R. 2002. The impact of the freezing stage in lyophilization: Effects of the ice nucleation temperature on process design and product quality. American Pharmaceutical Review 5:48-53.

Pikal MJ. 1985. Use of laboratory data in freeze drying process design: Heat and mass transfer coefficients and the computer simulation of freeze drying. J Parenter Sci Technol 39(3):115-39.

Pikal MJ, Roy ML, Shah S. 1984. Mass and heat transfer in vial freeze-drying of pharmaceuticals: Role of the vial. J Pharm Sci 73(9):1224-37.

Rambhatla S, Ramot R, Bhugra C, Pikal MJ. 2004. Heat and mass transfer scale-up issues during freeze drying: II. control and characterization of the degree of supercooling. Aaps Pharmscitech 5(4):54-62.

Rambhatla S and Pikal MJ. 2003. Heat and mass transfer scale-up issues during freeze-drying, I: Atypical radiation and the edge vial effect. AAPS PharmSciTech 4(2):111-20.

Rasetto Valeria, Marchisio Daniele L., Fissore Davide and Barresi Antonello A. 2008. Model-based monitoring of a non-uniform batch in a freeze-drying process. Proceedings of 18th european symposium on computer aided process Engineering–ESCAPE18 (edited by B. braunschweig, X. joulia). 1 p.

Rasetto V, Marchisio DL, Fissore D, Barresi AA. 2010. On the use of a dual-scale model to improve understanding of a pharmaceutical freeze-drying process. J Pharm Sci 99(10):4337-50.

Roy ML and Pikal MJ. 1989. Process control in freeze drying: Determination of the end point of sublimation drying by an electronic moisture sensor. PDA Journal of Pharmaceutical Science and Technology 43(2):60-6.

Sane P, Agarabi C, Pikal M, Bogner R. a. Quantifying the variation in product temperature and drying time within a lyophilized batch during primary drying. Manuscript in Preparation .

Sane P, Pikal M, Nail S, Bogner R. b. Measurement of heat transfer to vials on a freeze-dryer shelf during primary drying. Manuscript in Preparation .

Schneid SC, Gieseler H, Kessler WJ, Pikal MJ. 2009. Non-invasive product temperature determination during primary drying using tunable diode laser absorption spectroscopy. J Pharm Sci 98(9):3406-18.

Searles JA, Carpenter JF, Randolph TW. 2001. The ice nucleation temperature determines the primary drying rate of lyophilization for samples frozen on a temperature-controlled shelf. J Pharm Sci 90(7):860-71.

Varma N, Ganguly A, Sane P, Bogner R, Pikal M, Alexeenko A. Variation of pressure in lyophilization product chamber part 1: Computational modeling. Manuscript Submitted to AAPS PharmSciTech .

Zhang S and Liu J. 2012. Distribution of vapor pressure in the vacuum freeze-drying equipment. Mathematical Problems in Engineering 2012.

9. APPENDICES

I. Determination of the zero-point offset value for $\Delta P_{c \rightarrow e}$ measurements:

Unexpectedly, at conditions expected to produce no pressure variation, the differential CM displayed a non-zero value. For example, when the drying chamber door was closed, but before cooling the shelf to produce the ice slab (Protocol 1 in Table VII), there was no vapor flow from sublimation to produce a pressure drop; the differential CM was expected to produce a value close to zero for $\Delta P_{c \rightarrow e}$, but typically did not. Additionally, at the end of collecting $\Delta P_{c \rightarrow e}$ at each chamber pressure, the shelf with the ice slab was lowered to achieve maximum distance (i.e., 14 cm) from the false upper shelf (Protocol 2 in Table VII), where the pressure difference, $\Delta P_{c \rightarrow e}$, at this gap distance was expected to be negligible (Figure 2b).

However, neither Protocol in Table VII produced $\Delta P_{c \rightarrow e}$ readings that could be used as zero-point offset values to obtain meaningful data. Instead, values of $\Delta P_{c \rightarrow e}$ ranged from 0.4 to 45.0 mTorr, when a zero value was expected. There was no trend in the "zero point" $\Delta P_{c \rightarrow e}$ measurements with increasing chamber pressure (Table VIII). However, when the zero-point differential pressure readings were listed in order of collection date, there was an obvious increase in zero-point as a function of time (Table IX). The drift over time is most likely due to small permanent deflections of the diaphragm in the differential CM that result in hysteresis. The analysis of $\Delta P_{c \rightarrow e}$ in this report assumed that only the zero-point offset is affected and not the sensitivity of the diaphragm deflections to pressure changes.

The CFD studies of Varma et al. demonstrated a linear dependence of pressure difference on sublimation flux. If the raw $\Delta P_{c \rightarrow e}$ data were extrapolated to a sublimation flux of 0 $kg \cdot hr^{-1} \cdot m^{-2}$, the intercept should provide the most reliable value for the zero-point offset for pressure difference. Hence, as an alternative to either one of the directly measured values for zero-point

offset (i.e., Protocol 1 or 2), a third value (Protocol 3 in Table IX) was derived from extrapolation of the data for $\Delta P_{c \rightarrow e}$ as a function of sublimation rate (Figure 2a) using zero-point as determined from protocol 2 to zero sublimation rate. Clearly, at zero sublimation rate, the pressure difference must be zero, and as indicated above, the expectation is that the pressure difference should be essentially linear in sublimation rate.

II. Effect of variation in nucleation temperature on the resistance of the dry layer to water vapor transport

In a freeze-drying cycle, as the shelf temperature is lowered, not all vials contain ice at the equilibrium freezing point of the solution. In fact, normally none do! The product in the vial can exist in the liquid state well below the equilibrium freezing point (i.e., -10 to -20 °C). The degree of supercooling prior to ice nucleation during ramp freezing largely determines the size of the ice crystals (Roy and Pikal 1989). When ice leaves the frozen product by sublimation during primary drying, the porous structure of the solute it leaves behind is essentially a template of the ice removed. Any variation in degree of supercooling leads to a variation in the porosity of the freeze-dried solute and the resistance offered by the dried product to vapor flow during primary drying. Higher degrees of super-cooling are associated with smaller ice crystals, leading to the formation of small pores in the dried layer and greater resistance to water vapor transport.

Previous experience in our lab with 20 cc vials in a lab freeze dryer (Lyostar 2) has shown a range of ice nucleation temperatures from -6 °C to -20 °C, with 80% of vials undergoing ice nucleation between -8 °C and -17 °C (Sane et al. a). This range of ice nucleation temperatures leads to a range in dried layer resistance for vials within a batch, which was calculated as described next.

The dry layer resistance of both sucrose and mannitol at a concentration of 5% w/w was determined using Manometric Temperature Measurement (MTM) (Milton et al. 1997) at ice nucleation temperatures of -5°C and -10 °C using the Praxair *ControLyo™ Nucleation*. The product resistance as a function of the dry layer thickness, was fitted by the empirical relationship:

$$R_p = \left[R_o + \frac{A_1 \cdot l}{1 + A_2 \cdot l}\right] \qquad \text{Equation 4}$$

where R_p is the measured product resistance to the water vapor leaving the ice surface through the dried cake of thickness, l (Pikal 1985). The parameters, R_o, A_1, and A_2, are used to fit the shape of the R_p versus l curve. For both sucrose and mannitol, the resistance was related to nucleation temperature by an ice nucleation temperature-dependent factor, F_{Tnuc}, specific for that material as described below. The values of R_o, A_1, and A_2, were also material specific.

Equation 5

$$R_{p,nuc} = \mathrm{F}_{T_{nuc}} \cdot \left[R_o + \frac{A_1 \cdot l}{1 + A_2 \cdot l}\right]$$

The values of R_o, A_1, and A_2 were determined for each material such that multiplication of R_p (Equation 4) by a factors, $F_{T,nuc}$, described the resistance curves at both -5°C and -10°C, reasonably well. The temperature-dependent factor allowed for an increase in resistance as ice nucleation temperature decreased, while maintaining the general shape of the resistance versus dry layer thickness curve. In determining the values of $F_{T,nuc}$, several assumptions were made.

i. The change in resistance between -5°C and -10°C is linear and can be extrapolated to lower ice nucleation temperatures (This is perhaps the weakest assumption).

ii. The cake resistance, R_p, and the change in resistance with nucleation temperature, $\frac{dR_p}{dT_{nuc}}$, are about 25% lower for products in which ice nucleation was initiated at a single temperature as compared to product in vials where ice nucleated spontaneously, but at the same temperature.

iii. The average nucleation temperature in a batch without nucleation control is -15 °C[13].

Based on these assumptions, the average product resistance values for each material obtained from controlled nucleation runs were multiplied by factors such that the resistance linearly extrapolated to a nucleation temperature of -15 °C equaled that found during uncontrolled nucleation.

The measured average cake resistance values for 5% w/w sucrose at ice nucleation temperatures of -5°C and -10°C were 1.70 and 2.47 $cm^2 \cdot hr \cdot Torr \cdot g^{-1}$, respectively, and the average resistance for the same material without ice nucleation control was 3.91 $cm^2 \cdot hr \cdot Torr \cdot g^{-1}$ (Table X). When the value of the experimentally measured resistance of the 5% w/w sucrose cakes frozen using nucleation control is extrapolated to -15°C and multiplied by 1.25 (according to assumption ii above), it agrees well with resistance in the absence of nucleation control. The same factor 1.25 works well for both sucrose and mannitol.

Using the value for the change in resistance per degree ($\frac{dR_p}{dT_{nuc}}$), the average product resistance for a low ice nucleation temperature of -17 °C and a high ice nucleation temperature of

[13] The batch average nucleation temperature is based on compilation of 37 data points for ice nucleation in 20 cc vials in our lab (unpublished).

-8 °C were estimated. In the case of mannitol, the average product resistance varies from 6.15 $cm^2 \cdot hr \cdot Torr \cdot g^{-1}$ when ice nucleation occurs at -8°C to 8.13 $cm^2 \cdot hr \cdot Torr \cdot g^{-1}$ when ice nucleation occurs at -17°C. Sucrose at 5% has a lower dry layer resistance (i.e., 2.70 $cm^2 \cdot hr \cdot Torr \cdot g^{-1}$ when ice nucleation occurs at -8°C and 4.42 $cm^2 \cdot hr \cdot Torr \cdot g^{-1}$ when ice nucleation occurs at -17°C).

10. FIGURES

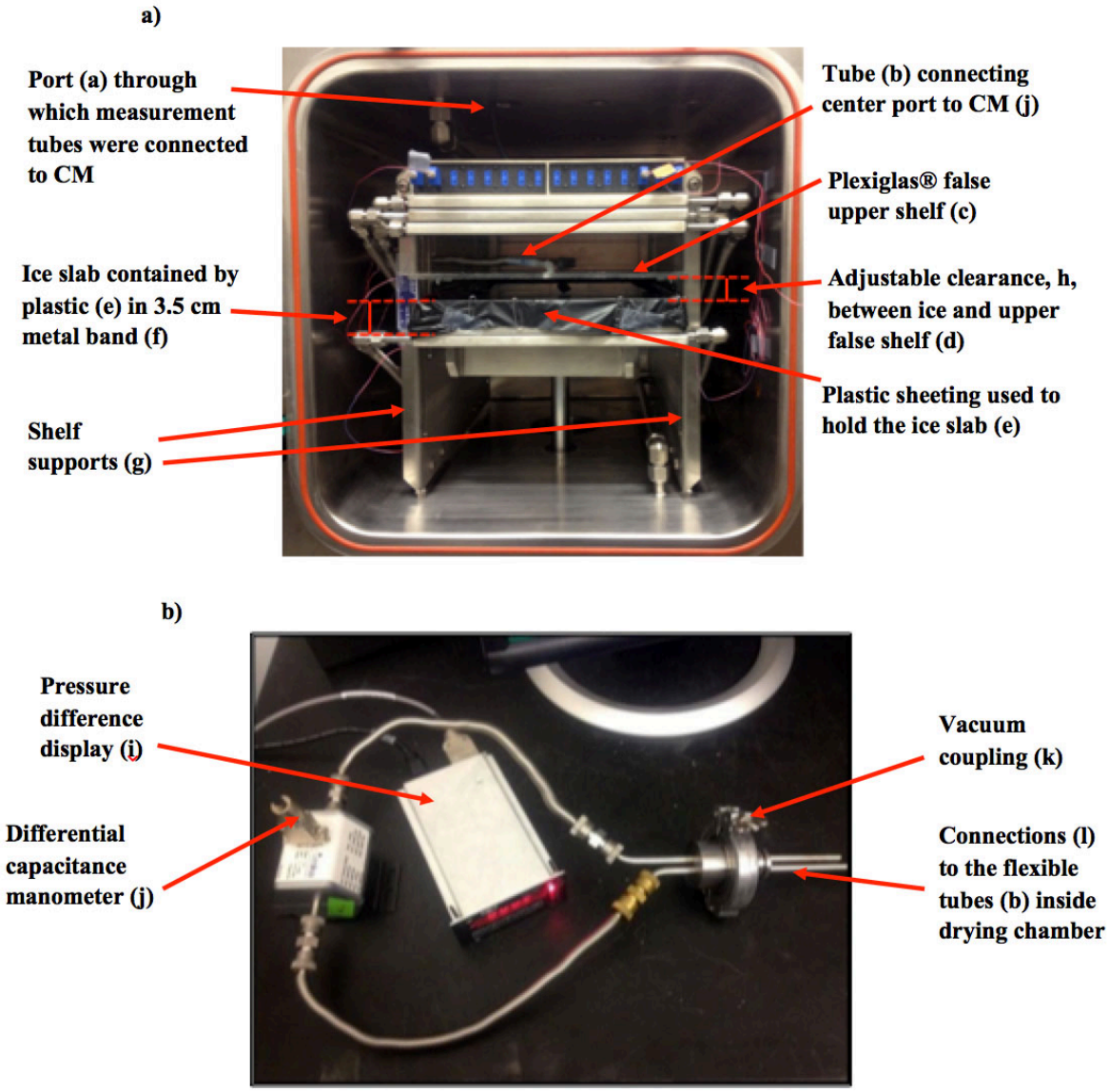

Figure 1- a) The drying chamber of Lyostar 3 with Plexiglas® shelf installed above the ice slab with adjustable clearance set at 2.6 cm as shown. b) Differential capacitance manometer (to the left) connected to a custom vacuum fitting (to the right) through the Pirani port on a LyoStar 3

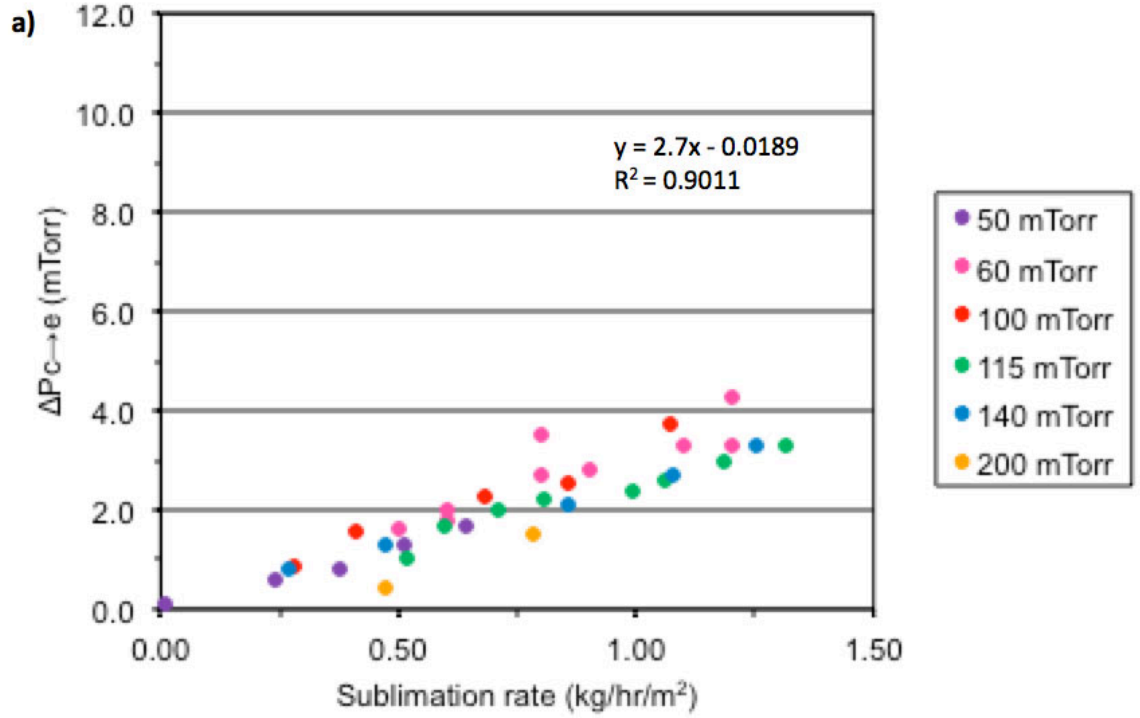
a)
12.0
10.0
8.0
6.0
4.0
2.0
0.0
ΔPc→e (mTorr)
y = 2.7x - 0.0189
R² = 0.9011
0.00
0.50
1.00
1.50
Sublimation rate (kg/hr/m²)
50 mTorr
60 mTorr
100 mTorr
115 mTorr
140 mTorr
200 mTorr

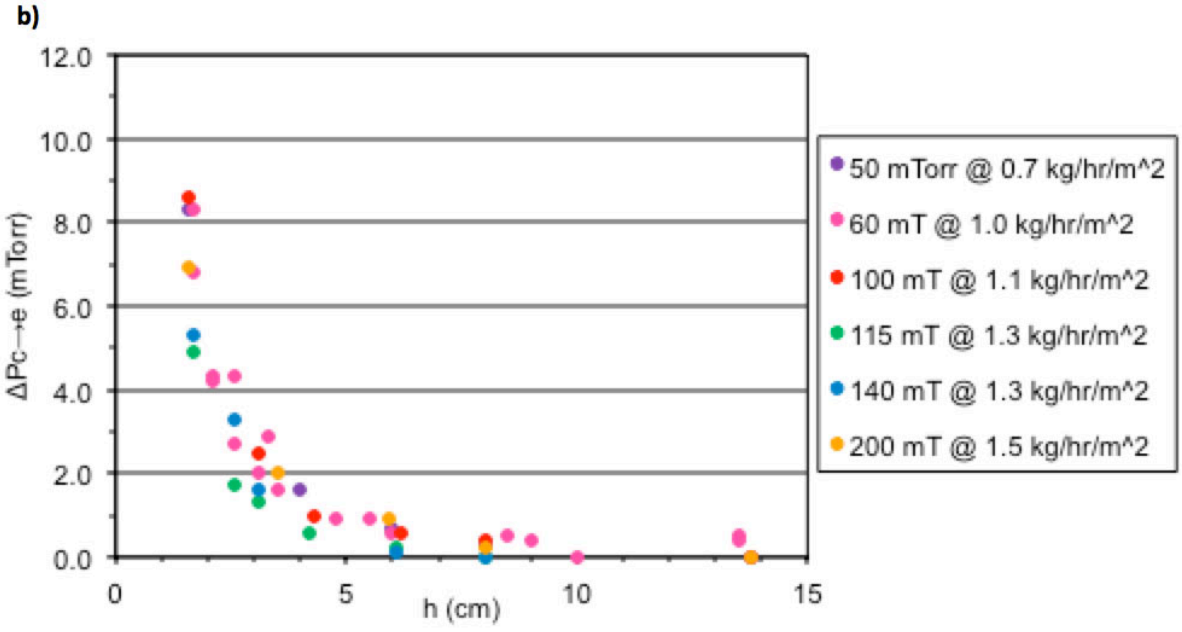
b)
12.0
10.0
8.0
6.0
4.0
2.0
0.0
ΔPc→e (mTorr)
0
5
10
15
h (cm)
50 mTorr @ 0.7 kg/hr/m^2
60 mT @ 1.0 kg/hr/m^2
100 mT @ 1.1 kg/hr/m^2
115 mT @ 1.3 kg/hr/m^2
140 mT @ 1.3 kg/hr/m^2
200 mT @ 1.5 kg/hr/m^2

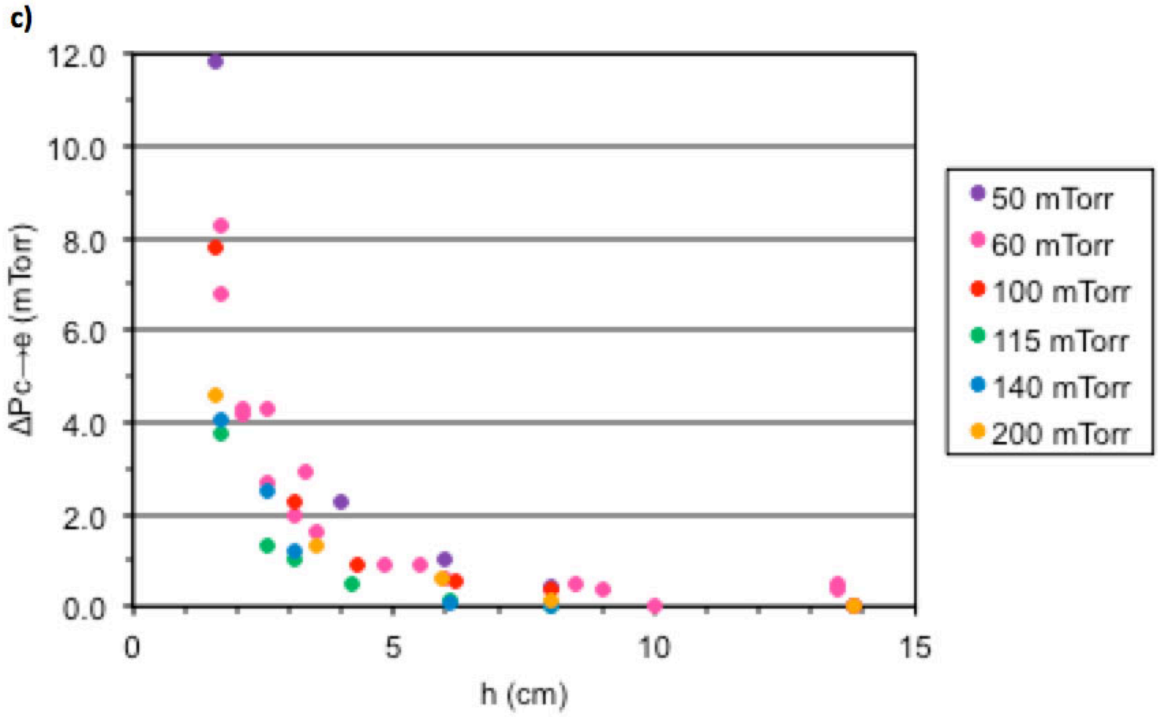

Figure 2- a) Experimental pressure difference from center to edge of the shelf ($\Delta P_{c\rightarrow e}$) for several sublimation rates at a series of chamber pressures at a clearance, h = 2.6 cm using Protocol 3 (refer to Appendix 1) as a zero point offset. b) Increase in pressure at center relative to edge of the shelf in a lab-scale freeze dryer during which sublimation of ice is taking place at the rates indicated in the box on the right side of the figure. Pressure differentials used the zero-point offset from the value at h = 14 cm at a shelf temperature of -35 °C and corresponding chamber pressure for a particular experiment. c) Data from 4b normalized to a fixed sublimation rate of 1 $kg \cdot hr^{-1} \cdot m^{-2}$

Table I - Comparison of vial heat transfer coefficient (K_v), primary drying time (t_{dry}), and maximum product temperature (T_p) at the nominal chamber pressure (P_c) versus the calculated higher local pressure at the center of the shelf. Results for two example materials – 5% sucrose and 5% mannitol – were calculated for lab-scale equipment at h = 2.6 cm based on a relatively low dry layer resistance (R_p), corresponding to a high ice nucleation temperature (T_{nuc}) of -8 °C for sucrose, and based on a relatively large R_p, corresponding to a T_{nuc} of -17 °C for mannitol (refer to appendix for details). Values for t_{dry} and T_p for each case were calculated using Excel®-based lyo-calculator Version 4 (Pikal, Roy, Shah 1984; Pikal 1985).

5% w/w sucrose				5% w/w mannitol			
T_{shelf} = -25°C				T_{shelf} = +30°C			
P_c (mTorr)	K_v x 10^4 (cal·cm^{-2}·sec^{-1}· K^{-1})	t_{dry} (hrs)	T_p (°C)	P_c (mTorr)	K_v x 10^4 (cal·cm^{-2}·sec^{-1}· K^{-1})	t_{dry} (hrs)	T_p (°C)
65.0	3.33	19.3	-36.6	150.0	5.49	5.6	-10.1
65.5	3.35	19.1	-36.3	152.5	5.51	5.6	-10.1

Table II - Comparison of vial heat transfer coefficient (K_v), primary drying time (t_{dry}), and maximum product temperature (T_p) at the shelf temperatures and chamber pressures shown. K_v values for 20cc edge and center vials (Sane et al. b) and a relatively low dry layer resistance (R_p), corresponding to a high ice nucleation temperature (T_{nuc}) of -8 °C for sucrose and based on a relatively large R_p corresponding to a T_{nuc} of -17 °C for mannitol (refer to appendix for details) were used to calculate t_{dry} and T_p for center versus edge vials using Excel®-based lyo-calculator Version 4 (Pikal, Roy, Shah 1984; Pikal 1985).

Vial Position	5% w/w sucrose			5% w/w mannitol		
	T_{shelf} = -25°C P_c = 65 mTorr			T_{shelf} = +30°C P_c =150 mTorr		
	$K_v * 10^4$ (cal·cm^{-2}·sec^{-1}·K^{-1})	t_{dry} (hrs)	T_p (°C)	$K_v * 10^4$ (cal·cm^{-2}·sec^{-1}·K^{-1})	t_{dry} (hrs)	T_p (°C)
Center	3.33	19.3	-36.6	5.49	5.6	-10.1
Edge	4.58	15.3	-35.4	6.13	5.2	-9.2

Table III - Comparison of the primary drying time (t_{dry}), and maximum product temperature (T_p) at the shelf temperatures and chamber pressures shown for product in vials in which ice nucleated at -8 °C versus at -17 °C. Vial heat transfer coefficients (Table II) and product resistance values (Table X in the Appendix) were used to calculate t_{dry} and T_p for center (C) versus edge (E) vials using a simple Excel®-based model for steady-state heat and mass transfer equations (Pikal, Roy, Shah 1984; Pikal 1985).

5% w/w sucrose						5% w/w mannitol					
T_{shelf} = -25 °C P_c = 65 mTorr						T_{shelf} = +30°C P_c = 150 mTorr					
T_{nuc} (°C)	$<R_p>$ (cm²·hr·Torr·g⁻¹)	t_{dry} (hrs)		T_p (°C)		T_{nuc} (°C)	$<R_p>$ (cm²·hr·Torr·g⁻¹)	t_{dry} (hrs)		T_p (°C)	
		C	E	C	E			C	E	C	E
-8	2.70	19.2	15.0	-36.5	-35.4	-8	6.15	5.3	4.9	-12.4	-11.5
-17	4.42	22.2	18.2	-34.8	-33.7	-17	8.13	5.6	5.1	-10.0	-9.1

Table IV - Comparison of product in edge vials versus center vials for the two example materials – 5% sucrose and 5% mannitol– at larger scale showing the effect of pressure difference across the shelf on vial heat transfer coefficient, K_v, maximum product temperature during primary drying, T_p, and primary drying time, t_{dry}. The K_v values for the edge vials are assumed equal to the values in the laboratory freeze-dryer. The K_v values for the center vials were adjusted for the locally higher chamber pressure calculated for the larger scale (i.e., center to edge distance of 36 inches and vial to upper shelf clearance of 1.6 cm).

Vial Position	5% w/w sucrose				5% w/w mannitol			
	T_{shelf} = -25 °C				T_{shelf} = +30 °C			
	P_c (mTorr)	K_v x 10^4 (cal·cm^{-2}·sec^{-1}·K^{-1})	t_{dry} (hrs)	T_p (°C)	P_c (mTorr)	K_v x 10^4 (cal·cm^{-2}·sec^{-1}·K^{-1})	t_{dry} (hrs)	T_p (°C)
Edge	65.0	4.58	15.0	-35.4	150.0	6.13	5.1	-9.1
Center	68.7	3.57	18.9	-36.4	177.1	5.73	5.4	-9.6

Table V - Chamber pressures, P_c, for sucrose and mannitol at: (1) nominal set chamber pressure, (2) accounting for pressure difference at lab-scale, and (3) accounting for pressure difference at manufacturing-scale with the vapor pressure of ice at the sublimation interface, P_o, calculated at the corresponding chamber pressure and vial heat transfer coefficient. The driving force for sublimation is proportional to P_o - P_c, which increases as chamber pressure increases.

	5% w/w sucrose			5% w/w mannitol		
	P_c (mTorr)	P_o (mTorr)	P_o - P_c (mTorr)	P_c (mTorr)	P_o (mTorr)	P_o - P_c (mTorr)
No $\Delta P_{c\rightarrow e}$	65	129	64	150	1439	1289
Accounting for $\Delta P_{c\rightarrow e}$ at lab scale	65.5	130	64.5	152.5	1445	1292.5
Accounting for $\Delta P_{c\rightarrow e}$ at larger scale	68.7	134	65.3	177.1	1505	1327.9

Table VI – Comparison of calculated edge versus center vial drying time, t_{dry}, and product temperature, T_p, at lab- and manufacturing-scales for a cycle set at P_c = 50 mTorr and T_s = +10 °C. The theoretical product was assumed to have sucrose-like low dry layer resistance with a fill volume of 5 ml in 20 cc vials. The K_v values take into account both the local pressure and radiation effects of position. Scale-up causes an inversion in temperatures of center and edge vials.

	Lab-scale		Manufacturing-scale	
	Edge	Center	Edge	Center
P_c (mTorr)	50.0	51.3	50.0	64.4
K_v x 10^4 (cal·cm^{-2}·sec^{-1}·K^{-1})	3.70	3.54	3.70	4.00
T_p (°C)	-23.7	-24.1	-24.0	-22.9
t_{dry} (hr)	10.0	10.3	10.0	9.5

Table VII- Conditions at which the pressure difference, $\Delta P_{c \rightarrow e}$, was recorded for potential use as a zero-point offset.

Protocol	Material on the shelf below the ports in the upper false shelf	Shelf Temperature (°C)	Chamber Pressure (Torr)	Clearance *h* (cm)
1	Water (i.e. ice slab prior to freezing)	20	760	2.6
2	Ice slab	35	x[a]	14

[a]x = Target chamber pressure for a particular experiment, see Table VIII

Table VIII- $\Delta P_{c \rightarrow e}$ values (mTorr) using the protocols in Table VII.

	Difference in Pressure (mTorr)	
Chamber Pressure (mTorr)	Protocol 1[b]	Protocol 2[b]
50	24.8	39.4
60	-	0.4
100	28.8	45.0
115	-	10.3
140	-	10.9
200	25.0	39.6

[b]Protocols described in Table VII

Table IX - Zero point differential pressure readings from Table VIII in order of date of collection

		Protocols [c]		
Date of Experiment	Chamber Pressure (mTorr)	1	2	3
25-Jan	60	-	0.4	0.4
25-Apr	115	-	10.3	8.7
29-Apr	140	-	10.9	9.9
16-Sep	100	28.8	45.0	43.5
17-Sep	50	24.8	39.4	41.6
18-Sep	200	25.0	39.6	42.8

[c]Protocols 1 and 2 from Table VII, protocol 3 derived from (Figure 2a) for zero sublimation flux.

Table X – Average Product Resistance for 5% w/w sucrose ($R_0 = 1.59, A_1 = 3.73, A_2 = 0.71$) and 5% w/w mannitol ($R_0 = 4.26, A_1 = 11.10, A_2 = 0.30$). Product resistance values for both sucrose and mannitol at two different nucleation temperatures were determined by MTM, except for uncontrolled nucleation of sucrose, which was estimated, based on thermocouple data and primary drying time.[14]

5% w/w Sucrose				
	Nucleation induced at (°C)		Uncontrolled Nucleation (Avg temp -15°C)	Extrapolated to ice nucleation at -15°C
	-5	-10		
Experimentally determined R_p ($cm^2 \cdot hr \cdot Torr \cdot g^{-1}$)	1.70	2.47	3.91	
R_p x 1.25	2.13	3.08	--	4.04
F	1.00	1.45		2.3
			$\frac{dR_p}{dT_{nuc}}$ = - 0.153	
5% w/w Mannitol				

[14] Due to difficulties determining the cake resistance of 5% sucrose at -10°C, the average resistance of the cake was estimated based on the primary drying time of the 5% sucrose batch.

	Nucleation induced at (°C)		Uncontrolled Nucleation (Avg temp -15°C)	Extrapolated to ice nucleation at -15°C
	-5	-10		
Experimentally determined R_p ($cm^2 \cdot hr \cdot Torr \cdot g^{-1}$)	4.39	5.27	7.75	
Rp x 1.25	5.49	6.59	--	7.68
F	1.00	1.20		1.75
			$\frac{dR_p}{dT_{nuc}}$ = - 0.176	

Chapter 5

Effect of Lyophilization Process on the Reconstitution of Amorphous Lyophilized Protein Formulations at High Concentrations

1. ABSTRACT

The number of biotherapeutics in the pharmaceutical market has been increasing since the advent of recombinant DNA technology. Due to the high dose requirements for some of these candidates such as the monoclonal antibodies (mAbs) combined with the volume restrictions (< 1.5 ml) from the subcutaneous route of delivery, development of high concentration liquid mAb formulations has become a necessity. However, these liquid formulations pose a variety of stability challenges due to their high concentrations. Lyophilization/freeze-drying is one of the preferred methods for removal of water in order to stabilize these formulations. Long reconstitution time prior to administration remains an undesirable quality attribute for these high concentration formulations, which limits their practical usage to the end user. In this study we propose three approaches to study the reconstitution behavior of completely amorphous high concentration mAb containing lyophilized formulations by exploring their wetting, disintegration and hydration behavior. Initially, these mechanisms were investigated for formulations containing 0 to 83 mg/ml mAb with 5% w/v sucrose in 10 mM Histidine buffer. As the protein concentration increased, the reconstitution times were found to be longer. Poor wetting with slow hydration and disintegration was observed as the protein concentration increased. Further, the effect of ice nucleation temperature (-5 and -10 °C) during freezing followed by the use of either conservative or aggressive drying conditions on the reconstitution times was explored at a mAb concentration of 40 and 83 mg/ml. No effect of either of the processing conditions was noted on the 40 mg/ml mAb containing formulations where the reconstitution times were less than a minute. At 83 mg/ml mAb, aggressive drying led to faster dissolution of the lyophilized cake causing shorter reconstitution times at both the nucleation temperatures. On comparing this study with the already published literature it was found that as the protein to sugar ratio increased

beyond 1, the reconstitution times increased non-linearly. Wetting, disintegration and hydration of the lyophilized cake were determined to be the key mechanisms contributing to its complete reconstitution in a vial for the amorphous systems containing high concentrations of proteins.

2. INTRODUCTION

Some of the liquid protein formulations especially those containing monoclonal antibodies (mAbs) need to be administered at high doses (greater than 1 mg/kg body weight) due to their low specificity (Sharma et al. 2009; Shire, Shahrokh, Liu 2004). Majority of the marketed formulations are administered via intravenous (IV) or subcutaneous (SC) route. Volume restriction (< 1.5 ml) posed by the SC route combined with the high dose requirements (> 100 mg/ml) for mAbs necessitates the development of these formulations at high concentrations. Development of these mAb formulations at high concentrations is very challenging due to the stability, manufacturing and delivery issues associated with them (Shire, Shahrokh, Liu 2004). Freeze-drying or lyophilization is one of the preferred methods to stabilize these formulations by removal of water at low temperatures (Pikal 2002). A lyophilized product has to be reconstituted into a solution using an appropriate diluent prior to patient administration. Presence of no visible particles in the reconstituted vial marks the end of reconstitution time. Lyophilized highly concentrated protein formulations tend to have long reconstitution times with some commercial products ranging from 15-40 minutes (Cao et al. 2013; Geidobler, Konrad, Winter 2013). Another high concentration lyophilized protein formulation exhibited a 4-hour reconstitution time when no swirling was performed after introducing the diluent in the vial (Tchessalov et al. 2010). Such long reconstitution times are undesirable from an administration perspective.

Reconstitution time is dependent on several lyophilized product attributes such as specific surface area, porosity, phase behavior of formulation components, presence of bubbles or foam and viscosity, that can primarily affect the dissolution behavior (Bhatnagar et al.). Limited data are available on reconstitution of high concentration protein formulations. Cao et al

showed that as the Fc-fusion protein concentration increased from 10 to 100 mg/ml when formulated in an amorphous matrix containing 4.5% sucrose and 2% mannitol the reconstitution time increased from less than a minute to about 15 minutes (Cao et al. 2013). The authors correlated the long reconstitution times for the high concentration amorphous protein cakes to their slow erosion rates using the model for dissolution of surface-eroding solids in liquid given by the equation:

$$\frac{M_t}{M_\infty} = 1 - [1 - \frac{(k_0 * t)}{(C_0 * a_0)}]^n \qquad \text{Equation 1}$$

where $\frac{M_t}{M_\infty}$ is the fraction of the amount of active molecules dissolved in time *t* versus at infinite time, k_0 is the constant for erosion rate, C_0 is the initial concentration and a_0 is the initial radius or thickness depending on the shape.

During the freezing step of lyophilization, ice does not nucleate spontaneously at the equilibrium freezing point of water (0 °C). The liquid state of water is retained well below the equilibrium freezing point, which is termed as supercooling. The degree of supercooling defined as the difference between the equilibrium freezing point of water and the actual ice nucleation temperature is dependent on the solution as well as the processing conditions (Rambhatla et al. 2004). This degree of supercooling affects the size of the ice crystals during the freezing step, which subsequently affects the size of the pores in the dried cake. A lower degree of supercooling (higher nucleation temperature) leads to larger sized pores and decreased specific surface area in the final lyophilized cake (Kasper and Friess 2011; Rambhatla et al. 2004; Searles, Carpenter, Randolph 2001a). Beech et al (Beech et al. 2015) studied the influence of cooling profile on the reconstitution times for completely amorphous systems using BSA and a

mAb. They related the long reconstitution times (3-4 minutes) for the quench cooled systems to the presence of small or closed pores which slowed the penetration of water into the cake. Another study (Geidobler et al) using BSA and another mAb as model proteins at concentrations ≥100 mg/ml, showed that by controlling ice nucleation at higher temperatures (-5 °C) a shorter reconstitution time can be achieved. The hypothesis was that the higher nucleation temperatures led to formation of larger pores, improved wetting and hence, faster dissolution of the lyophilized cake. In another study, Shire et al (Shire, Shahrokh, Liu 2004) observed a faster reconstitution at lower protein loading concentration versus at high concentrations with constant total solids content. On investigating the morphology of the lyophilized cake using scanning electron microscopy (SEM), they found a loosely packed structure at the low concentration versus a denser compact for the high concentrations. Though a transition between the two patterns of cake morphology was readily observed in the intermediate range, the SEM images are not very quantifiable. Several other studies showed that increase in the size of the pores either by controlled nucleation at low protein concentrations (1 mg/ml) (Awotwe-Otoo et al. 2013) or annealing at high protein concentrations (≥ 50 mg/ml) resulted in a faster reconstitution.

A four-step process has been described in the food literature for reconstitution of powders or agglomerates (Forny, Marabi, Palzer 2011; Schober and Fitzpatrick 2005; Shittu and Lawal 2007). These include initial wetting of the powders by the liquid, penetration of the liquid by capillary action to dissolve the bridges connecting the primary particles followed by dispersion and dissolution of the primary particles. Similar principles can be applied to the reconstitution of high concentration lyophilized protein cakes in vials along with an additional parameter of cake hydration. The best-case scenario for complete and fast dissolution of the lyophilized cake would involve wetting of the cake followed by disintegration of the cake into small fragments

(an effect of the microstructure) followed by hydration of the individual fragments. Though some of these concepts have been introduced in the reconstitution literature for high concentration lyophilized protein formulations qualitatively as shown above, there is a lack of quantitative and systematic analysis of these factors in understanding their contribution towards reconstitution times.

The overall objective of this work is to delineate the steps, which lead to complete dissolution of the lyophilized cake using a mAb at a high concentration in an amorphous matrix. Initially the effect of mAb concentration on the reconstitution times was investigated. Out of these, low and high mAb concentrations that exhibited completely different reconstitution behavior were selected. Effect of ice nucleation temperature (T_{nuc}) and drying conditions on the reconstitution times was then studied for these protein formulations. The wetting behavior, hydration and disintegration rates were also studied for all of these systems.

3. MATERIALS AND METHODS

3.1. Materials

A recombinant human IgG1 monoclonal antibody (mAb) (approximate molecular weight 147 kDa and solubility of 170 mg/ml) was used as a model protein in this work (Pfizer Inc., Andover, MA) at a concentration of 83 mg/ml with 5% w/v sucrose in 10 mM histidine buffer at pH 6. At a concentration of 83 mg/ml mAb with 5% w/v sucrose, the viscosity of the formulation was only 3 cP. This initial formulation was further diluted to obtain a range of mAb concentrations with same concentration of sucrose (5% w/v). Pure mAb devoid of any sucrose was prepared using an Ultrafiltration/Diafiltration unit. The concentrations for all formulations

were checked with SpectraMax Plus384 microplate spectrophotometer (Molecular Devices Corp., Sunnyvale, CA).

3.2. Lyophilization cycle

Lyophilization cycles were performed in either Virtis Benchmark 1000 or Lyostar 3 (SP Scientific, Warminster, PA). A 2 ml fill volume in a 6 ml vial (from Schott, Type I clear glass vial) with 13 mm neck opening was used. Apart from vials, hollow glass tubes about 4 cm in length cut out from 10 ml Corning® glass pipettes (Sigma-Aldrich Corp. St. Louis, MO) with an internal diameter of approx. 8.6 mm were filled with 1 ml of the same formulations (fill height 1.8 cm). These tubes were carefully fitted with a single layer of Parafilm® at one end to create a removable bottom. The protocols for freeze-drying cycles were different based on the two main objectives of the work.

Protocol 1: Effect of protein concentration:

Formulations containing 5% w/v sucrose in 10 mM histidine buffer with different protein concentrations (0-83 mg/ml) were freeze-dried using LyoStar 3. Ice nucleation was controlled during the freezing step at a product temperature of about -10 °C with a final freezing temperature of -45 °C at a ramp rate of 0.5 °C/min during the entire freezing cycle. Primary drying was carried out at a shelf temperature of -25 °C and chamber pressure of 10 mTorr followed by secondary drying at +25 °C shelf temperature and 10 mTorr chamber pressure.

Protocol 2: Effect of ice nucleation temperature and drying conditions

For this set of experiments formulations containing 40 and 83 mg/ml mAb with 5% w/v sucrose in 10 mM histidine buffer were used. The glass transition temperatures (T_g') for the mAb formulations at concentrations of 40 and 83 mg/ml were -30 and -23 °C, respectively.

Only one shelf was used for these freeze-drying experiments where the mAb formulations in vials and tubes were placed in the center of the shelf surrounded by at least 2 rows of 20 ml vials containing 5% sucrose. These sucrose-containing edge vials were used as shields to minimize the radiative heat transfer (Rambhatla and Pikal 2003) from the inner chamber walls to the mAb-containing center vials. The cooling rate used during the freezing stage was same irrespective of the drying conditions. Initially, the shelf was cooled at 0.5 °C/min to the temperature at which ice nucleation was to be initiated (-5 or -10 °C product temperature) and held there for at least 30 minutes for thermal equilibration. Ice nucleation using ice fog technique adapted from Patel et al (Patel, Bhugra, Pikal 2009)was initiated at this point. Once ice nucleated in all the vials (vial tray was pulled out at this point to check for nucleation), the shelves were immediately cooled to -45 °C at 0.5 °C/min and held there for 2 hours. At the end of 2 hours, the chamber was evacuated to the required set point and the primary drying was initiated at a set shelf temperature. Two drying conditions (conservative versus aggressive) were used following the freezing step with the following specifics:

Conservative drying (product temperature well below the T_g'): Primary Drying: Shelf heated at 0.5 °C/min to -20 °C at a chamber pressure of 30 mTorr; Secondary Drying: Shelf heated at 0.2 °C/min to +25 °C at a chamber pressure of 30 mTorr.

Aggressive drying (product temperature above the T_g'): Shelf heated at 0.5 °C/min to +45 °C at a chamber pressure of 400 mTorr.

Pirani gauge was used to determine the end point of primary drying. (Patel, Doen, Pikal 2010) Product temperatures from 2 vials at each concentration were recorded using 36 gauge copper-constantan (type-T) thermocouples (Omega Engineering Inc., Stamford, CT) with a resolution of ±0.1 °C placed in the bottom center of vials. The thermocouples were calibrated

for 0.0 °C before each freeze-drying cycle using a mixture of ice and deionized water. At the end of the cycle, mAb containing vials were manually stoppered at ambient pressure and the open ends of the tubes were covered with multiple layers of Parafilm® in a glove box.

3.3. Reconstitution times

Freeze-dried cakes from vials were equilibrated to ambient temperature before reconstituting with 2 ml of room temperature deionized water using 3 ml syringe and 21G gauge needle. The diluent (water) was added to the vial ensuring that the entire top surface of the cake was in contact with water and the vial was then swirled. In order to remove any user-specific bias in the swirling movement, the method of reconstitution was optimized. The reconstitution was controlled at ≈150 rpm while moving along the perimeter of a circle for one revolution drawn on a laboratory bench top. A total of 5 vials were reconstituted for each sample. Presence of no visible particles marked the end point of reconstitution.

3.4. Disintegration

Freeze-dried cakes from tubes were used for studying the disintegration rates. The Parafilm® layer at the bottom of the tube was removed. The tube (attached to a ruler) was lowered into water (equilibrated to room temperature) to a height of 5 mm from the bottom of the tube (Figure 1a). Photographs were obtained to document the height of cake loss / disintegration. The images were quantified for height of cake loss from enlarged images as a function of time. The data for cake height loss below the level of the water was designated as Phase 1 and that above the level of the water was designated as Phase 2. The slope of the cake height loss vs. time plots provided a disintegration rate (mm/min) for each disintegration phase. A total of 8 tubes were analyzed for each sample (n=8).

3.5. Hydration

A flow-through dissolution apparatus (Greco, Bergman, Bogner 2011) was used to study the hydration rates for the lyophilized mAb cakes from vials (Figure 1b.). Freeze-dried cakes were powdered and 20 mg of the powder was weighed and filled in the cavity of the flow cell inside a humidity-controlled glove box. A steel rod was placed over the powder and the entire assembly was placed on an Instron testing system, Model 5543 (Norwood, MA). The sample was compressed at 0.1 mm/min to 400N. The flow cell was then connected to two 60 ml syringes containing deionized water and placed under a microscope fitted with a camera. The flow rate of water was controlled at 4 ml/min from each syringe (total 8 ml/min) using a syringe pump. Once the flow was initiated, photographs were obtained every 30 seconds for 15 minutes. For each sample at least 3 hydration experiments were performed. The photographs were magnified with the magnification factor as the ratio of the "magnified" width of the flow cell channel to its real width (2 mm). The movement of the hydration front was measured and plotted versus time to determine the hydration rate for 3 samples (n=3).

3.6. Wetting behavior

The freeze-dried cakes from vials were powdered inside a controlled humidity glove box with a spatula. Approximately 25 mg of the powder was transferred to a weighing paper and sealed in a Ziploc® bag. The powder was then compressed using the following protocol on the Instron testing system, Model 5543 (Norwood, MA): compressed at 5 mm/min to 100 N, compressed at 1 mm/min to 300 N, compressed again at 1 mm/min to 300 N. The compressed pellet was then pulled out of the Ziploc® bag and a drop (10 μL) of saturated solution containing 70% w/v sucrose and 10% w/v mannitol was placed on it. Photographs were taken immediately after the drop was placed on the cake. Two pellets were prepared for each formulation and the

contact angles for at least 2 drops were determined per pellet (n=4). For each drop a tangent was drawn at the contact point of the drop with the cake on the horizontal line as shown in Figure 1c. The left and the right angles were measured and averaged for each drop.

3.7. Residual Moisture

Residual water content in the lyophilized cakes was determined using an Aquatest™ 2010 Karl Fischer Coulometric titrator (Photovolt Instruments, Minneapolis, MN). The vials were reconstituted with 5 ml of anhydrous methanol and vortexed for 2 minutes to break the cake. The vials were held for at least 2 hours to ensure complete extraction of water. At the end of 2 hours, 500 µL of the supernatant was injected into the titrator. The experiments were done in triplicates for each vial with 2 vials for each sample. The final residual moisture content for each sample, expressed in % w/w, was an average of 6 readings.

3.8. Specific Surface Area

A BET surface area analyzer, Flowsorb III 2305 (Micromeritics Instrument Corporation, Norcross, GA) was used to measure the specific surface area of the freeze-dried samples. Approximately 100 -150 mg of each freeze-dried sample was gently crushed and transferred into glass sample tubes. The sample was outgassed at least for 6 hours at room temperature. Calibration of the instrument was performed using 100% krypton gas at ambient temperature and pressure. A mixture of krypton and helium (0.1 mol% krypton in helium) was introduced into the sample with krypton being the adsorbate and helium, the inert carrier gas. Single point measurements at 0.1 mol% krypton were performed and the results were averaged from two measurements.

4. RESULTS AND DISCUSSION

High concentration protein formulations pose unique challenges involving stability, manufacturing and delivery. (Shire, Shahrokh, Liu 2004) Considerable data on undesirable long reconstitution times for lyophilized high concentration protein formulations exist in the published literature (Bhambhani, Meyer, Blue 2010; Cao et al. 2013; Dix, Bowers, Chimanlall 2006; Shire, Shahrokh, Liu 2004). While some of these highlight the differences in the morphology of the cake structure at different protein concentrations (Shire, Shahrokh, Liu 2004) some others discuss the importance of wetting and solubility in reconstitution when the processing conditions during the freeze-drying cycle for amorphous systems were altered. (Geidobler, Konrad, Winter 2013) The present report combines the effect of the processing conditions with a detailed study of some of the underlying mechanisms contributing to the long reconstitution times. Wetting, disintegration and hydration properties of the lyophilized mAb cakes were studied. First, the results for effect of protein concentration on the reconstitution times will be presented. Based on these studies, low and high concentration mAb formulations were selected for investigating the effect of lyophilization processing conditions on the reconstitution times. Data from these studies will be discussed in the later section.

4.1. Effect of protein concentration

The effect of mAb concentration on the reconstitution times is shown in Figure 2a. The end point of reconstitution was appearance of a clear solution devoid of any visible particles. As the protein concentration increased from 0 to 83 mg/ml, the reconstitution time increased exponentially from less than a minute to about 13 minutes. At the highest mAb concentration studied (83 mg/ml), though most of the cake dissolved earlier on, a small fragment remained undissolved that prolonged the reconstitution time. To better understand the reconstitution

behavior, several other studies to explore the wetting, disintegration and hydration behavior of the lyophilized cakes were carried out.

Wetting can be described as the ability of a liquid to spread over a surface due to a balance of the cohesive forces between the liquid molecules and the adhesive forces between the liquid and solid molecules (Martin 1993). A quick method to determine the degree of wetting between a solid and a liquid surface is by measuring the contact angle formed as a result of balance of three vectors acting along the phase lines formed by the solid, liquid and gas when a drop of liquid is placed on the solid (Figure 1c). The Young Equation can be used to describe the relationships between the surface energies for this three-phase system as follows:

$$\gamma_L cos\theta = \gamma_S - \gamma_{SL} \qquad \text{Equation 2}$$

where γ_L and γ_S denote the liquid and solid surface tensions, respectively, γ_{SL} is the interfacial tension between the solid and the liquid and θ is the contact angle (Martin 1993). There is an inverse relation between the contact angle and the wetting behavior. A contact angle of > 90° corresponds to poor wetting whereas < 90° indicates good wetting by the liquid drop on the solid surface.

To quantify the wetting behavior of the mAb containing lyophilized cakes, a previously published methodology was adapted (Zografi and Tam 1976). A drop of saturated solution containing 70% w/v sucrose and 10% w/v mannitol was placed on a pellet made by compressing the lyophilized powder. It is to be noted that the contact angle is measured for ideal surfaces, which are smooth, rigid, chemically homogenous and non-reactive (Zografi and Tam 1976). By using a pellet made out of compressed lyophilized powder in our studies, the contribution of surface porosity was minimized/removed. A saturated solution for the drop was used in order to

avoid any solubilization of the pellet during the measurement of the contact angle. Moreover, the contact angle values obtained from this experiment were determined for a range of protein concentrations to investigate the trend in the values and not really use the absolute values for any further calculations. Figure 2e. shows a panel of pictures for the drops placed on powder compacts of increasing protein concentration. The data on contact angles as determined from these pictures are plotted as a function of protein concentration in Figure 2b. The contact angle increased from 20° to 120° as the protein concentration increased from 0 to 20 mg/ml indicating poorer wetting with increasing protein concentration. However, beyond 20 mg/ml mAb concentration the value for contact angle reached a plateau implying no further change in the wetting behavior.

Dissolution rate is improved when the surface area of the dissolving solid is increased (Martin 1993). Disintegration of the lyophilized cake into smaller fragments increases the surface area, which leads to faster dissolution of the cake leading to a shorter reconstitution time. The Washburn method is a well-known procedure for determining the wetting behavior for powders through capillary rise of a liquid through the powder bed (Washburn 1921). Similar technique was used in this study to monitor the disintegration of the cake as the reconstitution fluid moved up a lyophilized cake due to capillary action. Instead of lyophilized cakes in a vial, cakes prepared by lyophilization of the solution formulation in open ended glass tubes with a removable bottom were used to study the disintegration rate which helped in displacement of air from the top as the cake disintegrated from the bottom end of the tube as the water moved up.

The disintegration rate as a function of protein concentration is shown in Figure 2c. Phase 1 in the tube refers to the cake disintegration, which is in contact with water (up to 5 mm) and can be compared to the initial part of cake reconstitution in a vial where the water is in direct

contact with the cake when added to the vial. Phase 2 refers to the cake disintegration in the tube beyond 5 mm and can be compared to the reconstitution of that last cake fragment, which remains undissolved and prolongs the reconstitution time. In contrast to the original Washburn experiment, which shows that the penetration distance of the liquid up the capillary is proportional to the square root of time, we observed a linear dependence between the decrease in cake height and time. This difference in the time dependence is attributed to the fact that the disintegration of the cake was being monitored in our experiments and not the movement of the water through the cake. Phase 1 was faster than Phase 2 at all mAb concentrations. A continuous decrease in the Phase 1 rates was observed as the protein concentration was increased to 83 mg/mL. An initial dramatic decrease in the Phase 2 rates was observed as the protein concentration was increased to 63 mg/ml followed by a very small change in the disintegration rates at higher concentrations.

Finally, the hydration behavior for the mAb formulations at the different concentrations was studied on lyophilized powder compacts placed as an insert in a flow-cell (Greco, Bergman, Bogner 2011). Instead of using the lyophilized cake as it is, the powder was compressed into a compact to resolve the role of hydration in the "absence" of the porous cake structure. The compact was flush with the channel wall and the reconstitution fluid was allowed to flow through a channel just above the compact such that the flow remained undisturbed. The hydration rates for the different protein concentrations are shown in Figure 2d. As the protein concentration increased the hydration rates decreased non-linearly.

Further, we compared our data on reconstitution times for amorphous lyophilized high concentration protein formulations with the recently published literature (Beech et al. 2015; Cao et al. 2013; Geidobler, Konrad, Winter 2013) as a function of protein to sugar ratio (Figure 3).

The proteins used in all four cases are different with some differences in the reconstitution methods as well. The averaged reconstitution times for lyophilized BSA-sucrose formulations containing 100 and 194 mg/ml protein were 2.7 and 20 minutes obtained via agitation at 400 rpm irrespective of the freezing protocol by Geidobler et al (Geidobler, Konrad, Winter 2013). Since the swirling method used in this study was about 3 times faster than our work (150 rpm) we used a factor of 3 to convert the shorter reconstitution times from Geidobler et al's work to an equivalent reconstitution time of 8.1 and 60 minutes for 100 and 194 mg/ml BSA concentrations, respectively. The reconstitution times from Beech et al (Beech et al. 2015) for lyophilized cakes containing BSA at 50 and 200 mg/ml with 7% w/v sucrose were also averaged irrespective of the freezing protocol. On adding the diluent to the vial, the vial was swirled once and then left aside to achieve complete reconstitution. We assumed a factor of 0.5 to convert the longer reconstitution time obtained without swirling the vial into equivalent reconstitution time if one were to swirl the vial, for the ease of comparison. Hence, the actual reconstitution times obtained from Beech et al's work, 1 and 40 minutes for 50 and 200 mg/ml BSA were converted to 0.5 and 20 minutes, respectively. The reconstitution times for different concentrations of Fc-fusion protein formulated with 4.5% sucrose and 2% mannitol in the amorphous phase from Cao et al's (Cao et al. 2013) work were used directly without any further modifications assuming that the vials were swirled manually. Figure 3 shows a strong correlation between the equivalent reconstitution time and the protein to sugar ratio. Below a ratio of 1 the reconstitution times were less than a minute. As the amount of protein increased when compared to the sugar content in a formulation, the reconstitution times increased non-linearly.

From the above results it was concluded that poorer wetting combined with decreased disintegration and hydration rates lowered the dissolution rates of the lyophilized cakes and

prolonged the reconstitution times as the protein concentration increased. The ratio of protein to saccharide contributes to the effects of wetting, disintegration and hydration of the cakes during reconstitution.

4.2. Effect of ice nucleation temperature and drying conditions

The processing conditions during a freeze-drying affect the microstructure of the final freeze-dried cake, which can further alter the reconstitution times. A few studies from the literature discussed the role of pore size, a consequence of the freezing step, on the reconstitution times of high concentration proteins (Beech et al. 2015; Geidobler, Konrad, Winter 2013). Also, Krishnan et al (Krishnan, Pallitto, Ricci) observed that using a lower secondary drying temperature of 25 °C versus 45 °C during the freeze drying cycle for Etanercept (50 mg/ml with mannitol and sucrose) decreased the reconstitution times from 90 to 41.6 seconds.

In our work, 40 and 83 mg/ml mAb were selected from the range of concentrations studied, to be further explored for the effect of processing conditions. Ice nucleation was controlled at two temperatures, -5 and -10 °C during freezing, using an ice fog method adapted from Rambhatla et al (Rambhatla et al. 2004). The freezing was followed by either of the two primary drying conditions, aggressive or conservative (details are provided in the methods section). Some cake shrinkage and cracking in the final lyophilized product was observed in all vials irrespective of the protein concentration. The average product temperature during primary drying was about -33 °C irrespective of the protein concentration and ice nucleation temperature (T_{nuc}) when conservative drying conditions were employed. The product temperatures in the tubes were recorded to be at least 2 °C higher than those in the vials for all formulations. This can be attributed to the increased resistance to vapor flow posed by the thicker dry layer in the

tubes versus that in the vials owing to the higher fill depths. Moreover, there can be a small difference in the heat transfer to the product from the shelf via the Parafilm® (in case of tubes) versus glass (in case of vials). At the aggressive conditions of primary drying, even when the product temperature (increases continuously from -35 to +40 °C) was well above the glass transition temperature (for 40 and 83 mg/ml were -30 and -23 °C respectively) no sign of macro-collapse or excessive cake shrinkage was seen. Such retention of the cake structure above glass transition temperature has been previously reported (Colandene et al. 2007). The primary drying times for the conservative cycles were 42.5 and 45.2 hours at a T_{nuc} of -5 and -10 °C respectively, where the end point of primary drying was determined based on equilibration of the Pirani gauge reading with the capacitance manometer (Patel, Doen, Pikal 2010). Use of aggressive conditions for drying significantly reduced the drying times to 12.5 and 16.8 hours for T_{nuc} of -5 and -10 °C, respectively. In general, a longer drying time was observed for T_{nuc} of -10 °C than at -5 °C because of the presence of smaller pores and a higher resistance to sublimation similar to (or our observations are in agreement with) previously published reports (Awotwe-Otoo et al. 2013; Searles, Carpenter, Randolph 2001a).

4.2.1. Reconstitution times

Reconstitution times for the freeze-dried formulations at both 40 and 83 mg/ml mAb using T_{nuc} of -5 and -10 °C followed by either conservative or aggressive drying are shown in Figure 4. At 40 mg/ml, the reconstitution times were less than a minute and appeared to be independent of the T_{nuc} and drying conditions (Figure 4a.). However, at the higher mAb concentration of 83 mg/ml significant differences in reconstitution times were observed (Figure 4b.). At conservative drying conditions, T_{nuc} of -10 °C led to slightly shortened reconstitution times than at -5 °C but the effect was reversed at the aggressive drying conditions. In general,

aggressive drying shortened the reconstitution times at 83 mg/ml and the effect was more pronounced when ice was nucleated at -5 °C. Since the product temperature at the both the protein concentrations was above the glass transition temperature, the aggressive drying probably caused restructuring of ice combined with an increase in the ice crystal size due to Ostwald ripening.(Searles, Carpenter, Randolph 2001b) The high temperature drying condition probably led to formation of larger pores in the final dried product causing easy displacement of air from the pores during reconstitution leading to a shorter reconstitution time. (Geidobler, Konrad, Winter 2013)

4.2.2. Disintegration rate

The disintegration rates for lyophilized cakes at the combination of four processing conditions are shown in Figure 5. Note the difference in the scales for the y-axis at the low and high mAb concentration. As expected, the disintegration rates for 40 mg/ml mAb are higher than those for 83 mg/ml, which is consistent with the reconstitution times (Figure 4). In general, Phase 1 (disintegration of first 5 mm of cake immersed in water) rates are faster than Phase 2 (disintegration of cake beyond 5 mm due to contact with water as a consequence of capillary rise). At 40 mg/ml the disintegration rates were much faster for the first phase than at the higher protein concentration of 83 mg/ml. The effect of slower disintegration in the second phase (as compared to Phase 1) does not seem to have an effect on the reconstitution times (less than a minute) for the 40 mg/ml protein systems (Figure 4a.). At 83 mg/ml, the first phase of disintegration was slower in the aggressively dried cakes at both nucleation temperatures. However, in contrast a shorter reconstitution time in vials was observed for the aggressively dried cakes at both the nucleation temperatures (Figure 4b.). Since the phase 2 disintegration rate refers to the dissolution of the cake fragment, which remains undissolved prolonging the

reconstitution time, reconstitution behavior for 83 mg/ml protein systems is probably best described by phase 2 than by phase 1.

4.2.3. Wetting behavior

Contact angles of lyophilized cakes at 40 and 83 mg/ml mAb and at both the drying conditions but only for the higher nucleation temperature of -5 °C were determined. Contact angle for a control formulation containing 83 mg/ml mAb in 10 mM His buffer (no sucrose) was also measured. The data on contact angles between the drop and the powder pellet are shown in Figure 6. Contact angles for all cases were found to be > 90° indicating poor wetting of the pellets. Since the reconstitution times for all the cakes at 40 mg/ml were less than a minute, the poor wetting of these cakes does not seem to impact the reconstitution behavior. At 83 mg/ml, while the aggressively dried cakes showed poorer wetting than the conservatively dried cakes, the reconstitution times were shorter for the former.

4.2.4. Hydration rate

Hydration rates for lyophilized cakes at 40 and 83 mg/ml at both the drying conditions but only for the higher nucleation temperature of -5 °C were determined (Figure 7). At 40 mg/ml, the hydration rates were found to be 2.5 times faster than those at 83 mg/ml. No effect of the drying conditions was observed on the hydration rates at a given mAb concentration. At 83 mg/ml mAb concentrations similar hydration rates were observed with and without sucrose in the formulation.

4.2.5. Specific surface area and residual moisture

The BET specific surface areas are plotted in Figure 8. The SSA values were found to be low, ranging from 0.2 to 0.5 m^2/g irrespective of the protein concentration. No correlation was found between the SSA and the vial reconstitution times. This observation is in agreement with the case studies for high concentration proteins in the existing published literature (Beech et al. 2015; Cao et al. 2013; Geidobler, Konrad, Winter 2013). The residual moisture contents (values not shown here) at the end of the freeze-drying cycle were found to be < 1% w/w in all cases.

To summarize, at a mAb concentration of 40 mg/ml, complete dissolution of the lyophilized cake was observed within a minute yielding very short reconstitution times irrespective of the ice nucleation temperature and drying conditions. While the wetting behavior was found to be poor at this concentration, the disintegration and the hydration rates were very fast and appear to be the dominant mechanism for faster reconstitution. At the higher mAb concentration of 83 mg/ml, the aggressive drying appeared to shorten the reconstitution times at both the nucleation temperatures. Though the Phase 1 disintegration rates in tubes were slower for the aggressively dried cakes, the Phase 2 rates were found to be similar irrespective of the drying conditions at any given ice nucleation temperature. No significant effect of the nucleation temperatures and drying conditions on the wetting and disintegration behavior was observed at 83 mg/ml mAb concentration.

5. CONCLUSIONS

A short reconstitution time is a key desirable attribute of a lyophilized product. However, long reconstitution times are encountered during the development of freeze-dried formulations of highly concentrated proteins, which are unfavorable from an administration perspective.

Existing published literature has emphasized on the role of the pore size in the lyophilized cake, the openness and the connectivity of the pores and the solubility limit of the proteins in the reconstitution of highly concentrated protein formulations in amorphous phase (Beech et al. 2015; Cao et al. 2013; Geidobler, Konrad, Winter 2013). Also, some empirical strategies to reduce the reconstitution times are described in the patent literature. However, there is a lack of systematic studies to understand the impact of formulation and processing variables on wetting, disintegration, and hydration during reconstitution.

This report describes three approaches to understand the contribution of wetting, disintegration and hydration mechanisms in the reconstitution of proteins as a function of protein concentration. As the protein concentration increased, poor wetting behavior combined with the slower hydration and disintegration resulted into long reconstitution times. An effect of protein to sugar ratio on the reconstitution time was explicitly pointed out by combining the data from our work with a few other studies (Beech et al. 2015; Cao et al. 2013; Geidobler, Konrad, Winter 2013). With this ratio less than 1 the reconstitution times were found to be less than a minute. However, as the protein to sugar ratio increased, a non-linear increase in the reconstitution times was observed. Further, the effect of ice nucleation temperature (-5 vs. -10 °C) and drying conditions (aggressive vs. conservative) on the reconstitution behavior of the at 40 and 83 mg/ml mAb concentrations was studied. At the lower protein concentration of 40 mg/ml none of the processing conditions affected the dissolution behavior leading to short reconstitution times (< 1 min). At higher protein concentration of 83 mg/ml, aggressively dried cakes exhibited shorter reconstitution times probably because of larger pores formed in the final lyophilized cake owing to the higher product temperature (exceeding the glass transition temperature). However, no significant effect of the drying conditions was observed on the wetting, disintegration and the

hydration rates at 83 mg/ml protein. No effect of specific surface area on recon times was observed. Thus, reconstitution of a lyophilized cake containing high protein concentration in a vial is a complex interplay between the cake properties such as the wetting behavior, hydration, disintegration and solubility combined with the hydrodynamics involved during the swirling motion of reconstitution.

6. ACKNOWLEDGEMENTS

The author would like to thank Sharon Bryant, Anthony Gudinas, Jennifer Juneau, Concepcion Kafka, Sheetal Pai and Brian Wilbur from Pfizer, Andover, MA for their help with regards to different aspects of this work.

7. REFERENCES

Awotwe-Otoo D, Agarabi C, Read EK, Lute S, Brorson KA, Khan MA, Shah RB. 2013. Impact of controlled ice nucleation on process performance and quality attributes of a lyophilized monoclonal antibody. Int J Pharm 450(1):70-8.

Beech KE, Biddlecombe JG, van der Walle, Christopher F, Stevens LA, Rigby SP, Burley JC, Allen S. 2015. Insights into the influence of the cooling profile on the reconstitution times of amorphous lyophilized protein formulations. European Journal of Pharmaceutics and Biopharmaceutics 96:247-54.

Bhambhani A, Meyer BK, Blue JT. 2010. Methods for producing high concentration lyophilized pharmaceutical formulations.

Bhatnagar BS, Tchessalov S, Lewis LM, Johnson R. Encyclopedia of pharmaceutical science and technology. .

Cao W, Krishnan S, Ricci MS, Shih L, Liu D, Gu JH, Jameel F. 2013. Rational design of lyophilized high concentration protein formulations-mitigating the challenge of slow reconstitution with multidisciplinary strategies. Eur J Pharm Biopharm 85(2):287-93.

Colandene JD, Maldonado LM, Creagh AT, Vrettos JS, Goad KG, Spitznagel TM. 2007. Lyophilization cycle development for a high-concentration monoclonal antibody formulation lacking a crystalline bulking agent. J Pharm Sci 96(6):1598-608.

Dix D, Bowers K, Chimanlall G. 2006. IL-1 Antagonist Formulations.

Forny L, Marabi A, Palzer S. 2011. Wetting, disintegration and dissolution of agglomerated water soluble powders. Powder Technol 206(1):72-8.

Geidobler R, Konrad I, Winter G. 2013. Can controlled ice nucleation improve Freeze-Drying of Highly-Concentrated protein formulations? J Pharm Sci 102(11):3915-9.

Greco K, Bergman TL, Bogner R. 2011. Design and characterization of a laminar flow-through dissolution apparatus: Comparison of hydrodynamic conditions to those of common dissolution techniques. Pharm Dev Technol 16(1):75-87.

Kasper JC and Friess W. 2011. The freezing step in lyophilization: Physico-chemical fundamentals, freezing methods and consequences on process performance and quality attributes of biopharmaceuticals. European Journal of Pharmaceutics and Biopharmaceutics 78(2):248-63.

Krishnan S, Pallitto MM, Ricci MS. Development of formulations for therapeutic monoclonal antibodies and fc fusion proteins. Formulation and Process Development Strategies for Manufacturing Biopharmaceuticals :383-427.

Martin A. 1993. Physical pharmacy: Physical chemical principles in the pharmaceutical sciences. BI Waverly. Pvt Ltd.

Patel SM, Doen T, Pikal MJ. 2010. Determination of end point of primary drying in freeze-drying process control. AAPS PharmSciTech 11(1):73-84.

Patel SM, Bhugra C, Pikal MJ. 2009. Reduced pressure ice fog technique for controlled ice nucleation during freeze-drying. AAPS PharmSciTech 10(4):1406-11.

Pikal MJ. 2002. Freeze drying. Encyclopedia of Pharmaceutical Technology, Marcel Dekker, New York 1299:1326.

Rambhatla S, Ramot R, Bhugra C, Pikal MJ. 2004. Heat and mass transfer scale-up issues during freeze drying: II. control and characterization of the degree of supercooling. Aaps Pharmscitech 5(4):54-62.

Rambhatla S and Pikal MJ. 2003. Heat and mass transfer scale-up issues during freeze-drying, I: Atypical radiation and the edge vial effect. AAPS PharmSciTech 4(2):111-20.

Schober C and Fitzpatrick J. 2005. Effect of vortex formation on powder sinkability for reconstituting milk powders in water to high solids content in a stirred-tank. J Food Eng 71(1):1-8.

Searles JA, Carpenter JF, Randolph TW. 2001a. The ice nucleation temperature determines the primary drying rate of lyophilization for samples frozen on a temperature-controlled shelf. J Pharm Sci 90(7):860-71.

Searles JA, Carpenter JF, Randolph TW. 2001b. Annealing to optimize the primary drying rate, reduce freezing-induced drying rate heterogeneity, and determine tg' in pharmaceutical lyophilization. J Pharm Sci 90(7):872-87.

Sharma VK, Chih H, Mrsny RJ, Daugherty AL. 2009. The formulation and delivery of monoclonal antibodies. Therapeutic Monoclonal Antibodies: From Bench to Clinic :673-709.

Shire SJ, Shahrokh Z, Liu J. 2004. Challenges in the development of high protein concentration formulations. J Pharm Sci 93(6):1390-402.

Shittu T and Lawal M. 2007. Factors affecting instant properties of powdered cocoa beverages. Food Chem 100(1):91-8.

Tchessalov S, Kantor A, Li L, Luksha N, Warne N. 2010. Slow dissolution method for reconstitution of lyophilized material.

Washburn EW. 1921. The dynamics of capillary flow. Physical Review 17(3):273.

Zografi G and Tam SS. 1976. Wettability of pharmaceutical solids: Estimates of solid surface polarity. J Pharm Sci 65(8):1145-9.

8. FIGURES

(a)

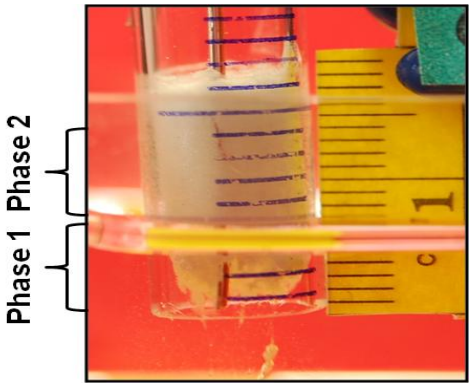

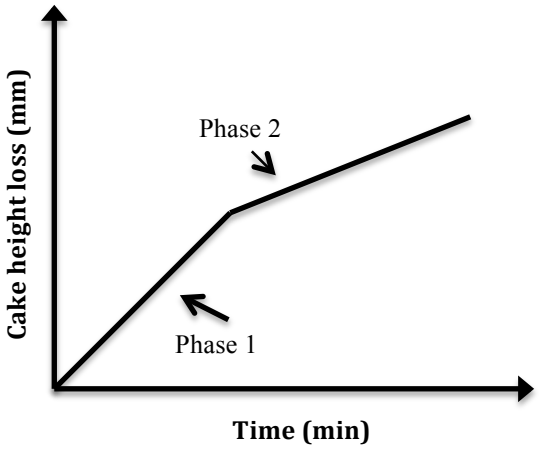

(b)

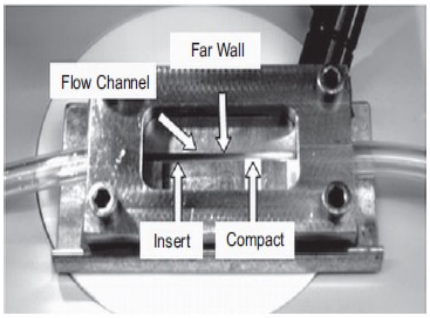

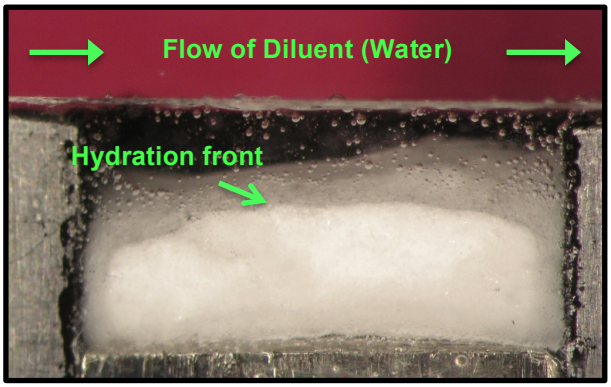

(c)

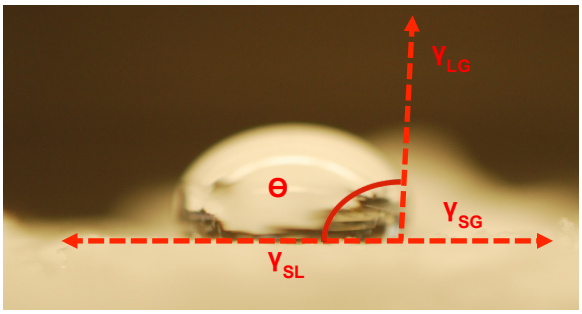

Figure 1 - (a) Left image: Picture of a tube containing lyophilized cake attached to a ruler and immersed into water up to 5 mm. Disintegration of first 5 mm of cake refers to Phase 1 and beyond 5 mm is Phase 2. Right image: A representative graph of cake height loss (in mm) plotted against time (in minutes) for Phase 1 and 2. (b) Left image: Top view of a miniaturized flow-cell connected to a tube used for determination of the hydration rates with the different parts marked. Right image: A magnified image of the compacted cake placed in the cell as observed through a camera. The direction of diluent flow and the hydration front are shown. (c) A drop of saturated solution containing 70% sucrose and 10% mannitol placed on a compacted lyophilized powder pellet. Contact angle θ is the angle formed between the vectors γ_{SL} and γ_{LG} denoting the solid-liquid and liquid-gas interfacial tensions.

(a)

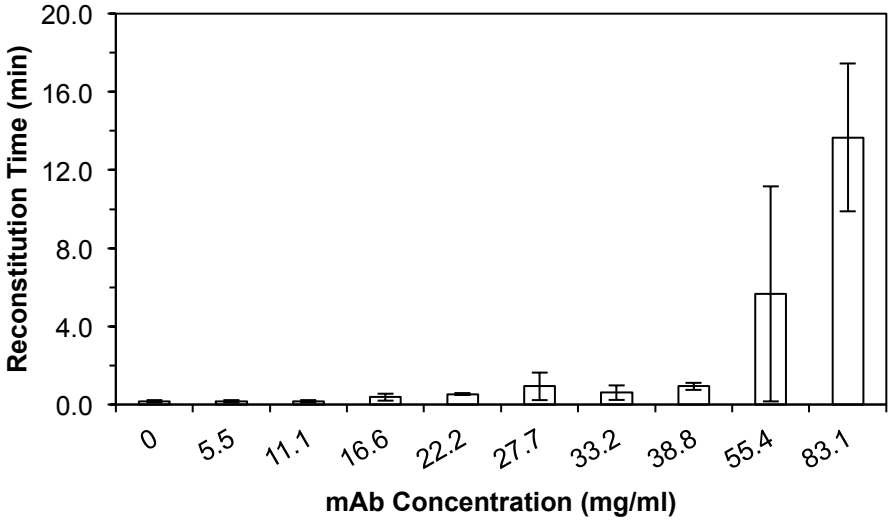
20.0
16.0
12.0
8.0
4.0
0.0
Reconstitution Time (min)
0
5.5
11.1
16.6
22.2
27.7
33.2
38.8
55.4
83.1
mAb Concentration (mg/ml)

(b)

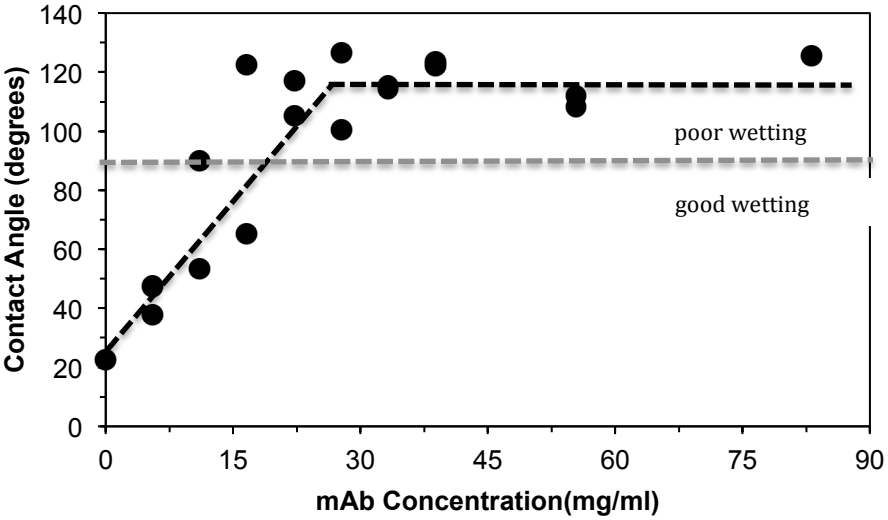
140
120
100
80
60
40
20
0
Contact Angle (degrees)
poor wetting
good wetting
0
15
30
45
60
75
90
mAb Concentration(mg/ml)

(c)

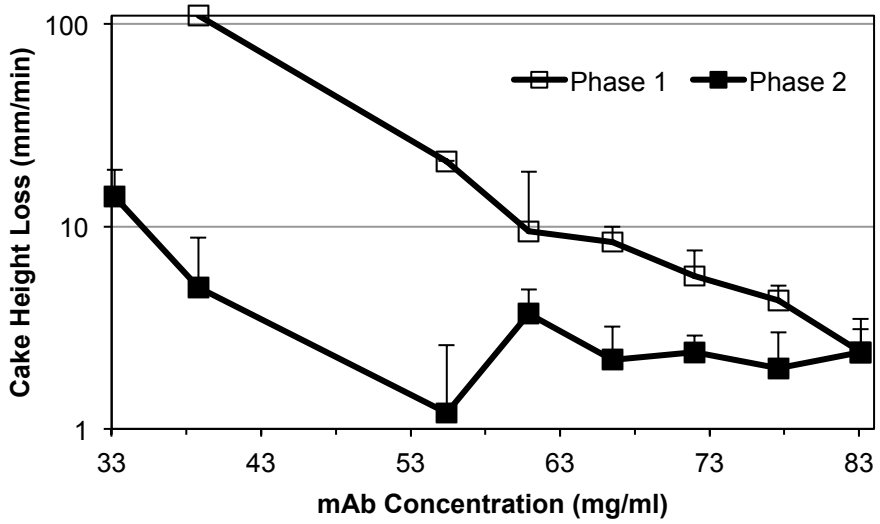
100
10
1
Cake Height Loss (mm/min)
Phase 1
Phase 2
33
43
53
63
73
83
mAb Concentration (mg/ml)

(d)

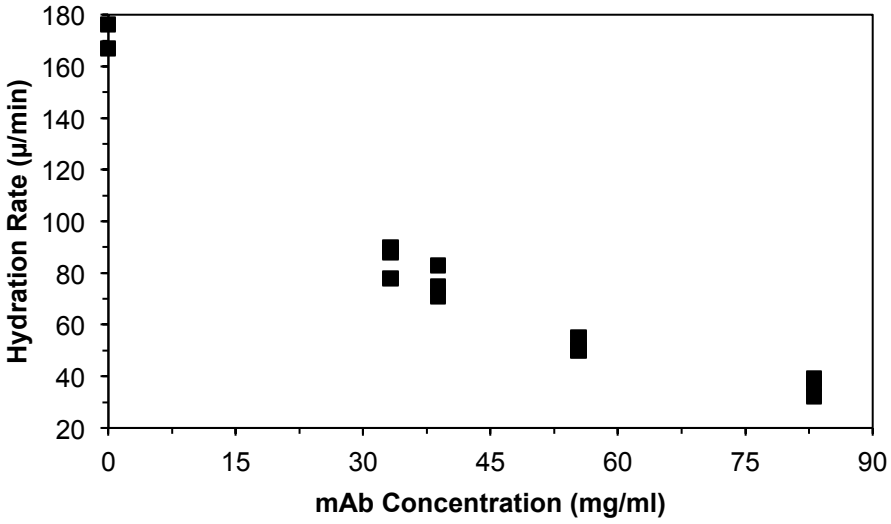
180
160
140
120
100
80
60
40
20
Hydration Rate (µ/min)
0
15
30
45
60
75
90
mAb Concentration (mg/ml)

(e)

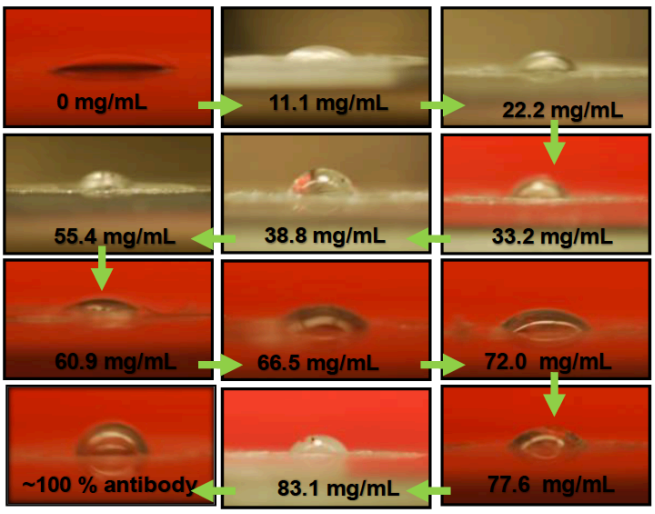

Figure 2 - Effect of protein concentration on (a) reconstitution times in vials (b) wetting behavior determined by contact angles between a drop of saturated solution containing 70% sucrose and 10% mannitol placed on a powder pellet, the grey dashed line (at 90°) demarcates the transition between the good (<90°) and the poor wetting (>90°) (c) disintegration rate: Phase 1 (open squares), Phase 2 (closed squares) in tubes measured by monitoring the loss in cake height with time, and (d) hydration rates determined in a miniaturized flow cell using powder compacts. (e) Pictures of drops placed on lyophilized powder pellets for determination of contact angles with an increasing protein concentration.

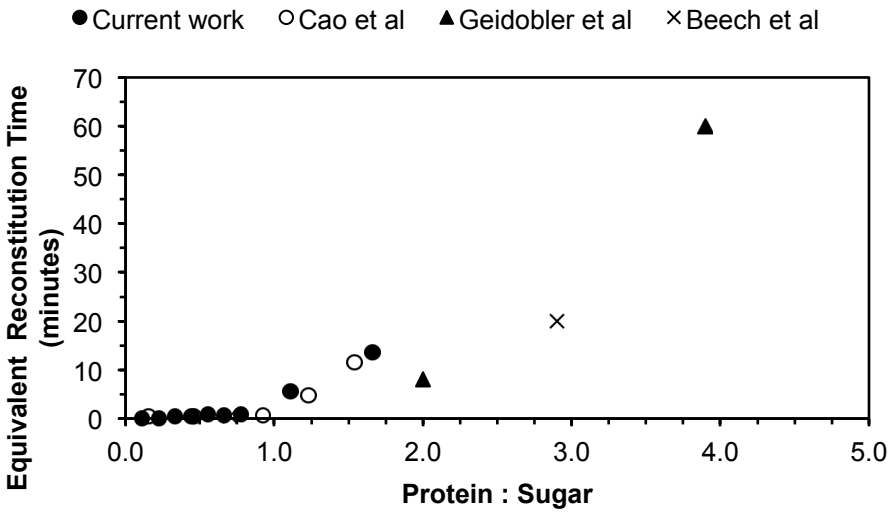

Figure 3 - A plot of equivalent reconstitution times with protein to sugar ratio. Data shown represents reconstitution times pooled from four different case studies involving different proteins and slightly different reconstitution methods. The reconstitution times from different studies shown in the graph were adjusted using a factor to obtain the equivalent reconstitution times for ease of comparison as explained in the text.

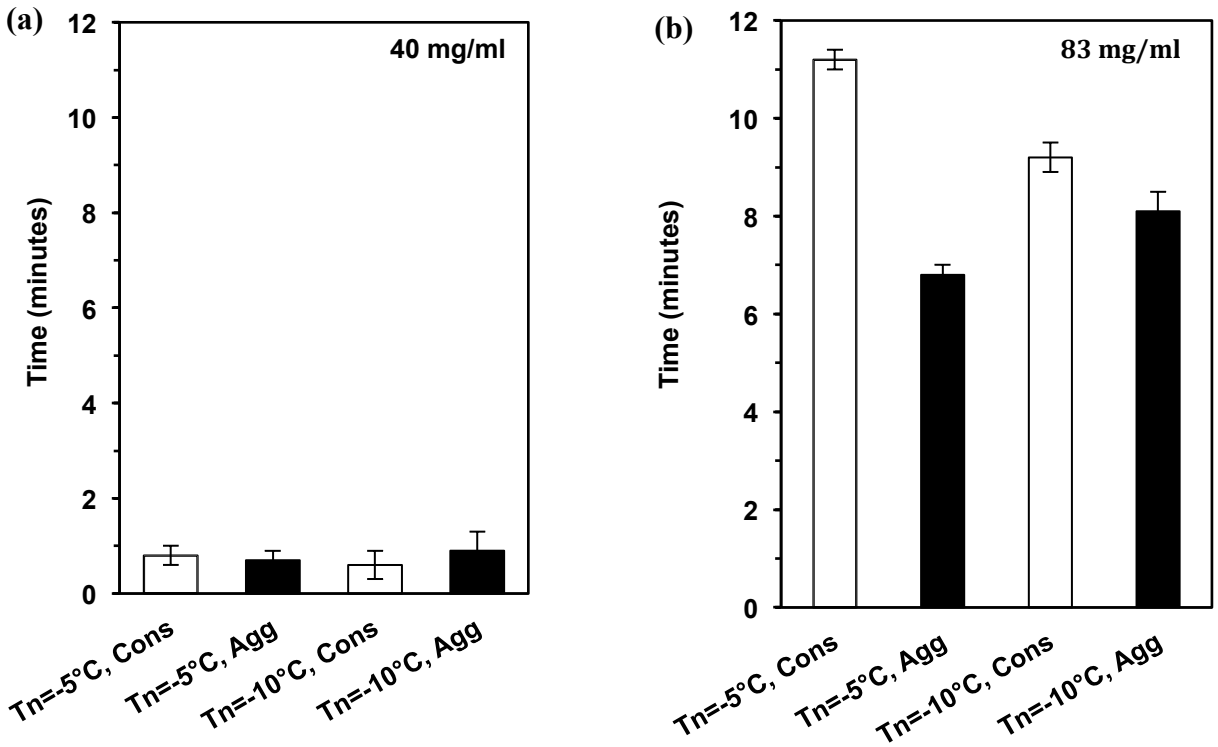

Figure 4 - Reconstitution times in vials at different ice nucleation temperatures and drying conditions at (a) 40 mg/ml mAb and (b) 83 mg/ml mAb with 5% w/v sucrose in 10 mM His buffer. □ represents conservative drying conditions and ■ represents aggressive drying conditions. The results are averaged from 5 samples (n=5).

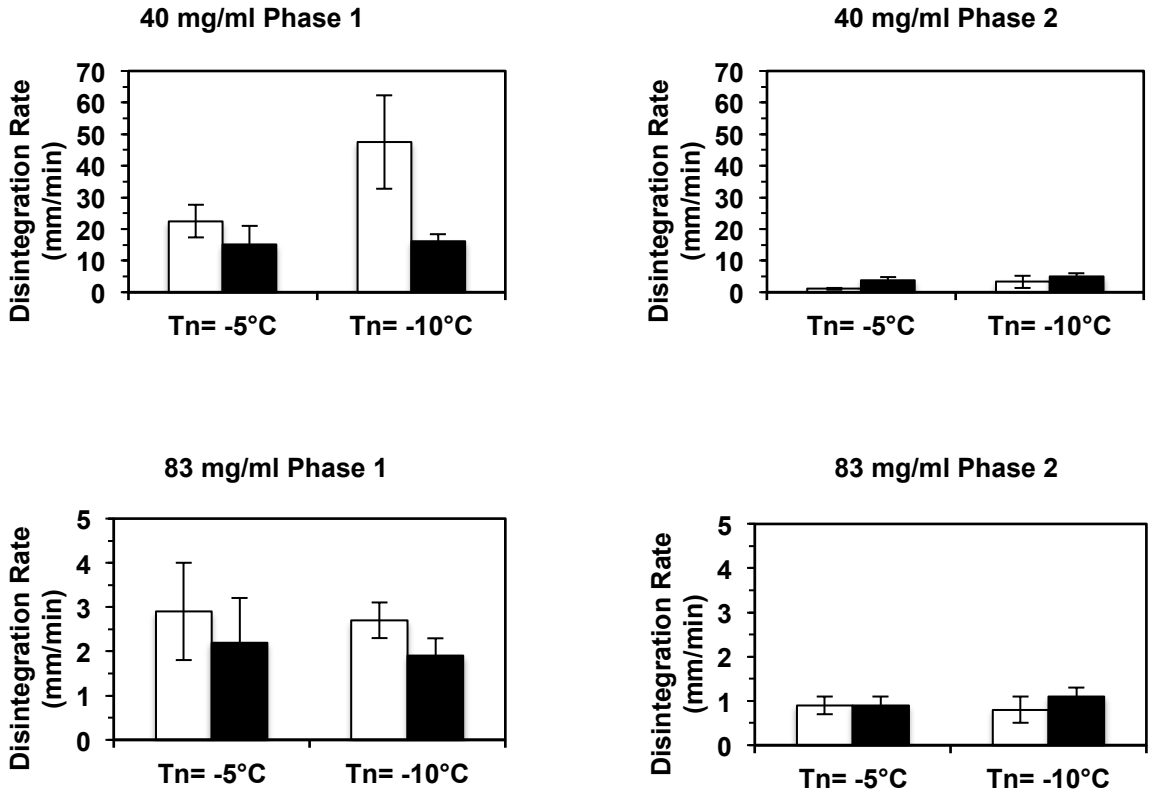

Figure 5 - Disintegration rates in tubes for 40 mg/ml mAb (upper panel) and 83 mg/ml mAb (lower panel). □ represents conservative drying conditions and ■ represents aggressive drying conditions. Phase 1 refers to cake disintegration of first 5 mm and Phase 2 denotes cake disintegration beyond 5 mm. The results are averaged from 8 samples (n=8).

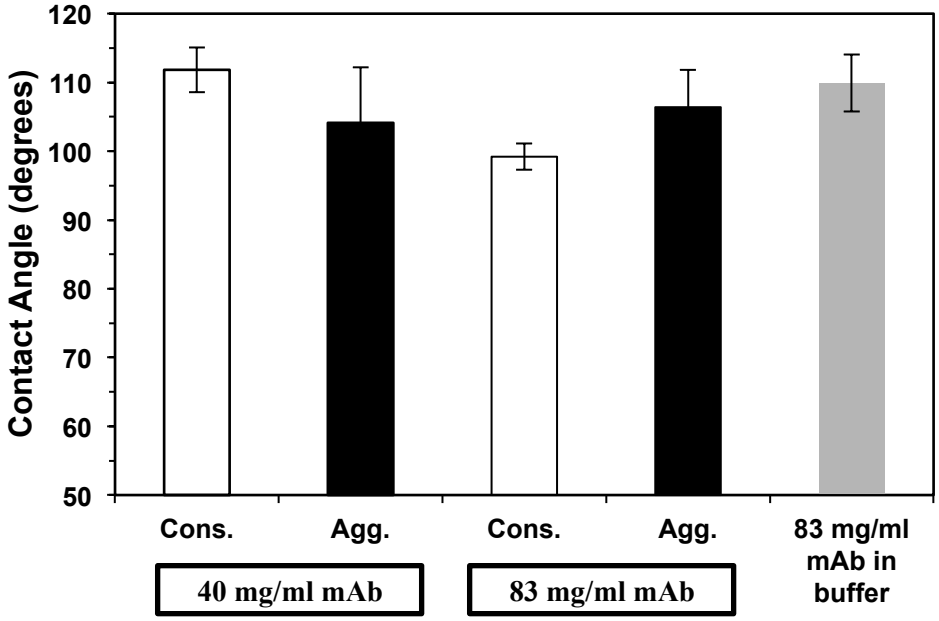

Figure 6 - Contact angles for 40 and 83 mg/ml mAb at conservative and aggressive drying conditions using an ice nucleation temperature of -5 °C. □ represents conservative drying conditions and ■ represents aggressive drying conditions. ■ represents the contact angle for pure mAb in buffer without any sucrose dried aggressively. The results are averaged from 8 samples (n=8).

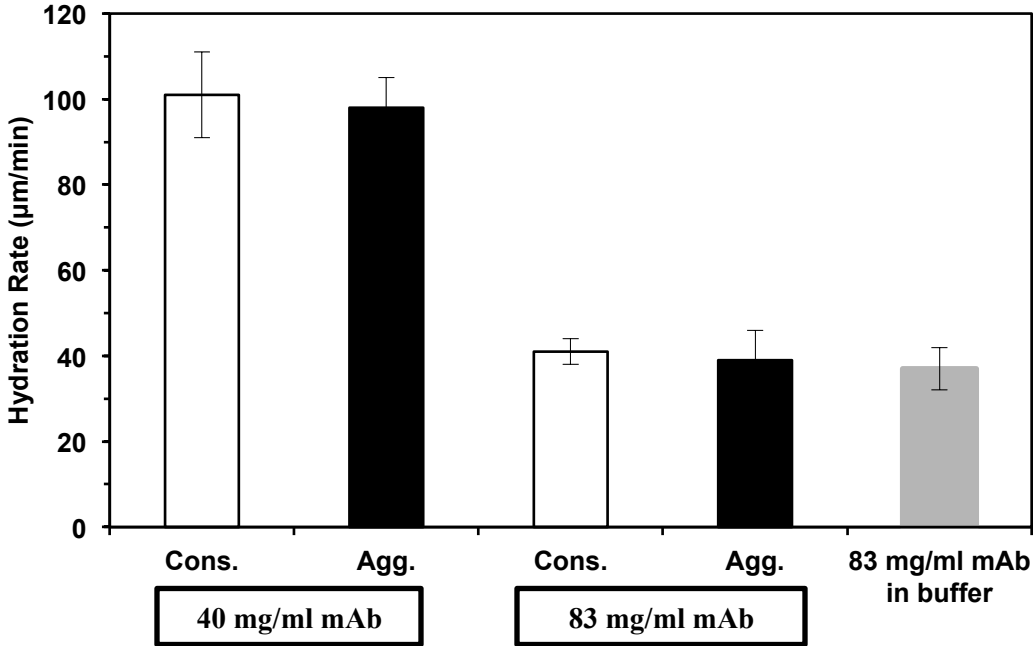

Figure 7 - Hydration rates for 40 and 83 mg/ml mAb at conservative and aggressive drying conditions using an ice nucleation temperature of -5 °C. □ represents conservative drying conditions and ■ represents aggressive drying conditions. ■ represents the hydration rate for pure mAb in buffer without any sucrose dried aggressively. All experiments were performed in triplicates (n=3).

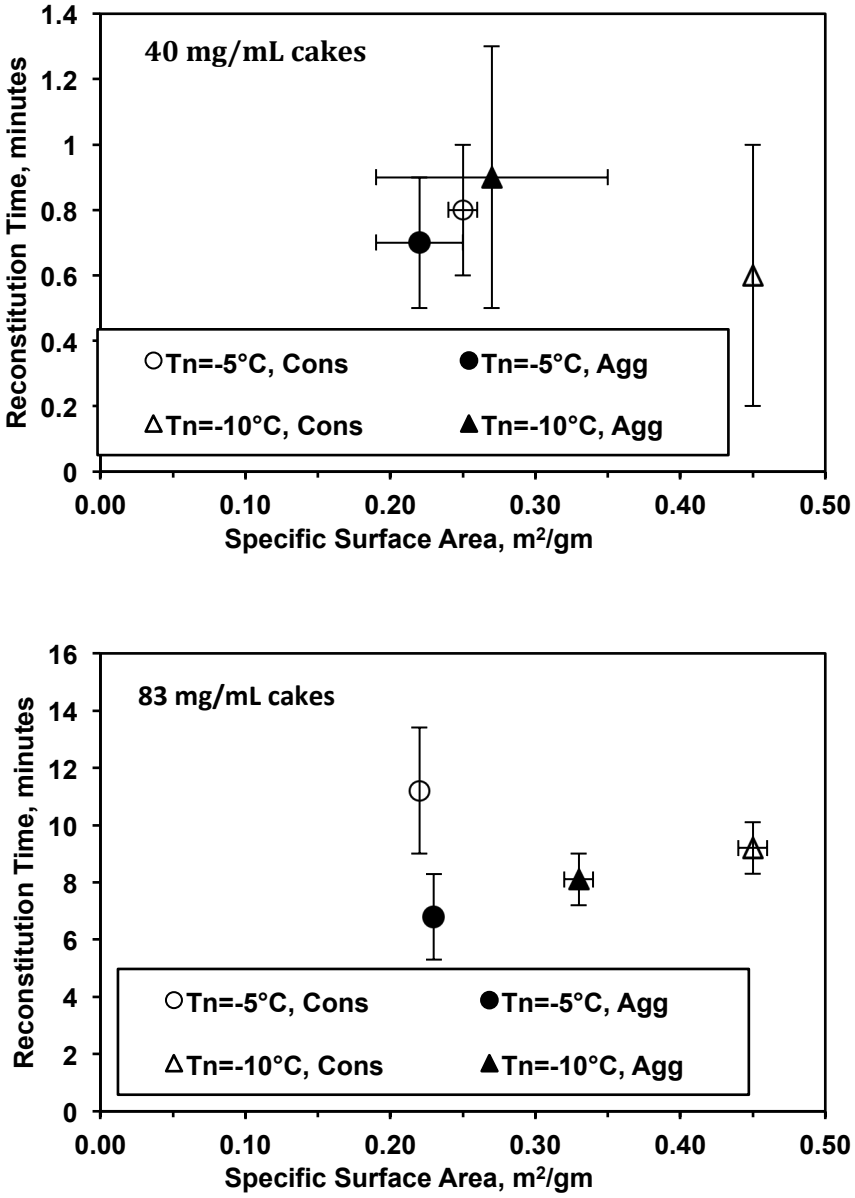

Figure 7 - Specific surface areas for 40 mg/ml (top panel) and 83 mg/ml (bottom panel) mAb concentrations. All experiments were performed in duplicates (n=2).

Chapter 6

Summary

Freeze-drying or lyophilization is the process of choice for converting sterile solutions of some labile drugs to be administered parenterally, into solids for enhanced long-term storage stability and ease of handling during transportation. In addition to physical and chemical stability, quality attributes for a lyophilized product include elegant cake structure and short reconstitution time. These quality attributes are influenced by all three stages of lyophilization namely, freezing, primary drying and secondary drying. Both intra- and inter-batch heterogeneities in these stages lead to a variation in the quality of the final product, which produce variable product performance. Heterogeneity in heat transfer across the batch during the process leads to extended freeze-drying cycle times to assure all vials have completed each stage, resulting in a higher processing cost and expensive final product to the end user. A thorough understanding of the heterogeneities in heat and mass transfer during the lyophilization process can aid in further optimization of a cycle to achieve a better quality product at a reduced cost consistently.

The vial heat transfer coefficient, K_v, is a parameter used to quantify the heat flow required for sublimation of ice from the frozen product. This coefficient is used in a heat and mass transfer model to develop an optimized primary drying cycle. **Chapter 2** describes in detail the effect of processing conditions on the calculation of vial heat transfer coefficients using sublimation rates measured by Tunable Diode Laser Absorption Spectroscopy (TDLAS) and a gravimetric method. Based on the method to measure sublimation rate as well as product temperature, the K_v can be calculated i) as a function of time or as an average over a period of time, and ii) for a single vial, group of vials or the entire batch. Using TDLAS as a rapid method for determining the batch-averaged K_v at different combinations of chamber pressure and shelf

temperature demonstrated that K_v is a strong function of chamber pressure and has only a weak dependence on the shelf temperature. However, shelf temperature was shown to alter the distribution in K_v across a single shelf, particularly at the higher shelf temperatures more recently used for lyophilization of biotech products. Furthermore, though there was no significant effect of fill volume or solutes in the frozen product on the batch-averaged time-averaged K_v, the distribution in K_v across the batch does depend on these parameters.

The aim of **Chapter 3** was to determine the ability to predict the distribution of drying times and maximum product temperature within a batch from measured distributions in key input parameters, a) vial heat transfer coefficient, b) the resistance of the product dry layer to sublimation, c) fill volume and d) shelf temperature, using a quasi steady-state heat and mass transfer model of primary drying. This required development of protocols to accurately characterize the input parameters. The input distribution most difficult to characterize was the resistance of the product dry layer to sublimation. Ultimately, good agreement was achieved between the predicted drying times and experimental results using a 5% w/v sodium chloride solution as a model system. Further studies using the model to predict the primary drying time and maximum product temperature for different pharmaceutical materials at a range of concentrations will improve confidence in using the protocols for input characterization and the modeling.

Chapter 4 discusses the measurement of spatial variation of pressure in the freeze-drying chamber using a differential capacitance manometer positioned at the center and the back edge of a laboratory-scale freeze-dryer. The pressure difference was found to be a function of sublimation flux and clearance between the sublimation front and the upper shelf during sublimation from an ice slab placed on the shelf of a lab-scale freeze-dryer. While only a modest

3 mTorr pressure difference was observed when the sublimation flux was doubled from 0.5 to 1.0 $kg \cdot hr^{-1} \cdot m^{-2}$ at a clearance of 2.6 cm, an 8-fold increase in the pressure drop was noted as the clearance (from the point at which water vapor enters the chamber to the upper shelf) was decreased from 4.0 to 1.6 cm at a constant sublimation flux of 1.0 $kg \cdot hr^{-1} \cdot m^{-2}$. On calculating the pressure drop for a manufacturing scale freeze-dryer for representative pharmaceutical materials (mannitol and sucrose at 5% w/w), an increased uniformity in the drying rates across the batch was predicted. However, at a combination of atypical primary drying conditions, calculations predict that the product temperature in the center vials was higher than product temperature in the vials at the edge of the array on the shelf, which is opposite to the usual distribution of product temperatures. Since the initial pressure drop measurements were performed at lab-scale using ice slabs, next steps would include determining the spatial variation in the chamber when using product in vials and if possible, verify the scale-up calculations presented in this work by actual measurements in a manufacturing-scale freeze-dryer.

Lastly, the underlying causes of long and variable reconstitution times of lyophilized protein formulations at high concentrations were explored in **Chapter 5**. Three new approaches to investigate the wetting, hydration and disintegration of the lyophilized cakes were applied in **Chapter 5** to better understand barriers to the reconstitution of amorphous lyophilized protein systems. Reconstitution times increased 1) as a measure of wetting declined, 2) as hydration rates decreased, and 3) as a measure of disintegration rates decreased over a range of 0 to 83 mg/ml protein. At a low protein concentration of 40 mg/ml, the reconstitution time was less than a minute irrespective of the process conditions. At the higher protein concentration of 83 mg/ml, aggressive primary drying conditions provided a modest reduction in reconstitution time when compared to the conservative drying conditions. There was no effect of specific surface area on

reconstitution time. Studies aimed towards exploring the effect of lyophilized cake structure on the underlying mechanisms of wetting, hydration and disintegration and hence, reconstitution are ongoing.